MULTIBLOCK COPOLYMER BASED ANION EXCHANGE MEMBRANES AND IONOMERS

A Dissertation
Presented to
The Academic Faculty

by

Lisha Liu

In Partial Fulfillment
of the Requirements for the Degree
Doctorate of Philosophy in the
School of Materials Science and Engineering

Georgia Institute of Technology
May 2018

MULTIBLOCK COPOLYMER BASED ANION EXCHANGE MEMBRANES AND IONOMERS

Approved by:

Dr. Paul A. Kohl, Advisor
School of Chemical and Biomolecular Engineering
Georgia Institute of Technology

Dr. Vladimir Tsukruk
School of Materials Science and Engineering
Georgia Institute of Technology

Dr. Seung Soon Jang
School of Materials Science and Engineering
Georgia Institute of Technology

Dr. William J. Koros
School of Chemical and Biomolecular Engineering
Georgia Institute of Technology

Dr. Meilin Liu
School of Materials Science and Engineering
Georgia Institute of Technology

Date Approved: December 12, 2017

Dedicated to my family

ACKNOWLEDGEMENTS

First, I would like to express my sincere appreciation to my academic advisor Dr. Paul A. Kohl for his support and guidance of my Ph.D work, for his patience, motivation, and immense knowledge. I would also like to thank my committee members: Dr. Seung Soon Jang, Dr. Meilin Liu, Dr. Vladimir Tsukruk, and Dr. William Koros, who provided tremendous support to my research work by sharing their expertise, insights, and instruments.

Second, I would like to thank all Kohl group members for all their help and for all the happy and tough times we have been through together. Particularly, I would like to thank Dr. Johanna Stark Goodman, Dr. Sarah Kim, Dr, Brennen Mueller, Dr. Erdal Uzunlar, Dr. Jared Schwartz, Dr. Bharat Suthar, John Ahlfield, Oluwadamilola Phillips, Jisu Jiang, Garrett Huang, Anthony Engler, Wenjiao Huang, and Dr. Mrinmay Mandal. Special thanks go to John Ahlfield, who helped me to initiate my thesis work. Two undergraduates that have worked with me, Andrew Tricker and Beth Qu, also helped a lot with accomplishing this thesis.

I would like to thank my family who support me with their love and encouragement in all my pursuits. Thanks to my Mom and Dad for their understanding that I cannot be with them all the time. Finally, I cannot thank my lovely husband, Changsheng Wu, enough for his support, patience, and encouragement during my Ph.D. We have been through a lot of hard times together. He has my deepest appreciation and love.

TABLE OF CONTENT

LIST OF TABLES

LIST OF FIGURES

LIST OF ABBREVIATIONS

ABCO	1-azabicyclo[2,2,2]octane
AEI	Anion exchange ionomer
AEM	Anion exchange membrane
AFM	Atomic force microscopy
BPFL	4,4’-(9-fluorenylidene)diphenol
BTMA	Benzyl trimethyl ammonium
CL	Catalyst layer
CPE	Constant phase elements
DCM	Dichloromethane
DFBP	Decafluorobiphenyl
DMA	Dynamic mechanical analysis
DMAc	N,N’-dimethylacetamide
DMF	Dimethylformamide
DSC	Differential scanning calorimetry
EIS	Electrochemical impedance spectroscopy
GDL	Gas diffusion layer

GPC	Gel permeation chromatography
HER	Hydrogen evolution reaction
HFBPA	4,4’-(hexafluoroisopropylidene)diphenol
HSQC	Heteronuclear single quantum coherence
IEC	Ion exchange capacity
MEA	Membrane electrode assembly
NMP	1-methyl-2-pyrrolidone
NMR	Nuclear magnetic resonance
NOE	Nuclear Overhauser effect
OER	Oxygen evolution reaction
ORR	Oxygen reduction reaction
PAE	Poly(arylene ether)
PEM	Proton exchange membrane
PPD	Peak power density
PPO	Poly(phenylene oxide)
QA	Quaternary ammonium
SAXS	Small angle X-ray scattering
STEM	Scanning transmission electron microscopy

TEM	Transmission electron microscopy
TGA	Thermogravimetric analysis
THF	Tetrahydrofuran
TMA	Trimethylamine
TMHA	Trimethyl hexyl ammonium
TTMPP	Tris(2,4,6-trimethoxyphenyl)phosphonium
WU	Water uptake

LIST OF SYMBOLS

σ	Ionic conductivity
λ	Hydration number
q	Wave vector of scattering
d	Characteristic separation length
D	Diffusivity
P	Permeability
S	Solubility
χ	Flory-Huggins interaction parameter

SUMMARY

Anion exchange membranes (AEMs) have been a subject of research as hydroxide conducting polymer electrolytes in electrochemical devices like fuel cells and electrolyzers in recent years due to the alkaline conditions facilitating reaction kinetics and allowing for non-precious metal catalysts, which greatly reduces the cost. However, the wide-scale commercialization of the AEMs is impeded by the low ionic conductivity, high water uptake, poor alkaline stability, and poor mechanical properties of current materials. The primary objective of this study is to create anion exchange membranes and ionomers with improved properties, including high ionic conductivity (*i.e.* greater than 100 mS/cm), excellent chemical stability under alkaline conditions, and low water uptake for better dimensional stability, compared to existing materials in the applications of fuel cells and electrolyzers. To achieve this objective, several new structures for polymeric anion exchange membranes were designed, and the corresponding structure-morphology-property relationship was investigated.

First, multiblock copolymers with partial fluorination and long head-group tethers was designed to improve the ionic conductivity, the alkaline stability, and lower water uptake of AEMs. A systematic study of the effect of the hydrophilic and hydrophobic block lengths and ion exchange capacity of partially fluorinated multiblock copolymer mPEs with long head-group tethers was undertaken to explore the relationship of the chemical structure, morphology and properties of the AEMs. The formation of ion conductive nano-channels for hydroxide ion transport due to nanophase separation of the multiblock copolymers greatly improved the ionic conductivity and reduced the water

uptake. Multiblock copolymer mPE-$X_{5.4}Y_7$-2 showed the highest ionic conductivity, 119 mS/cm at 80 ℃, but not the highest IEC, because it formed efficient channels. Partial fluorination of the polymer backbone was used to lower water uptake of the membrane by increasing the hydrophobicity. From DSC measurements of the number of freezable water and bound water molecules, the number of bound water molecules per ion of two-tether polymers was 4.5 to 5. In addition, the bound water played the dominant role in the hydroxide ion transport within the channels. The multiblock copolymer AEM showed good thermal, mechanical stability and excellent alkaline stability. Long head-group tether was used to improve the chemical stability of the membrane at high pH, as this structure prevents several possible degradation mechanisms of the commonly used benzylic structure. The ionic conductivity was hardly changed after soaking the membrane in 1 M NaOH solution at 60 ℃ for 1000 h. The mPEs AEM with higher ionic conductivity showed lower oxygen diffusivity and permeability, which means that the oxygen crossover problem was less severe.

Second, the effect of the number of ionic groups in the hydrophilic segment on the morphology and properties of AEMs was studied. Multiblock copoly(arylene ether)s (mPEs) were synthesized with different ion exchange capacity (IEC) by attaching a different number of cationic head-groups via long alkyl chain tethers. The multiblock copolymer mPEs with 1, 2, 3 and 4 long alkyl chain tethered ionic groups on each repeat unit in hydrophilic block, resulting in different IECs, were compared. Only one head-group tether can be attached on each hydrophilic repeat unit at a time. Thus, the tether amount can be precisely controlled. As the ionic concentration increased, the ionic conductivity and water uptake of the membranes increased. This was due to the increase

of the size of ion conductive channels. 3-tether membrane showed the highest ionic conductivity/IEC, which means that its ionic groups were most efficient for contributing to the ionic conductivity. In addition, the number of freezable and non-freezable water molecules were investigated. 2, 3, 4-tether membrane showed similar number of bound water, while the number of freezable water increased with the number of ionic groups. The excess freezable water led to high water uptake and low ionic conductivity/IEC ratio. Therefore, 3-tether membrane showed the best properties, 130.6 mS/cm ionic conductivity and 58.3% water uptake, with an IEC of 1.83 meq/g. As the number of ion groups increased, the mechanical strength of the membranes declined.

Third, the effect of the cationic groups (*i.e.* size, central atom, *etc.*) was investigated. Multiblock copoly(arylene ether)s (mPEs) with partial fluorination and two long alkyl head-group tethers on each hydrophilic repeat unit with quaternary trimethyl mmonium (TMHA), quinuclidium (ABCO), and tris(2,4,6-trimethoxyphenyl)phosphonium (TTMPP) were synthesized. Their morphology and properties (*i.e.* ionic conductivity, water uptake, alkaline stability, mechanical and thermal properties) were compared in order to understand the effects of the size and type of cations on the morphology and physical properties. A larger cation led to larger ion channels. However, larger cation also caused lower IEC and consequently lower ionic conductivity despite the channel size of the cation. Quinuclidium showed low water uptake with a lower number of bound water for each ion pair. Tris(2,4,6-trimethoxyphenyl)phosphonium showed high water uptake due to a large number of bound water. TMHA is the most stable cation after exposure to 1 M NaOH solution at 60 ℃ after 30 days, while quinuclidium showed a 22% ionic conductivity loss due to high

hydroxide ion concentration in the local area of ionic groups caused by low bound water content. TMHA also had the best mechanical properties, while phosphonium was the poorest. Therefore, alkyl trimethylammonium appears to be the best cation head group among the three cations studied for this backbone. In addition, the membrane preparation method impacts the morphology and properties of the AEMs. Quaternization before membrane casting resulted in better properties than quaternization after membrane casting due to greater phase segregation.

Lastly, a series of anionic ionomers was synthesized and tested in fuel cells and electrolyzers. These ionomers are based on a series of materials which include block copolymer AEMs with alkyl tethers that have been modified to be used as anion conductors. The ionomers were tested for their viability as anion conductors in the cathodic electrode for the cathode hybrid fuel cell and as the anodic electrode of an alkaline electrolyzer. In this case, the selected materials will be evaluated in both oxygen-consuming (*i.e.* oxygen reduction reaction (ORR)) and oxygen-producing electrodes (*i.e.* oxygen evolution reaction (OER)). The two sets of results show similar trends: for a homopolymer, lower molecular weight materials provide superior performance compared to their higher molecular weight counterparts. Additionally, the introduction of phase segregation via block copolymer further increased performance in both types of devices. Future work on optimizing anionic ionomer materials in oxygen-based electrodes should be focused on reducing the molecular weight of phase segregated materials in order to optimize ionomeric performance.

CHAPTER 1. INTRODUCTION

1.1 Anion exchange membranes and ionomers in electrochemical energy systems

In recent years, attention has been paid to the development of environmentally benign and renewable energy technologies, which includes fuel cells as power sources for automotive and stationary use,[1-3] water electrolyzers for hydrogen production,[4-5] redox-flow batteries for large-scale energy storage,[6] and reverse electrodialysis for energy production.[2, 7] The use of polymeric ion exchange membrane materials in these electrochemical energy conversion and storage systems have attracted increasing worldwide interests.

Ion exchange membrane materials consist of polymer backbones with ion exchange sites that require water of solvation for effective ion transport to provide adequate device performance. The ion exchange groups are usually bound covalently to the polymer backbone.

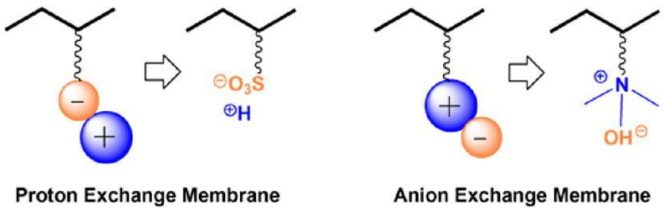

Figure 1.1 Representation of typical proton exchange membranes (left) and anion exchange membranes (right).[3]

According to the ions being transported, the membranes can be divided into proton exchange membranes (PEMs), with fixed, negatively charged functional groups such as sulfonic acid, and anion exchange membranes (AEMs), with fixed positively

charged functional groups such as quaternary ammonium, as shown in Figure 1.1[3]. PEMs have been developed and commercialized for many years.[1-2, 8] Nafion® (DuPont) is the most well-known and widely used PEM material.[1, 8] The high cost of the membrane materials and precious metal catalysts used in electrochemical devices due to the acidic condition are the main drawbacks of current PEMs. In the past decade, more and more attention has been attracted to AEM materials mainly due to the alkaline condition facilitating reaction kinetics, which enables the use of cheaper catalysts.[2, 9-12]

Anion conductive materials have two main applications in the electrochemical devices.[2] One is anion exchange membranes (AEMs) containing alkaline anions (*i.e.* OH^-, Cl^- and Br^-), which are used as solid-state electrolytes to provide ion conduction between anode and cathode and separate the two electrodes. Another is anion exchange ionomers (AEIs), which are usually low molecular weight polymer electrolytes in either solution or dispersion form. AEIs are used as polymer binders to introduce anion conductivity in the catalytic layer of electrodes, mixed with catalysts and electron-conductive materials to form a three-phase boundary as the active reaction site.

Anion conducting materials have a wide application in electrochemical systems. This work will focus on their applications in AEM fuel cells and water electrolyzers.

1.1.1 AEM fuel cells

As an alternative energy source to traditional fossil fuels, fuel cells have received more and more attention in recent years owing to their high efficiencies and low emissions.[1-2] Fuel cells are electrochemical devices that directly convert chemical energy stored in fuels, such as hydrogen, to electrical energy. Ion exchange membrane fuel cell,

which uses ion exchange polymeric membrane as the solid electrolyte, is one of the most developed fuel cells. Basically, there are two types of ion exchange membrane fuel cells: proton exchange membrane (PEM) fuel cell and anion exchange membrane (AEM) fuel cell.

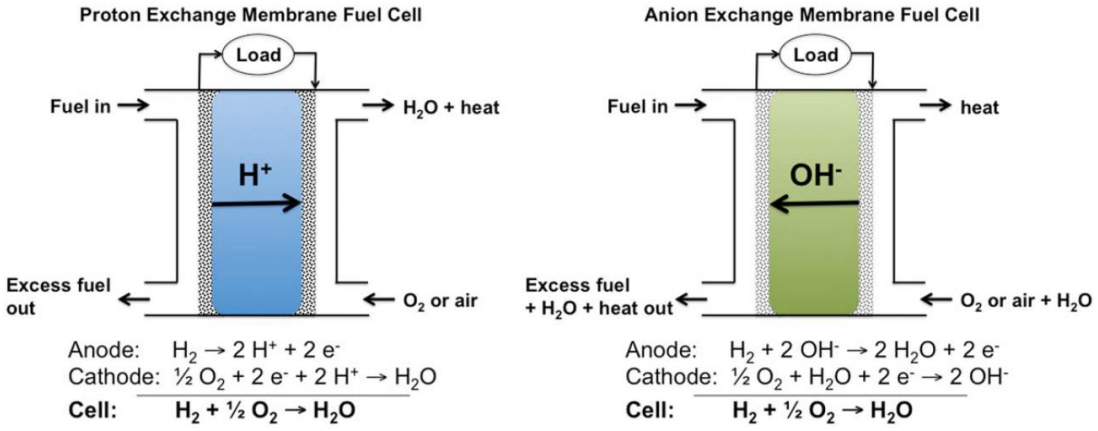

(a) (b)

Figure 1.2 Schematic of (a) proton exchange membrane (PEM) fuel cell and (b) anion exchange membrane (AEM) fuel cell using hydrogen as fuel.[9]

PEM fuel cells have been developed for a long time and have certain applications in portable devices and vehicle transportation.[1, 8] However, the wide-scale commercialization is impeded by several obstacles, including sluggish oxygen reduction kinetics at the cathode due to acidic reaction condition, high cost of noble catalyst platinum, complex water management, and fuel crossover problem. The configuration of PEM is shown in Figure 1.2(a)[9]. Recently, more and more attention has been attracted to AEM fuel cells, which use anion exchange membranes as the electrolyte to conduct OH^- ions.[2, 9-12] The configuration of AEM fuel cell is demonstrated in Figure 1.2(b)[9]. Oxygen flows into the fuel cell and reacts with water and electrons to form OH^- ions at the

cathode. OH^- ions go through the anion exchange membrane to the anode and then combine with hydrogen to produce water and electrons. The high pH environment of AEM fuel cells addresses many of the shortfalls with PEM fuel cells: facile reaction kinetics, potential use of non-precious metal catalyst, and mitigated fuel crossover because of the opposite transportation directions of ions and fuels. However, the performance of AEM fuel cells is not as good as PEM fuel cells. It is mainly due to the limitations of current anion exchange membrane materials, including low ionic conductivity, high water uptake, and poor stability in high pH environment.

1.1.2 AEM water electrolyzers

Advanced water electrolysis is one of the most efficient and reliable approaches to produce hydrogen, which is an excellent energy storage medium, from renewable energy. Currently, two types of low-temperature water electrolysis have been developed: alkaline liquid electrolyte water electrolysis,[5, 13] and proton exchange membrane (PEM) water electrolysis.[14-15] In alkaline liquid electrolyte water electrolysis, non-noble metals can be used as the catalysts for the hydrogen and oxygen evolution reactions. The low cost of this approach makes it possible for large-scale hydrogen production. However, the insoluble carbonates precipitate formed by high concentration alkaline electrolyte and CO_2 in the air can block the transport of reagents and products. Precise pressure control is also required to prevent gas crossover problem. PEM water electrolysis can overcome these drawbacks with the use of solid-state electrolyte. However, it has the disadvantage of high cost of precious metal catalyst and PEM materials.

Anion exchange membrane (AEM) water electrolysis is emerging from recent research, as it combines the advantages of PEM water electrolysis and liquid alkaline electrolyte water electrolysis.[2, 4, 16] High pH operation condition makes it possible to employ non-precious metal catalyst and reduce the cost. In addition, the quaternary ammonium based membrane eliminates carbonate precipitation due to the absence of metal cations. The main limitations of AEM materials for water electrolysis, similar to fuel cells, include low ionic conductivity, poor alkaline stability, and poor mechanical stability.[2, 4, 16-17]

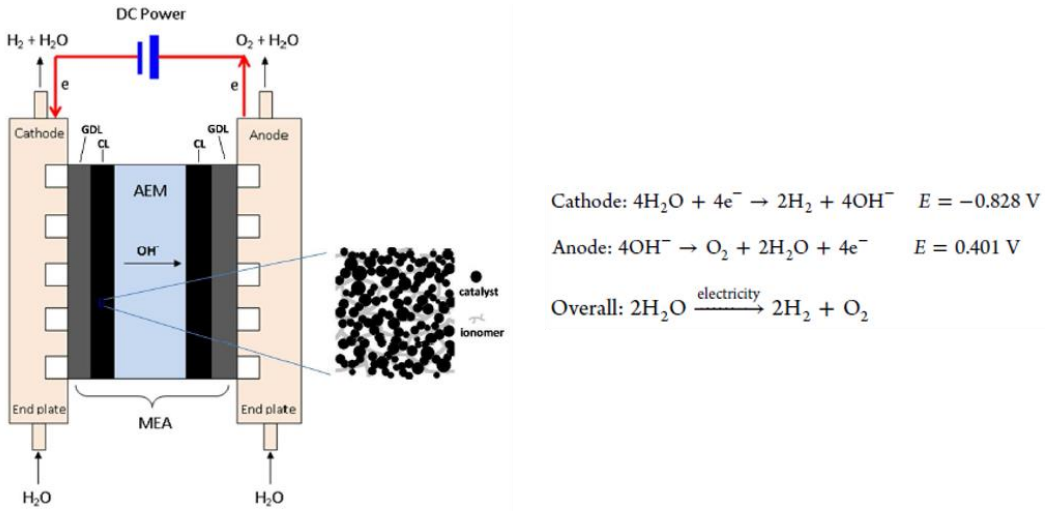

Figure 1.3 Schematic of an alkaline membrane electrolyzer, and electrode and overall reactions.[4]

The configuration of a typical AEM water electrolysis cell is shown in Figure 1.3[4]. In general, an alkaline membrane water electrolysis cell is comprised of an anode for oxygen evolution reaction (including an anode gas diffusion layer (GDL) and anode catalyst layer (CL)), a cathode for the hydrogen evolution reaction (including cathode GDL and CL), bipolar plates, and an anion exchange membrane as the solid electrolyte. The insert figure (Figure 1.3) shows the porous microstructure of electrode catalyst layers,

where a three-phase boundary is formed by catalysts, ionomers, and gas pores. The hydrogen and oxygen evolution reactions take place on the three phase boundaries, which are the electrochemically active sites. Typically, water is fed into the cathode since water is consumed for the hydrogen evolution reaction to produce OH^- ions. The OH^- ions are then transported through the AEM to the anode, where hydroxide ions are oxidized to produce oxygen gas and water. The thermodynamic cell voltage for the overall reaction is 1.23 V at 25 ℃. For effective production of hydrogen, the applied voltage is required to be greater than 1.23 V to overcome the overpotential of the electrochemical reaction processes and ohmic drop in the cell.

1.2 Properties of AEM materials

1.2.1 Desired properties of AEM materials

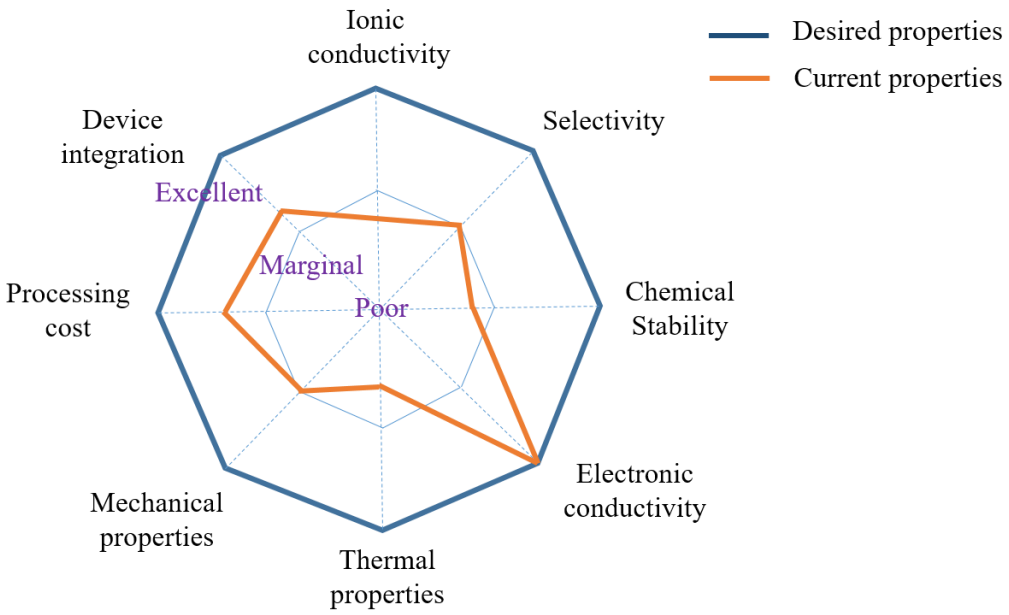

Figure 1.4 Radar diagram of current and desired properties of anion exchange membranes.[18]

The desired properties of AEM membrane materials include high ionic conductivity, sufficient chemical, thermal and dimensional stabilities, mechanical toughness, and low permeability to gas or liquid fuels.[2, 9-12] The radar diagram, as shown in Figure 1.4, demonstrates the current and desired properties of anion exchange membranes.[18]

Ionic conductivity is an intrinsic property of membranes, which characterizes the ion transport ability in the membrane. High ionic conductivity is essential to minimize the resistance of membrane electrolytes. Ionic conductivity is usually tested by an electrochemical impedance spectrometer. Water uptake is the percentage difference of the weight of the membrane in wet and dry form. Proper hydration is necessary for efficient ion transport in the membrane. AEMs need hydrated ions for efficient ion transport. However, excess water uptake can swell the membrane, leading to poor mechanical toughness of the membrane and flooding of the ion conductive channels, which will result in poor performance of the electrochemical devices. Chemical and thermal stabilities are of great importance as the typical operation conditions of AEM based electrochemical devices are high pH and relatively high temperature. Mechanical stability of AEMs is essential during the membrane fabrication process and device operation since a pressure difference usually exists between the two electrodes. Inhibiting gas or liquid fuel transport through the membrane also an important property since high permeability results in fuel crossover, which leads to the direct reaction of the reagents. This reduces the efficiency of the electrochemical devices.

Most of the desired properties of AEM ionomers are the same as AEM membrane materials, including high ionic conductivity, low water uptake, and good alkaline

stability.[2, 19] However, the requirement for the fuel and oxygen diffusivity and permeability are different from that of membranes. High fuel and oxygen transport is needed for efficient supply of reagents for electrode reactions.[19] In addition, high mechanical toughness is not essential for AEM ionomers, as AEM ionomers are desired to have good solubility in common solvent and be easy to rearrange in the catalytic layer during the electrochemical device operation. So AEM ionomers are usually low molecular weight anion conductive polymers. However, AEMs membranes are typically high molecular-weight polymers, which can be cast into a stable and robust membrane without much deformation during fabrication and operation processes.

1.2.2 Limitations of current AEM materials

Compared to PEM materials, the main limitations of current AEM materials include low ionic conductivity, high water uptake, poor alkaline stability at high temperature, and poor mechanical stability.[2, 9-12]

1.2.2.1 Low ionic conductivity

The lower ionic conductivity in AEMs compared to PEMs is due to the inherently lower mobility of hydroxide ions and the weak basicity of the cation site.[3] For example, the ratio of ion mobility between OH^- and H^+ is 0.57 in the limiting case of an infinitely dilute solution at 298K.[20] Moreover, the ionic exchange group sulfonic acids in PEM are strong acids as the pK_a of aryl sulfonic acid is estimated to be on the order of 1.[20] However, quaternary ammoniums are comparatively weak bases with a pK_b on the order of 4.[20] Therefore, a considerable theoretical barrier to the dissociation of hydroxide ions

from quaternary ammonium ions exists, which impedes the efficient hydroxide ion conduction in AEMs.

1.1.1.2 Degradation and alkaline stability

Stability under alkaline condition is another obstacle to AEM development and commercialization.[2, 9] Extreme conditions, such as high pH and high temperature, are usually required in electrochemical devices employing anion exchange membranes. The presence of hydroxide ions is required for facile reaction kinetics, and high temperature is desirable to decrease the use of catalyst by improving the kinetics, increase ionic conductivity, and aid in the removal of carbon dioxide form the system, where carbonates will be formed due to the presence of hydroxide ions. Therefore, the stability of AEMs in strongly alkaline environments (*e.g.* in the presence of nucleophilic OH^- ions) has become the primary concern with the use of AEMs in electrochemical devices.

The alkaline stability and degradation mechanism of AEMs have been studied for different cations and chemical backbones.

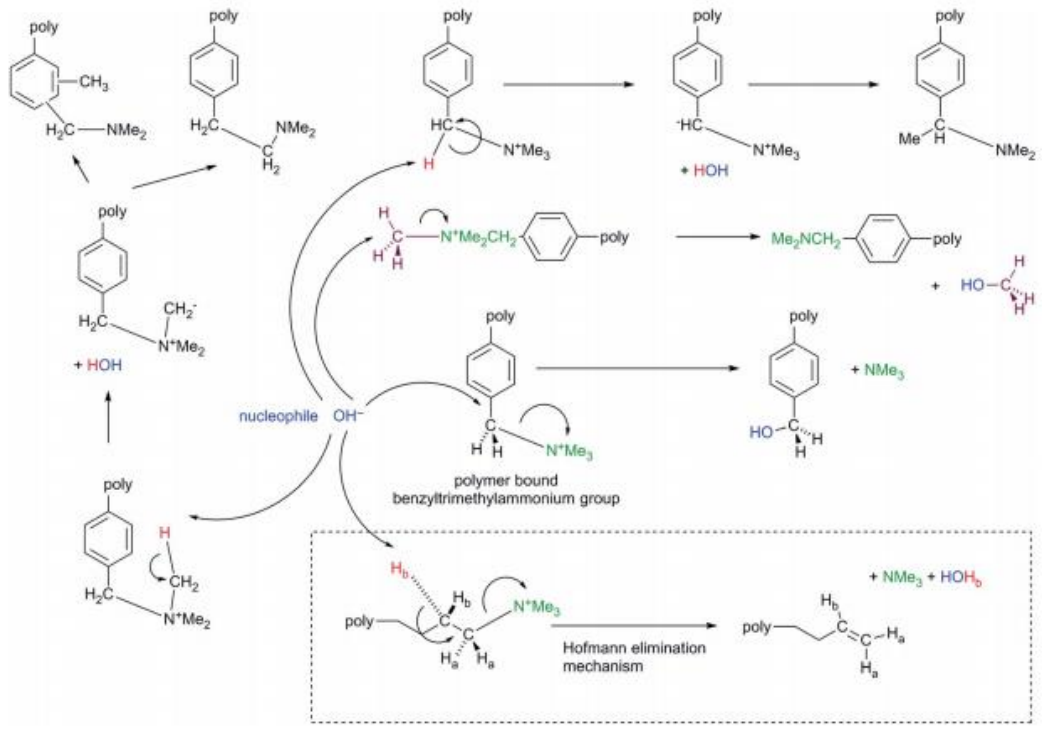

Figure 1.5 Degradation pathways for the reaction of OH- nucleophiles with benzyltrimethylammonium cationic (anion-exchange) groups. The dashed box shows the Hofmann Elimination degradation mechanism that can occur with alkyl-bound QA groups.[2]

Benzyl-trimethyl ammonium (BTMA) is the most common cation group. Figure 1.5 shows the possible degradation processes in the presence of OH^- nucleophiles. The main degradation mechanism for benzyl trimethyl ammonium groups is via direct nucleophilic substitution (displacement) on the benzylic carbon or methyl carbon.[21-22] Elimination via ylide formation also exists.[21, 23] Hofmann elimination can only occur when there are β-Hs present. Therefore, it cannot occur with BTMA structure.[24] It used to be concerned that Hofmann elimination can occur with quaternary ammonium groups bound to longer alkyl chains, as shown in Figure 1.5 in dashed box, which makes it less stable than BTMA groups.[25] However, more recent evidence suggests that this may not be the case. Several studies reported that long alkyl chain (especially >4 carbon atoms

long) tethered quaternary ammonium groups showed surprisingly good alkaline stability.[26-29] The possible hypothesis is that the high electron density around the β-Hs in long alkyl side chains can inhibit Hofmann elimination.[30] In addition, the steric shielding in the β-positions may also play a role in the good stability with long alkyl chains.[31] Only in some very extreme conditions, Hofmann elimination reaction was reported in long alkyl chain tethered cationic groups.

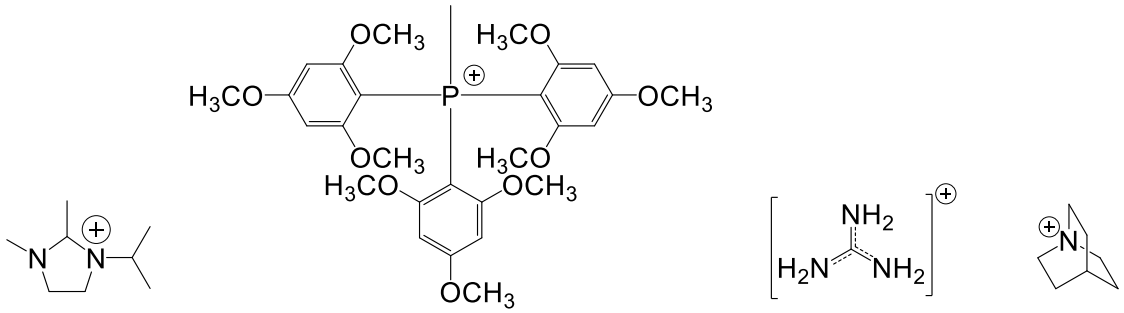

Figure 1.6 Structures of (a) imidazolium cations with isopropyl substitute,[32] (b) phosphonium,[33] (c) guanidinium,[34] and (d) quinuclidium.[19]

Other cation groups, such as imidazolium,[35-36] phosphonium,[33] and guanidinium[37] have also been studied as alternatives of BTMA. For instance, Xu and co-workers[38] synthesized PPOs based AEMs with imidazolium cationic groups, which showed OH^- conductivity higher than 100 mS/cm at 80 ℃ and good chemical stability. Gu et al.[32] investigated the alkaline stability of a variety of imidazolium cations with various N_3-substitutes including methyl, butyl, heptyl, dodecyl, isopropyl, and diphenylmethyl groups via NMR analysis and density functional theory calculations. Their results showed that the isopropyl substituted imidazolium cation with the highest LUMO energy value, which is shown in Figure 1.6(a), exhibited the highest alkaline stability in aqueous NaOH. The imidazolium cations exhibited higher alkaline stability than BTMA. Yan et al.[33]

reported a bulky phosphonium cation structure as the ionic exchange groups in AEMs, which is shown in Figure 1.6(b). It showed a high ionic conductivity of 45 mS/cm at 20 ℃ and no degradation in 1 M NaOH at 60 ℃ for one month. A guanidinium cation, as shown in Figure 1.6(c), was also investigated in AEMs with a higher ionic conductivity due to the high alkalinity (high pKa) of guanidinium hydroxide, which leads to an augmentation of both the number of dissociated hydroxides and water molecules.[39] The inherent charge delocalization from the resonance structure of the guanidinium also improved the chemical stability of the material.[39] For example, Xu and co-workers[38] synthesized PPO based AEMs with guanidinium cations. A high ionic conductivity of 71 mS/cm at room temperature and no degradation in 1 M NaOH at 25 ℃ for 200 h were observed. Zhou and co-workers[40] synthesized poly(arylene ether) ionomers with pendant quinuclidium cations, as shown in Figure 1.6(d). Higher fuel cell performance was observed using these ionomers than their counterparts with BTMA cations in the electrodes.

In addition to cation stability, backbone stability is another issue. A wide range of polymer backbone structures including, polyphenylenes,[41] poly(phenylene oxide)s,[28, 42] poly(arylene ether sulfone)s,[40, 43] and poly(arylene ether)s[44] have been investigated. No systematical study of polymer backbone stability has been reported. However, some[45-46] observed degradation of AEMs containing aryl ether (C_{sp2}-O) bonds under alkaline conditions.

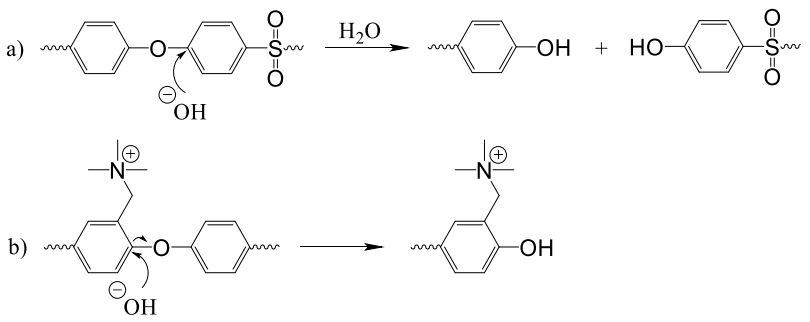

Figure 1.7 Potential degradation mechanism of aryl-ether cleavage occurring (a) at the polymer backbone with sulfone and ketone groups, [46] (b) in the ether linkage with BTMA substituted aryl group of PAEs.[45]

The presence of electron-withdrawing groups such as sulfone and ketone groups in the aromatic polymer backbone will activate aryl-ether linkage for hydrolysis via nucleophilic attack, as shown in Figure 1.7(a).[46] The aryl-ether cleavage of quaternized poly(arylene ether)s (PAEs) is likely to occur in the ether linkage with BTMA substituted aryl group, as shown in Figure 1.7(b).[45] No degradation was observed in non-functionalized PAEs without BTMA groups after storage in 0.5 M NaOH at 80 ℃ for 2 days.

In order to design AEMs with better alkaline stability, it is essential to understand the degradation mechanisms. NMR has been the most commonly used technique to monitor degradation. Other techniques have been reported as well, such as Raman, ultraviolet-visible spectroscopy (UV/Vis) and gas chromatography-mass spectrometry (GC-MS).

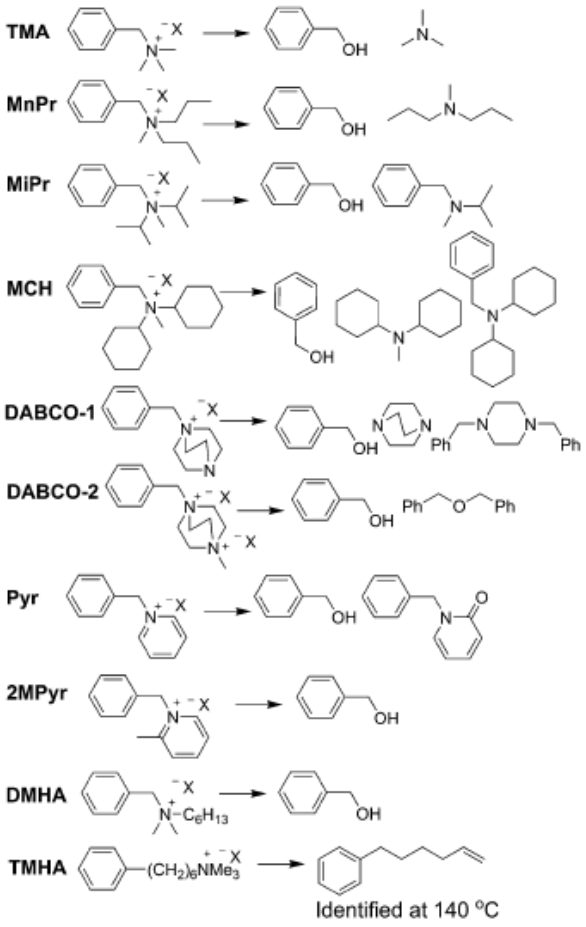

Figure 1.8 Byproducts identified after cation degradation studies (where X = OH or OD).[27]

Bae and co-workers[27] reported the byproducts after degradation of a variety of cationic groups attached on small molecule benzene, as shown in Figure 1.8. The cation stability was investigated in pure OH^- (or OD^-) form in water without excess alkaline solution by utilizing an Ag_2O-mediated ion exchange reaction. From quantitative NMR analysis, three cation structures including MnPr, MCH, and TMHA, showed greater alkaline stability than the well-known TMA. Two QA-model compounds (DABCO-1 and DMHA) showed comparable stability. The other six compounds showed worse stability compared to TMA. The degradation products shown in Figure 1.8 will be good

indications of degradation mechanisms, such as Hofmann elimination and nucleophilic substitution.

Pivovar et al.[47] developed a reliable and standardized method to determine cation degradation under conditions similar to those expected in electrochemical devices. They investigated a number of experimental variables including reaction vessel, heating method, the use of internal (NMR) standards, ionic group concentration, and different aqueous environments (most notably D_2O and H_2O). The resulting method employed a relatively high base concentration of 2 M, a relatively low cation concentration of less than 0.1 M, the removal of deuterated solvents, and Teflon lined Parr reactors placed in convention ovens. This method allowed reproducible degradation rates at accelerated temperatures.

1.3 Multiblock copolymer AEMs and phase segregation

AEMs with high ionic conductivity (i.e. > 100 mS/cm at 80 °C) and low water content are desired for efficient fuel cell operation.[2, 9, 48] The ionic conductivity is determined by two factors: ionic mobility and ion exchange capacity (IEC).[48] Increasing IEC by attaching more cationic groups is easier but with the sacrifice of higher water uptake. Improving ionic mobility is more promising by constructing more efficient ionic channels.

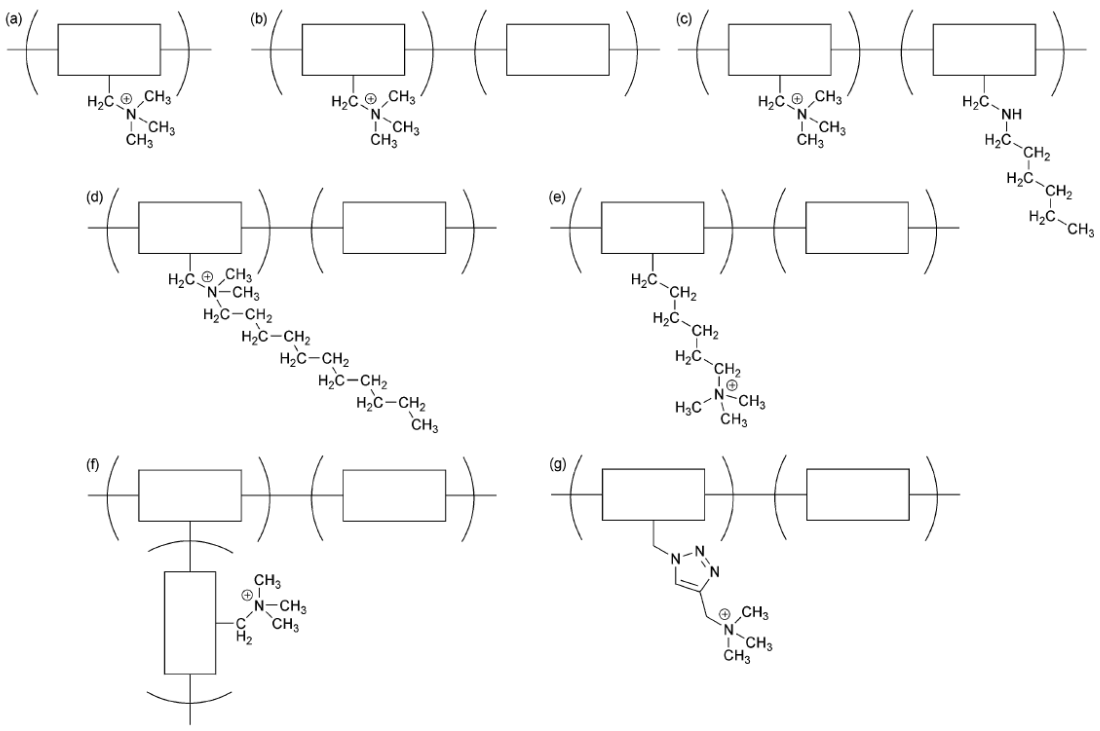

Figure 1.9 General strategies for the development of phase segregated AEMs (b-g) compared to a benchmark homopolymer system (a).[2] (The rectangles represent a polymer block.)

Using a block copolymer structure is one of the strategies to obtain well-defined nano-channels, because block copolymers can form nanophase separation on a nanometer scale due to the thermodynamic incompatibility between hydrophilic and hydrophobic blocks. These can form a variety of self-assembled morphologies including spheres arranged on a cubic lattice, hexagonally packed cylinders, interpenetrating gyroids, and alternating lamellae.[49] General strategies for the development of block copolymers with phase segregation are shown in Figure 1.9[2].

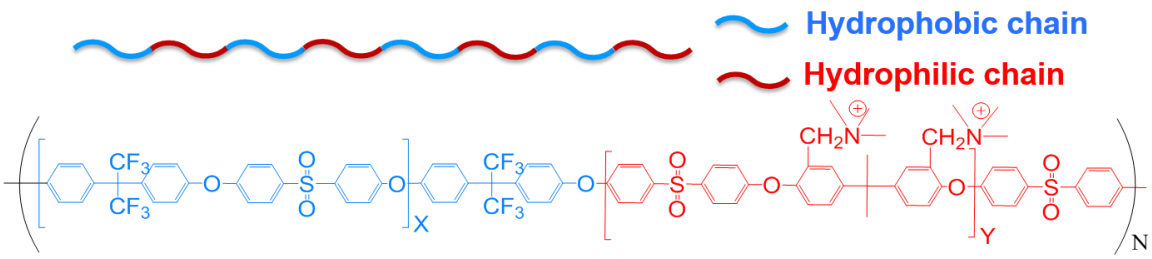

Figure 1.10 Representation of structure of multiblock copolymers and multiblock copoly(arylene ether sulfone)s with benzyl trimethyl ammonium.[40]

It has been reported that multiblock copolymers have higher ionic conductivity and lower water uptake than their corresponding random copolymers with the same IEC.[40, 50] Park et al.[40] prepared anion conductive aromatic multiblock copoly(arylene ether sulfone)s, shown in Figure1.10, by polycondensation, chloromethylation and quaternization reactions. It was found that the multiblock copolymer membrane had higher ionic conductivity (37.7 mS/cm) than that of the random copolymer counterpart (13.6 mS/cm) at 60°C with the same IEC. Watanabe and co-workers[50] synthesized multiblock copoly(arylene ether)s with clustered ionic groups in the hydrophilic blocks. Similarly, higher hydroxide conductivity was observed in the multiblock copolymer membranes than in the random copolymer ones. They attributed this to interconnected ion transport pathways formed by phase separation, which was confirmed by scanning transmission electron microscopy (STEM). Therefore, utilizing multiblock copolymer structures with well-developed phase-separated nano-channels appears to be effective for improving the ionic conductivity of AEMs without sacrificing other essential properties such as mechanical and dimensional stability. In multiblock copolymer membranes, the ionic groups are locally concentrated to hydrophilic domains to form channels for ion and water transportation.

Multiblock copolymer membranes with different hydrophilic and hydrophobic block lengths show different ionic conductivity and water uptake properties. The reason is that ionic channels of different sizes are formed due to phase separation of different block lengths. In addition, the IEC will be different for different block lengths. Li et al.[51] prepared multiblock copolymers with fluorene-containing hydrophilic segments densely functionalized by side-chain quaternary ammonium groups. They showed that AEMs had different ionic conductivity and water uptake with different block lengths, and found that at a given length of hydrophilic block, the membrane peaks in small angle X-ray scattering (SAXS) patterns shifted slightly towards higher q values (smaller domain size) as the length of hydrophobic block increased, which could be attributed to hydrophobic structures driving the ion clusters to be aggregated. Lai and co-workers[52] synthesized phenolphthalein-based poly(arylene ether sulfone nitrile)s multiblock copolymers with different hydrophilic block lengths but the same hydrophobic block length. They observed larger hydrophilic domain sizes as well as more pronounced and developed interconnectivity of ion domains in atomic force microscopy (AFM) phase images and SAXS patterns, as shown in Figure 1.11[52], by increasing the hydrophilic block length. Ionic conductivity and water uptake also increased with the increase of the hydrophilic block length.

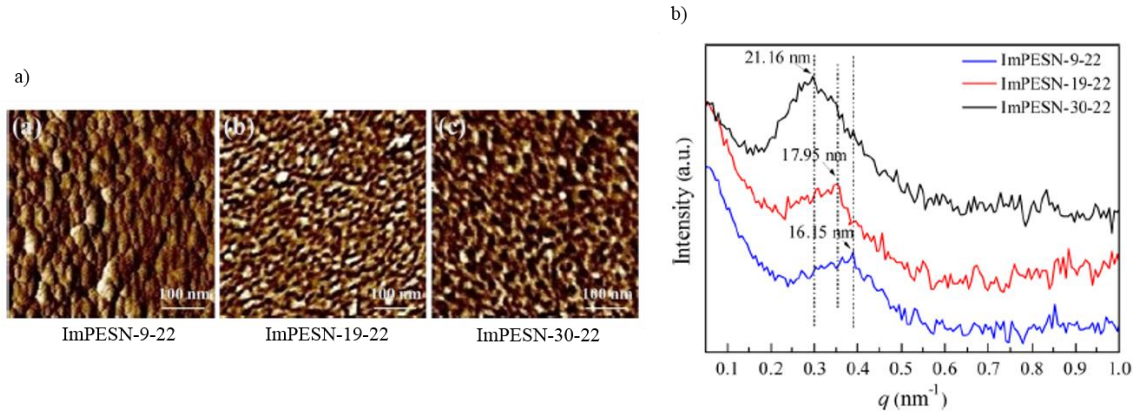

Figure 1.11 (a) AFM phase images (b) SAXS patterns of AEMs with different hydrophilic block lengths and same hydrophobic block lengths.[52]

The presence and morphological structure of the nano-channels are usually characterized by AFM, transmission electron microscopy (TEM), and SAXS.[3] AFM phase images provide information of the surface morphology of membranes. TEM experiments are usually performed on ~100 nm cross-sectioned films cut by ultramicrotomy. SAXS gives information on the domain size averaged over the entire sample but not visualized.

1.4 AEMs with tailored side chains

Ionic exchange groups, which are cationic groups in AEMs, can be attached to polymer backbones via different strategies and configurations. Among all the side chain configurations in recent research, tethering cations via pendant long alkyl spacers appears to be more effective in improving microphase separation, hydroxide ion conductivity, and alkaline stability.[29]

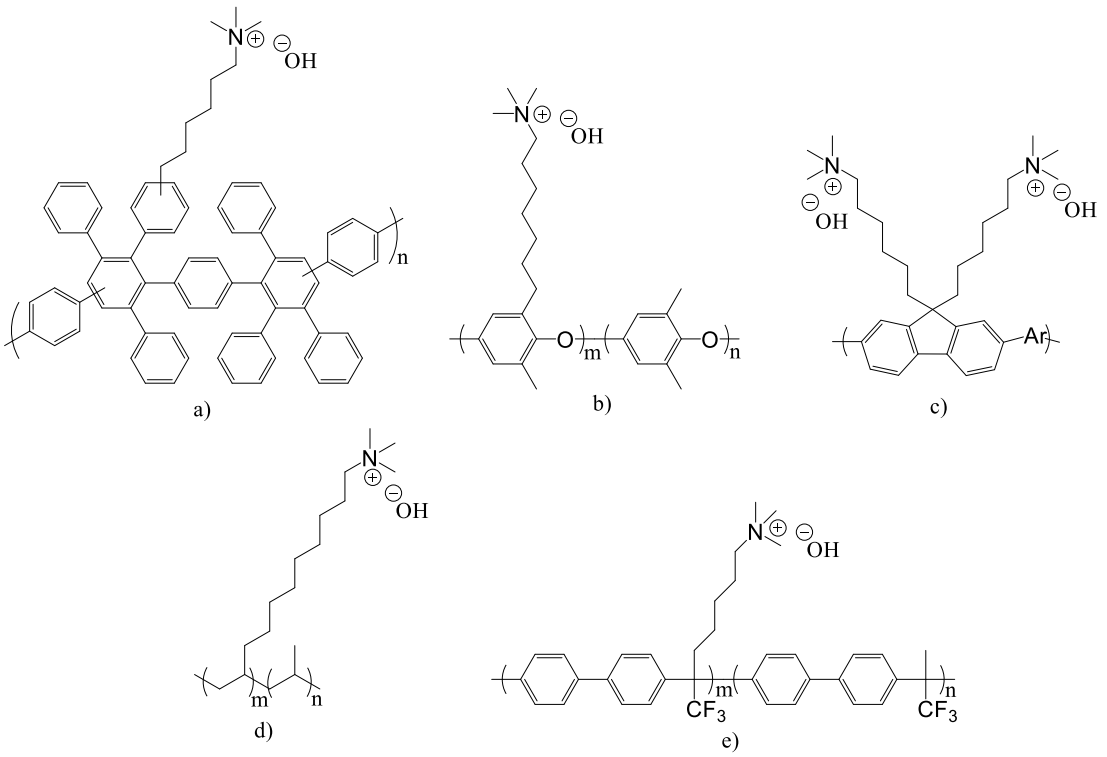

Figure 1.12 Structures of different polymers with cationic groups on flexible alkyl spacers: (a) polyphenylene,[41] (b) PPO-7Q,[28] (c) polyfluorene,[26] (d) polypropylene,[53] (e) poly(biphenyl alkylene).[54]

Figure 1.12 summarizes the structures of polymers with cationic groups on flexible alkyl spacers in the literature. Several synthetic approaches to these structures were reported. Hibbs[41] prepared poly(phenylene)s based anion exchange membrane carrying QA groups via hexyl spacers, as shown in Figure 1.12(a) by Friedel-Crafts acylation, reduction of the resulting ketone linker, and quaternization using trimethylamine. Less than 5% loss in ionic conductivity was observed in 4 M NaOH solutions after 14 days. Dang et al.[28] synthesized poly(phenylene oxide)s (PPO) functionalized with QA via heptyl spacer (Figure 1.12(b)). PPO was first lithiated in solution, and then reacted with an excess of 1,6-dibormohexane to introduce heptylbromide side chains before quaternization by trimethylamine. With an IEC of 1.8

mmol/g, the conductivity of the membrane reached 85 mS/cm at 80 ℃. No structural change in ^{1}H NMR spectra was observed over 192 h in 1 M NaOH solution at 80 ℃. Lee and co-workers[26] synthesized polyfluorenes (Figure 1.12(c)) with QA groups attached on hexyl spacers using Pd catalyzed Suzuki coupling of premade bromoalkylated monomers, followed by quaternization using trimethylamine. The OH^- conductivity was reported to be 24 and 85 mS/cm at 30 and 80 ℃, respectively. No significant change in the ^{1}H NMR shifts or IEC was observed in the AEMs after being soaked in 1 M NaOH at 80 ℃ for 720 hours. Semicrystalline polypropylene (PP) with QA groups on hexadecyl spacers (Figure 1.12(d)) was reported by Zhang et al.[53] via heterogeneous Ziegler-Natta catalyzed polymerizations. The AEMs maintained OH^- conductivity at 57 mS/cm at 80 ℃ with a low water uptake of 21%. The membranes retained more than 85% of OH^- ionic conductivity after storage in 5 M NaOH solution at 80 ℃ for 700 hours.

By tethering cations via long alkyl spacers instead of benzylic groups, the alkaline stability of AEMs at high temperature (*i.e.* 80 ℃) is greatly improved, as the new structure avoids the unstable BTMA groups. For instance, Hibbs[41] reported that the membrane with trimethylammonium cations attached by a hexamethylene spacer showed better stability than the membrane with benzyl trimethylammonium cations in 4 M KOH at 90 ℃. Bae and co-workers[27] reported that QA groups attached via six-carbon alkyl spacer was the more stable structure in alkaline solutions by comparing various cationic groups and configurations on small molecules.

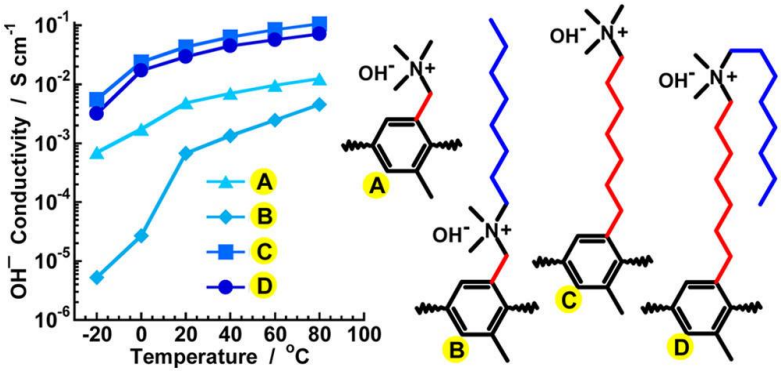

Figure 1.13 Structures and properties of PPO functionalized with different cationic alkyl side chain designs.[28]

Attaching long alkyl side chains is also one of the strategies to facilitate the formation of nano-channels as ion transport pathways. With the addition of the long alkyl side chains, the polymer becomes a comb-shaped or a grafted polymer configuration. This configuration can facilitate the nanophase separation between the conductive domains and nonconductive domains. For instance, Jannasch and co-workers[28] prepared and compared the morphology and properties of a series of PPOs with cationic alkyl side chains of different lengths and configurations, as shown in Figure 1.13. In particular, they investigated the effect of different side chain configurations based on spacer unit in-between the QA groups and the polymer backbone, as well as alkyl extension pendant to the QA group. It was showed by SAXS results that the flexible spacer units greatly facilitated efficient ionic phase separation, regardless of the location of the extender chain. In addition, the membrane with only long alkyl spacers had the highest OH^- conductivity, exceeding 100 mS/cm at 80 ℃, as well as the best alkaline stability. No change in ^1H NMR was observed after storage in 1 M NaOH solution for 8 days.

1.5 Water mobility in ion exchange membranes

Water absorbed in the ion exchange membrane exists in three different states: (1) free water that are identical to bulk water frozen at 0 ℃, (2) freezable water that is slightly interacted with ion exchange groups frozen at subzero temperatures, but still moves freely in the membrane, (3) non-freezable water that is strongly bound to ion exchange groups or a polar polymer matrix. It is essential to understand the states of water in the membranes for the operation of polymer electrolyte fuel cells and eletrolyzers, particularly at high and low temperatures. As only non-freezable water remains in the membrane under the dehydrated condition at high or low temperature (*i.e.* above 100 ℃ or below 0 ℃), the cell start-up speed and electrical properties are mainly determined by non-freezable water content.[55-56] The state of water is also crucial to improve the ionic conductivity. Several studies have attempted to elucidate the relationship between the amount of water in different states and ionic conductivity.[57-58] The types of ion transporting mechanism in the membranes can also be explained by studies about the water state because various ion transporting mechanisms are closely related to the proximity of water to the ion exchange groups.

Several techniques have been employed to study the states of water in the membranes, including NMR relaxation time,[40] FT-IR,[58] dielectric relaxation spectroscopy,[59] and differential scanning calorimetry (DSC),[60-62] etc.

DSC measurements can quantitatively identify the amount of water in different states by analyzing the different freezing behaviors. Since non-freezable water is strongly interacted with ion exchange groups and polymer matrix, it is not able to crystallize. Therefore, non-freezable water yields no heat flow in DSC thermogram. However, the

freezable water moves freely in the membranes and weakly interacts with the ion exchange groups. This state of water produces an exothermic peak at temperatures below 0 ℃ during a cooling scan in DSC thermogram. Then the amount of freezable water can be calculated by the value of freezing temperature depression and the freezing enthalpy of the exothermic peak. DSC technique is very facile and efficient in differentiating the two states of water and quantifying the amount. Several studies have been attempted to use DSC to study the water mobility in PEMs and correlate it with ionic conductivity.[60-62]

NMR relaxation times can sensitively reflect the rate and the nature of molecular motions within a confined geometry, as the principle of NMR relaxation process is the energy exchange of one proton spin with other proton spins and the energy exchange between the spin system and the surrounding lattice. NMR spin-lattice (T_1) and spin-spin (T_2) relaxation times provide direct indications of the restricted motions of water in confined environments or near surfaces. NMR relaxation time can be used to obtain quantitative water mobility in the membranes. Relaxation time T_1 has been used to examine water confinement and physical interactions of water molecules with the polymer in Nafion.[63] Park et al.[40] compared water mobility in random and block copolymer AEMs by analyzing bound versus free water through relaxation time T_2. It was indicated that block copolymer membrane showed shorter T_2, which means water is interacted with ionic groups more closely and utilized more efficiently in ion conducting.

1.6 Research objectives and strategies

The primary objective of this study is to create anion exchange membranes and ionomers with improved properties, including high ionic conductivity (*i.e.* greater than 100 mS/cm), excellent chemical stability under alkaline conditions, and low water uptake for better dimensional stability, compared to existing materials in the applications of fuel cells and electrolyzers. To achieve this objective, several new structures for polymeric anion exchange membranes were designed, and the corresponding structure-morphology-property relationship was investigated. The strategies have been proposed and implemented as follows.

1.6.1 Multiblock copolymer with partial fluorination and long head-group tethers

The molecular structure was designed to improve the ionic conductivity, the alkaline stability, and lower water uptake of AEMs: (1) Multiblock copolymer backbone was used to construct ion conductive channels through its phase segregation. The ionic channels can facilitate the ion transport and improve the ion mobility in the membrane. (2) Long head-group tether was used to improve the chemical stability of the membrane at high pH, as this structure prevents several possible degradation mechanisms of the commonly used benzylic structure. Long head-group tether also facilitates the phase segregation of the polymers. (3) Partial fluorination of the polymer backbone was used to lower water uptake of the membrane by increasing the hydrophobicity. Multiblock copolymer with different hydrophilic and hydrophobic block lengths, and different number of head-groups tethered in hydrophilic segments were synthesized and compared

to study the structure-morphology-property relationship and to identify the optimum AEMs. The details will be discussed in Chapter 3.

1.6.2 Different number of ionic groups in hydrophilic segments

This design was aimed at investigating the effect of ionic concentrations (or number of ionic groups) in hydrophilic block of the multiblock copolymers, which determines the ion exchange capacity, on the morphology and properties (i.e. ionic conductivity, water uptake, and mechanical strength) of AEMs. More ionic groups result in higher ionic exchange capacity. Typically, high ion exchange capacity can be achieved by increasing the number of ionic groups, which leads to high ionic conductivity, but high water uptake as well. The optimum number of ionic groups were selected with high ionic conductivity and acceptable level of water uptake. The details will be discussed in Chapter 4.

1.6.3 Long alkyl chain tethered quaternary trimethylammonium, quinuclidium, and phosphonium cations

Multiblock copolymers with long alkyl side chain tethered three cationic groups: trimethylammonium, quinuclidium, and phosphonium were designed and compared to understand the relationship between cation structure (*i.e.* size, central atom, etc.) and properties of AEMs, especially ionic conductivity and alkaline stability. Quinuclidium, or 1-azaoniumbicyclo[2,2,2]octane, a quaternary ammonium cation formed by quaternization of a polycyclic amine 1-azabicyclo[2,2,2]octane (ABCO), was first reported by Zhou et al.[19] as the ionomer for alkaline electrode in fuel cells. Quinuclidium has a larger van der Waals volume than the trimethyl ammonium head group, which may

facilitate the formation of larger ion conductive channels to enhance ion mobility in the membrane. Phosphonium cation has a central atom of phosphorus instead of nitrogen. Yan et al.[33, 64] developed a stabilized quaternary phosphonium cation, benzyl tri(2,4,6-trimethoxyphenyl)phosphonium, designed with nine methoxy groups to provide strong electron donation and steric hindrance. Quinuclidium and tri(2,4,6-trimethoxyphenyl)phosphonium with long alkyl tethers were evaluated and compared with alkyl trimethylammonium. The details will be discussed in Chapter 5.

1.6.4 Anion exchange ionomers performance in fuel cell and electrolyzer

A series of low molecular weight multiblock copoly(arylene ether)s and hydrophilic oligomers with 1 or 2 head-group tethers in each hydrophilic repeat unit based anion conductive ionomers were synthesized and tested in fuel cells and electrolyzers. The ionomers were tested for their viability as anion conductors in the cathodic electrode of fuel cells and as the anodic electrode of an alkaline water electrolyzer. In other words, the ionomers were evaluated in oxygen-consuming (i.e. oxygen reduction reaction (ORR)) and oxygen-producing electrodes (i.e. oxygen evolution reaction (OER)). The relationship between polymer properties (molecular weight, tether amount, and multiblock copolymer vs. homopolymer) and cell performance were systemically studied to find the optimum structure design for ionomer materials. The details will be discussed in Chapter 6.

CHAPTER 2. EXPERIMENTAL METHODS

2.1 Materials

N,N'-dimethylacetamide (DMAc) was obtained from Alfa Aesar and dried by vacuum distillation at 130 °C over CaH_2. Decafluorobiphenyl (DFBP), 4,4'-(hexafluoroisopropylidene)diphenol (HFBPA), 6-bromohexanoyl chloride, $AlCl_3$, 1,2-dichloroethane, triethylsilane, trifluoroacetic acid, and quinuclidine were also obtained from Alfa Aesar. 4,4'-(9-fluorenylidene)diphenol (BPFL) was obtained from TCI Co. Ltd. Potassium carbonate (K_2CO_3) and dichloromethane (DCM) were purchased from BDH chemicals. Tris(2,4,6-trimethoxyphenyl)phosphine and 1-methyl-2-pyrrolidone (NMP) were purchased from Sigma Aldrich. All chemicals were used as received unless otherwise noted.

2.2 Synthesis methods

2.2.1 Synthesis of hydrophobic and hydrophilic oligomers

The synthetic procedure for the hydrophobic oligomer with x = 3.1 repeat units is as follows: DFBP (1.67 g, 5 mmol) and HFBPA (1.68 g, 5 mmol) were dissolved in 20 mL DMAc in a 100 mL three-neck round bottom flask with a condenser under N_2 atmosphere at room temperature. K_2CO_3 (1.66 g, 12 mmol) was added to the solution and then the mixture was heated to 80 ℃ for 1 h. DFBP (0.5 g) was added to the mixture and allowed to react at 40 ℃ for 4 h to ensure that all the oligomers were hydroxyl-terminated. The viscous solution was poured into deionized water to precipitate the product. The white solid was isolated by filtration, washed three times with deionized

water and dried overnight at 80 ℃ in a vacuum oven. Hydrophobic oligomers with a different number of repeat units were synthesized by controlling the reaction time.

Fluoro-terminated hydrophilic oligomer with y = 3.6 repeat units was synthesized via a similar procedure. BPFL (1.75 g, 5 mmol) and DFBP (1.67 g, 5 mmol) were dissolved in 20 mL DMAc under N_2 atmosphere. K_2CO_3 (1.66 g, 12 mmol) was added to the solution and the mixture was reacted at 80 ℃ for 1 h. BPFL (0.6 g) was added to the mixture and reacted at 40 ℃ for 4 h. After precipitation, filtration and drying, a white solid was yielded. Similarly, hydrophilic oligomers with different amount of repeat units were obtained by varying reaction time.

2.2.2 Synthesis of multiblock copoly(arylene ether)s (mPEs)

The hydrophobic oligomer (1.15 g, 0.5 mmol, x = 3.1) and hydrophilic oligomer (1.33 g, 0.5 mmol, y = 3.6) were dissolved in 20 mL DMAc at room temperature under N_2. K_2CO_3 (0.15 g, 1.1 mmol) was added to the solution and the mixture was reacted at 80 ℃ for 4 h. The viscous solution was poured into deionized water and white solid was precipitated out. The product was filtrated, washed with deionized water and dried overnight at 80 ℃ in a vacuum oven.

2.2.3 Synthesis of BrKC6-mPEs (Friedel-Crafts acylation reaction)

The synthesis method of BrKC6-mPEs was modified from literature[41]. Multiblock copolymer mPE-$X_{3.1}Y_{3.6}$ (1.00 g, 0.74 mmol hydrophilic repeat units) was dissolved in 20 mL DCM in a flask under nitrogen atmosphere. The flask was chilled in an ice bath. 6-bromohexanoyl chloride (0.45 mL, 2.96 mmol) and $AlCl_3$ (0.40 g, 2.96 mmol) were added to the solution and warmed to room temperature. The mixture was reacted for 5 h

at room temperature. The solution was poured into 200 mL deionized water and heated to 60 ℃ to evaporate the solvent. The product was dissolved in DCM and precipitated in deionized water three times to obtain a purified light yellow solid.

2.2.4 Synthesis of BrC6-mPEs (reduction reaction)

BrKC6-mPE-$X_{3.1}Y_{3.6}$ (1.14 g, 0.74 mmol hydrophilic repeat units) was dissolved in 20 mL 1,2-dichloroethane in a three-neck round bottom flask with a condenser at room temperature under nitrogen. Trifluoroacetic acid (3.1 mL, 40.7 mmol) and triethylsilane (0.59 mL, 3.7 mmol) were added to the solution. The solution was heated to reflux for 24 h. Then it was cooled to room temperature and poured into a NaOH solution (1.63 g NaOH, 200 mL deionized water). The mixture was heated to 80 ℃ to evaporate the solvent. The product was isolated by filtration. The product was dissolved in DCE and precipitated in deionized water three times producing a white solid product.

2.2.5 Synthesis of multi-tether BrKC6-mPEs and BrC6-mPEs

Multi-tether BrKC6-mPEs and BrC6-mPEs were synthesized via repeated Friedel-Crafts reaction and reduction reaction described in the previous 2.2.3 and 2.2.4 steps.

2.2.6 Membrane casting, then quaternization, and ion exchange of membranes with quaternary ammonium

BrC6-mPEs (0.20 g) was dissolved in 5 mL 1,2-dichloroethane and the resulting solution was filtered through a 0.45 μm poly(tetrafluoroethylene) (PTFE) membrane syringe filter into a 4-cm diameter aluminum dish. The solvent was evaporated in a tube

furnace at 40 ℃ under nitrogen for 18 h. The free-standing membrane was about 40-μm thick.

The membrane with was quaternized as follows: immersion in 45 wt% trimethylamine aqueous solution at room temperature for 48 h. After being removed from the solution, the quaternized membrane with a bromide counter ion was washed with deionized water three times.

The membrane was soaked in 1 M KOH solution under nitrogen for 24 h to exchange the bromide ions for hydroxide ions. After being washed with deionized water three times, the membrane was stored in deionized water.

2.2.7 Quaternization and then casting of membranes with trimethyl quaternary ammonium

0.5 g BrC6-mPEs polymer was soaked in 45% trimethylamine aqueous solution at room temperature for 48 h. After being dried, the polymer was dissolved in 10 mL 1-methyl-2-pyrrolidone (NMP). The solvent was removed by pouring the mixture into a 4-cm diameter aluminum dish to dry in a tube furnace at 40 ℃ under nitrogen for 5 days to obtain the membrane.

2.2.8 Quaternization and then casting of membranes with quaternary quinuclidium

0.5 g BrC6-mPEs polymer was dissolved in 10 mL 1-methyl-2-pyrrolidone (NMP), followed by the addition of quinuclidine (1:1 molar ratio). The reaction mixture was stirred at 60 ℃ for 48 h in an N_2 atmosphere. After reaction, the solvent was

removed by pouring the mixture into a 4-cm diameter aluminum dish to dry in a tube furnace at 40 ℃ under nitrogen for 5 days to obtain the membrane.

2.2.9 Quaternization and then casting of membranes with quaternary phosphonium

0.5 g BrC6-mPEs polymer was dissolved in 10 mL 1-methyl-2-pyrrolidone (NMP), followed by the addition of tris(2,4,6-trimethoxyphenyl)phosphine (1:1 molar ratio). The mixture was reacted at 80 ℃ for 12 h under nitrogen. The mixture was then poured into a 4-cm diameter aluminum dish. The solvent was evaporated in a tube furnace at 40 ℃ under nitrogen for 5 days to obtain the membrane.

2.3 Characterization

2.3.1 Nuclear magnetic resonance (NMR) spectra

The chemical structure of the oligomers and polymers were analyzed by a variety of NMR techniques, including one-dimensional ^{1}H NMR and ^{19}F NMR obtained with a Varian Mercury Vx 400 MHz spectrometer, two-dimensional heteronuclear single quantum coherence (HSQC) and one-dimensional nuclear Overhauser effect (NOE) obtained with a Bruker 500 MHz spectrometer. HSQC and NOE NMR spectra were used to identify the position of the tether attachment on the polymer backbone. Chloroform-*d* was used as the solvent for non-ionic samples and N, N-dimethylformamide-d_7 was used for polar samples. Quantitative ^{19}F NMR spectra were collected at 376.273 MHz with a 12.5 s relaxation delay. The HSQC analysis employed 8 scans, 256 increments along t_1, 1024 data points along t_2, and 145 Hz as one-bond coupling constant. The one-

dimensional NOE spectra were used the DPFGSE-NOE pulse program, a mixing time of 0.2 s, a relaxation delay of 2 s, and an acquisition time of 3.28 s.

2.3.2 Gel permeation chromatography (GPC)

The molecular weight of the polymers was determined by gel permeation chromatography (GPC) (Shimadzu) equipped with an LC-20 AD HPLC pump and a refractive index detector (RID-10 A, 120 V). Tetrahydrofuran (THF) was used as the eluent with at a flow rate of 1.0 mL/min at 35 ℃. The molecular weight was measured by a calibration curve based on polystyrene standards.

2.3.3 Ionic conductivity

The ionic resistance of the membranes was measured with a four-probe, in-plane electrochemical impedance spectrometer over the frequency range from 1 Hz to 1MHz with a PAR 2273 potentiostat. All samples were tested in HPLC-grade water under nitrogen to minimize the effect of CO_2. The samples were equilibrated for 30 min prior to measurement. The in-plane ionic conductivity was calculated using Equation 1.

$$\sigma = \frac{L}{WTR} \tag{1}$$

In Equation 1, σ is the ionic conductivity in S/cm, L is the length between sensing electrodes in cm, W and T are the width and thickness of the membrane in cm, respectively, and R is the resistance measured in ohms.

2.3.4 Ion exchange capacity (IEC)

The ion exchange capacity was calculated by quantitative NMR analysis of the number of tethers with respect to the number of monomer units. We assumed 100% quaternization of the alkyl bromide tether. The IEC was calculated by Equation 2.

$$IEC = \frac{N_{tether} y}{M_b} \quad (2)$$

N_{tether} is the number of tethers attached to each hydrophilic repeat unit, y is the number of repeat units for the hydrophilic block, and M_b is the molecular weight of block copolymer repeat unit for the overall IEC or the molecular weight of hydrophilic block for local IEC.

2.3.5 Water uptake (WU)

The water uptake of the membranes was calculated by Equation 3.

$$\mathrm{WU}(\%) = \frac{M_w - M_d}{M_d} \times 100 \quad (3)$$

In Equation 2, M_d is the dry mass of the membranes measured after being dried in vacuum for 24 h and M_w is the wet mass of the membranes without surface water. Both dry and wet membranes were in the OH^- form and measured at room temperature.

2.3.6 Hydration number (λ)

The number of water molecules per ionic group, hydration number λ, was calculated using Equation 4.

$$\lambda = \frac{1000 \times WU\%}{IEC \times 18} \quad (4)$$

2.3.7 Number of freezable water (N_{free}) and bound, non-freezable water (N_{bound}) molecules

The number of freezable water (N_{free}) and bound water (or non-freezable water) (N_{bound}) were determined by differential scanning calorimetry (DSC). DSC measurements were carried out on a DSC Q200 (TA Instruments). The membrane samples were fully-hydrated by soaking in deionized water at least for one week. After the water on the membrane surface was wiped off, a 3 to 5 mg sample was quickly sealed in an aluminum pan. The sample was cooled to -50 ℃ and heated at a rate of 5 ℃/min under N_2 (20 mL/min). The quantity of freezable and non-freezable water was determined by Equations 5 to 7[60-62].

$$N_{free} = \frac{M_{free}}{M_{tot}} \times \lambda \tag{5}$$

M_{free} is the mass of freezable water and M_{tot} is the total mass of water absorbed in the membrane. The weight fraction of freezable water was calculated by Equation 6.

$$\frac{M_{free}}{M_{tot}} = \frac{H_f / H_{ice}}{(M_W - M_d)/M_w} \tag{6}$$

H_f is enthalpy obtained by the integration of the DSC freezing peak and H_{ice} is enthalpy of fusion for water, corrected for the subzero freezing point according to Equation 7.

$$H_{ice} = H_{ice}^{o} - \Delta C_p \Delta T_f \tag{7}$$

ΔC_p is the difference between the specific heat capacity of liquid water and ice. ΔT_f is the freezing point depression.

2.3.8 Morphological characterization

Small angle X-ray scattering (SAXS) was used to analyze the morphology of AEMs. Dry membranes in Br^- form were tested in a Malvern Panalytical Empyrean XRD (Netherlands) with a Pixel 3D detector. The scattering experiments were performed using Cu Kα radiation with a wavelength (l) of 1.542 Å generated within a high brilliance micro focus sealed tube with shaped multilayer optics operating at 45 kV and 40 Ma. The wave vector (q) was calculated as:

$$q = \frac{4\pi}{l \sin 2\theta} \tag{8}$$

where 2θ is the scattering angle. The characteristic separation length (d) (i.e. the Bragg spacing) was calculated as:

$$d = \frac{2\pi}{q} \tag{9}$$

The surface morphology of the membranes was analyzed by tapping mode atomic force microscopy (AFM) with an Asylum Research instrument. The probe (AC240TM-R3, Olympus) with a cantilever spring constant of 1.5 N/m was used to take images of the samples at ambient temperature and 50% relative humidity. The Amp InvOLS was 109 nm/V. The scanning frequency was 1 Hz. The measurements were conducted under the same conditions for each sample to keep consistency.

Transmission electron microscopy (TEM) was also used to analyze the morphology of the membranes. TEM was performed on a JEOL JEM-1400 Transmission Electron Microscope. The membranes in bromide ion form were stained with osmium tetroxide at room temperature prior to examination. The stained membranes were

embedded within an epoxy resin, sectioned into approximately 50 nm thick samples with a Leica UC6rt Ultramicrotome, and placed on copper grids for observation.

2.3.9 Thermal stability

Thermal stability of the hydroxide form of the membranes was analyzed by thermogravimetric analysis (TGA) on a TA Instruments Q50 analyzer. The thermal degradation was evaluated at a heating rate of 5 ℃/min up to 800 ℃ in nitrogen.

2.3.10 Mechanical properties

The stress-strain relationship was investigated by dynamic mechanical analysis (DMA) using TA Instruments Q800 with controlled force mode. Rectangular membrane samples were fully hydrated and tested using tension clamps after removing surface water at 100% relative humidity. The experimental parameters were set as: preload force 0.05 N, isothermal at 30 ℃, soak time 1 min, force ramp rate 0.5 N/min and upper force limit up to 18 N[36].

2.3.11 Alkaline stability

The alkaline stability of the membranes was evaluated by soaking the OH^- form membranes into 1 M NaOH in a Teflon lined Parr reactor at 60˚C for up to 1000 h to measure the changes in ionic conductivity. Before measurement, each membrane was thoroughly washed with deionized water. The ionic conductivity was determined in HPLC-grade water at room temperature.

2.3.12 Oxygen solubility, diffusivity and permeability

The oxygen transport properties, including solubility, diffusivity and permeability, were measured using an intelligent gravimetric analyzer by Hiden Analytical Ltd. (IGA-1). A membrane sample was placed in the chamber which was then evacuated for 24 h. Oxygen gas was introduced into the chamber in step increments of 250 mbar from vacuum to 1 bar. At each step, the mass was recorded until equilibrium was reached at each pressure to give the amount of oxygen absorbed by the sample at a given pressure. The oxygen solubility S (mass % per bar) of the membrane was calculated by the weight percent increase from vacuum to 1 bar oxygen pressure. The mass vs. time data for the step from vacuum to 250 mbar was used to estimate the oxygen diffusion coefficient, or diffusivity D (cm^2/s), in the membrane according to Equation 10.

$$\frac{M_t}{M_\infty} = \frac{2}{l}\left(\frac{D}{\pi}\right)^{\frac{1}{2}} t^{\frac{1}{2}} \tag{10}$$

M_t is the mass of the membrane and absorbed oxygen at time t, M_∞ is the mass at equilibrium and l is half of the thickness of the membrane in cm. The oxygen permeability, P, in mol/(bar·cm·s) was calculated by Equation 11.

$$P = \rho \frac{S}{M_{oxygen}} D \tag{11}$$

ρ is the density of the membrane (g/cm^3), which was measured by pycnometer to be 1.1 g/cm^3, and M_{oxygen} is the molecular weight of oxygen.

CHAPTER 3. SYNTHESIS AND CHARATERIZATION OF ANION CONDUCTING MULTIBLOCK COPOLYMER WITH PARTIAL FLUORONATION AND LONG HEAD-GROUP TETHERS

3.1 Introduction and objectives

Anion exchange membranes with high ionic conductivity, low water uptake, and excellent mechanical and chemical stability are needed for the electrochemical devices, such as fuel cells and electrolyzers.[2] In order to achieve these goals, a series anion conductive polymers composed of partially fluorinated multiblock copoly(arylene ether)s (mPEs) with long head-group tethers were designed, synthesized and characterized in this work. The multiblock copolymer structure was designed to utilize its nanophase segregation to form ion-conductive nano-channels to improve the ionic conductivity. Partial fluorination of the polymer backbone was used to reduce the water uptake of the membrane due to its high hydrophobicity. This design also targeted to improve the chemical stability by keep hydroxide ions away from the polymer backbone. The long alkyl chain as the head-group tether was designed to improve the alkaline stability by reducing the hydroxide ion attach of the ionic groups.

In this work, multiblock copoly(arylene ether)s (mPEs) with partial fluorination and long head-group tethers were synthesized via polycondensation reaction, Friedel-Crafts acylation reaction, reduction reaction, and quaternization. To our knowledge, this is the first time the long alkyl spacer structure was combined with multiblock copolymer backbone in AEM materials. Different hydrophobic and hydrophilic block lengths

containing one or two tethers per hydrophilic repeat unit were prepared. The size of the ion conductive nano-channels, ionic conductivity, water uptake, and the number of freezable water and bound water molecules per head-group were evaluated. The comparison is intended to help understand the relationship between structure, morphology and physical properties. The properties of multiblock copolymer membranes and pure hydrophilic oligomer were also compared. In addition, the oxygen solubility, diffusivity and permeability of the membranes were analyzed.

3.2 Results and discussion

3.2.1 Synthesis of anion conductive multiblock copolymer with long alkyl tethers

The synthesis route is shown in Figure 3.1. The multiblock copoly(arylene ether)s (mPEs) backbone was synthesized via polycondensation reaction of individually prepared hydroxyl-terminated hydrophobic oligomers (X) and fluorine-terminated hydrophilic oligomers (Y). The long tethers connecting the ionic head-groups to the polymer backbone were attached to mPEs backbone via Friedel-Crafts acylation reaction with 6-bromohexanoyl chloride and $AlCl_3$. It was found that only one tether was attached per hydrophilic repeat unit in BrKC6-mPEs, even though there was excess 6-bromohexanoyl chloride reactant during the Friedel-Crafts reaction. This is due to the strong electron-withdrawing effect of the ketone group within the tether, which reduced the reactivity of the aromatic rings. The ketone groups of side chains in BrKC6-mPEs were reduced to methylene groups by triethylsilane to produce BrC6-mPEs for better alkaline stability. After the ketone groups were reduced to methylene groups, the electron-withdrawing effect of the tether was eliminated and the aromatic rings were again susceptible to the

Friedel-Crafts acylation reaction. A second tether was attached on each hydrophilic repeat unit via Friedel-Crafts reaction and reduction reaction to synthesize two-tether 2BrC6-mPEs. The reduction reaction products BrC6-mPEs and 2BrC6-mPEs were then quaternized by trimethylamine (TMA) with bromide counter ion. After soaking in NaOH solution, the bromide counter ions were exchanged with hydroxide ions. A series of multiblock copoly(arylene ether)s with different hydrophilic and hydrophobic block lengths and one or two tethers for ionic exchange groups were synthesized.

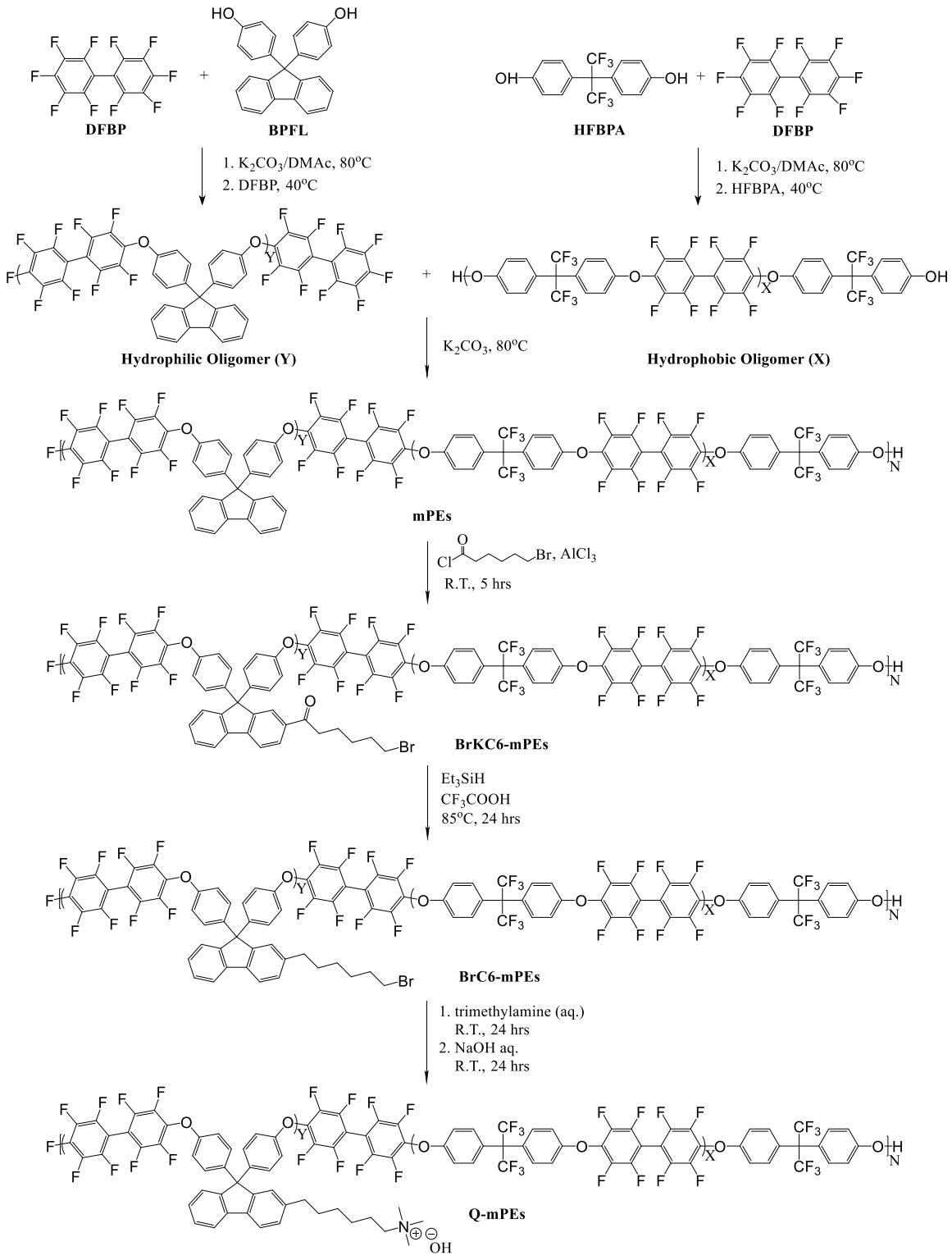

Figure 3.1 Synthesis of multiblock copoly(arylene ether)s with long alkyl tethers for ionic head-groups.

3.2.2 Structural analysis

The chemical structure of the oligomers and polymers were analyzed by a variety of NMR techniques, including one-dimensional ^{1}H NMR and ^{19}F NMR, two-dimensional heteronuclear single quantum coherence (HSQC) and one-dimensional nuclear Overhauser effect (NOE).

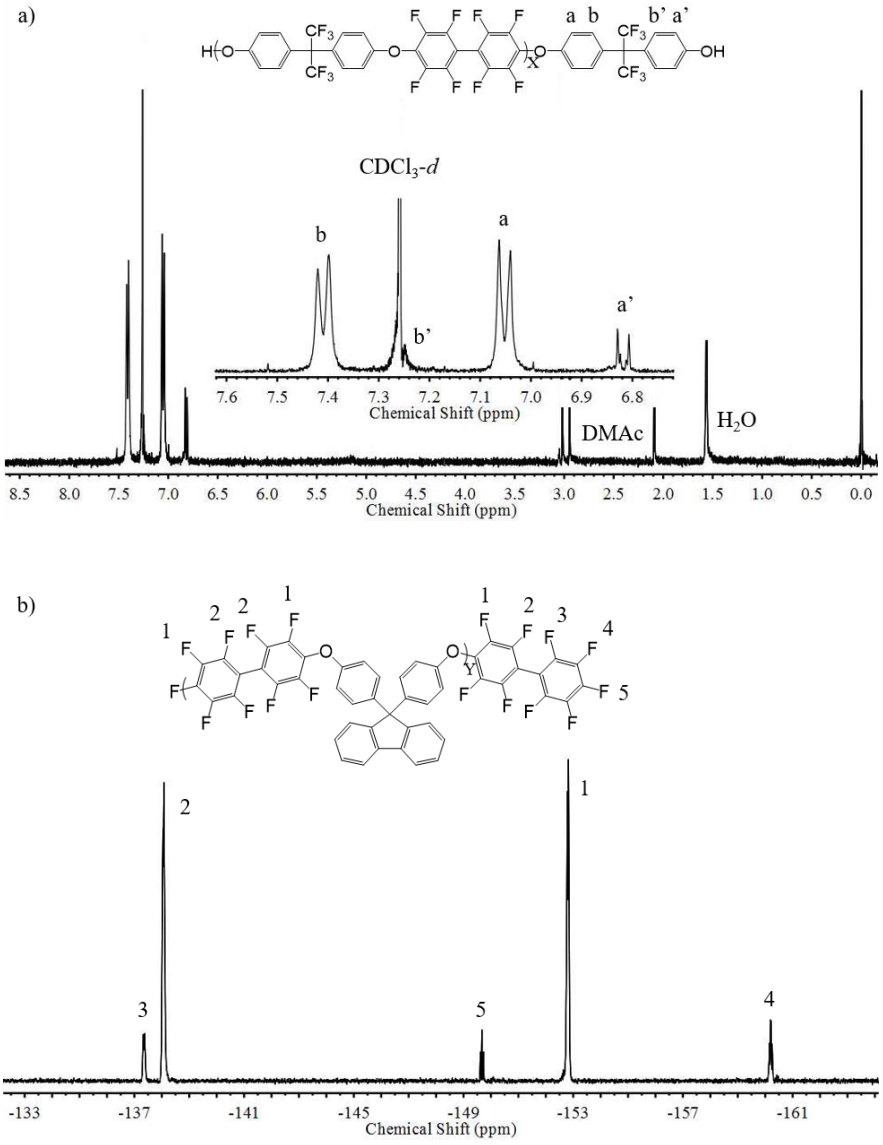

Figure 3.2 (a) ^{1}H NMR spectrum of OH-terminated hydrophobic oligomer, and (b) ^{19}F NMR spectrum of F-terminated hydrophilic oligomer.

The number of repeat units (x) of the hydroxyl-terminated hydrophobic oligomers was calculated according to the ratio of the integration of peaks a and a' in the ^{1}H NMR spectra shown in Figure 3.2(a). Similarly, the length of F-terminated hydrophilic oligomers (y) was determined by the ratio of peak 2 and 3 shown in Figure 3.2(b). The F-terminated oligomers were converted into ion conducting hydrophilic blocks after attachment of the long tether and ionic head-groups. The hydrophobic and hydrophilic block lengths were summarized in Table 3.1.

Table 3.1 Structural characteristics of mPEs multiblock copolymers.

[a]Multiblock copolymer	[b]x	[c]y	[d]N	[e]M_n	[f]PDI
H-1	/	8	/	18K	1.81
$X_{3.1}Y_{3.6}$	3.1	3.6	18.0	88.6K	2.27
$X_{5.4}Y_{7}$	5.4	7	8.0	68.2K	1.97
$X_{3.1}Y_{8}$	3.1	8	7.2	55.9K	1.83
$X_{5.9}Y_{5}$	5.9	5	7.8	59.0K	2.22

[a]H-1: pure hydrophilic oligomer; [a]X: hydrophobic blocks; [a]Y: hydrophilic blocks; [b]x: number of repeat units in hydrophobic blocks; [c]y: number of repeat units in hydrophilic blocks; [d]N: number of repeat units in block copolymer; [e]M_n: number-average molecular weight from GPC; [f]PDI: polydispersity index.

The number-average molecular weight (M_n) and polydispersity (PDI) of mPEs were obtained by gel permeation chromatography (GPC), as shown in Table 3.1. The target molecular weight of mPEs was >50 kg/mol in order to obtain stable, free-standing, solvent-cast membranes.

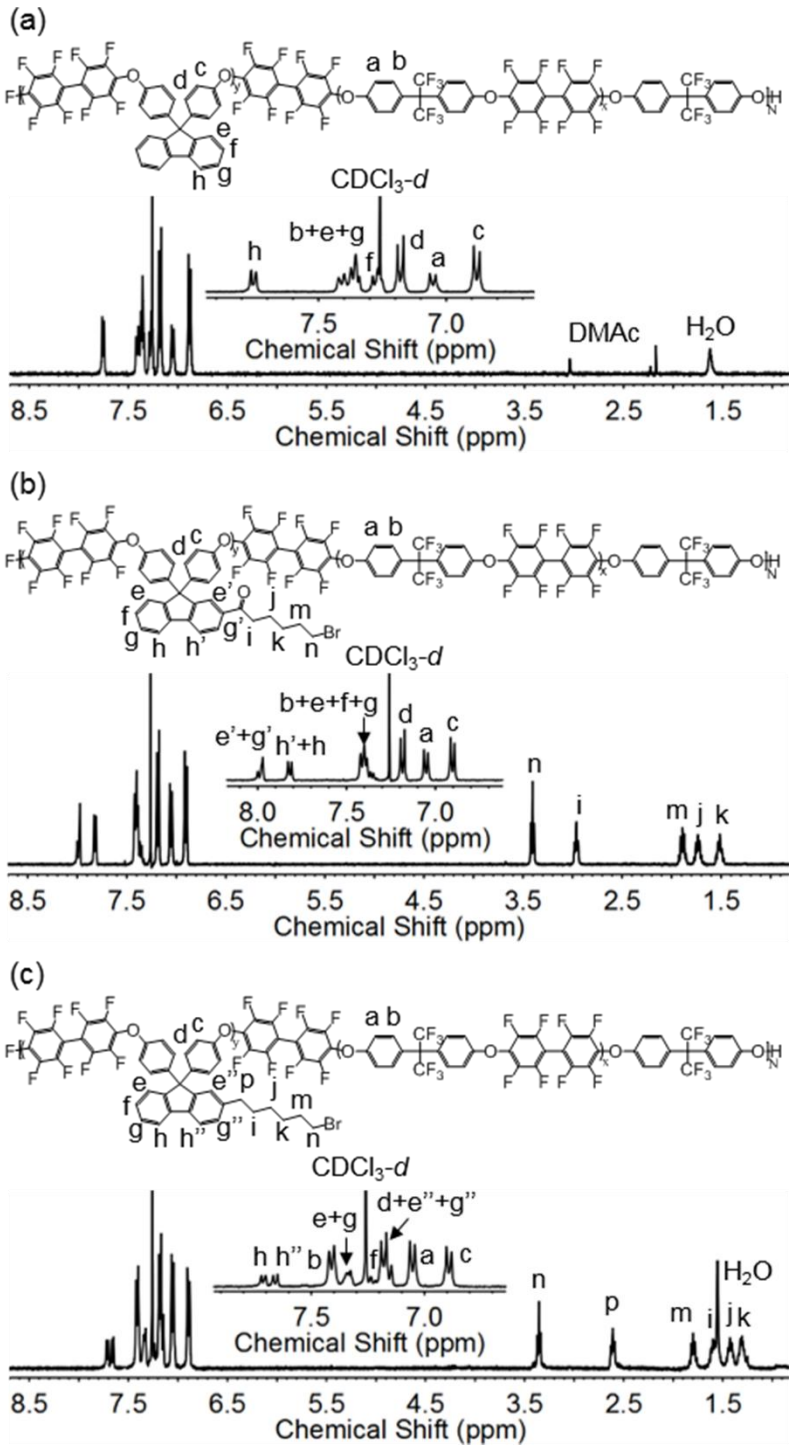

Figure 3.3 ^{1}H NMR spectra of (a) multiblock copolymer mPEs, (b) BrKC6-mPEs, and (c) BrC6-mPEs.

The long tethers connecting the ionic head-groups to the polymer backbone were attached to mPEs backbones via a Friedel-Crafts acylation reaction with 6-bromohexanoyl chloride and $AlCl_3$. The successful attachment of the tethers was confirmed by the ^1H NMR spectrum of the acylation product BrKC6-mPEs, as shown in Figure 3.3(b). A new peak i at 2.95 ppm appeared after acylation compared to the ^1H NMR spectrum of mPEs backbone structure, as shown in Figure 3.3(a). The new peak is attributed to methylene protons adjacent to benzyl carbonyl group. The appearance of the new peak at 7.95 ppm, the shift of peak h from 7.77 ppm to 7.81 ppm, and the disappearance of peak f at 7.28 ppm also confirmed the successful acylation reaction.

Since there was no change in the peak positions and peak areas for the aryl protons a, b, c, and d in Figure 3.3(a) and 3.3(b), these sites are not possible locations for attachment of the tether. Due to the strong electron-withdrawing effect of the trifluoromethyl groups, the aryl protons a and b adjacent to them are unfavorable sites for the Friedel-Crafts reaction. This was shown separately by the unsuccessful Friedel-Crafts acylation of the pure hydrophobic oligomers. Aryl protons c and d on the hydrophilic blocks are sterically hindered. In addition, they are deactivated by the electron-withdrawing effect of fluorine atoms on DFBP monomers.

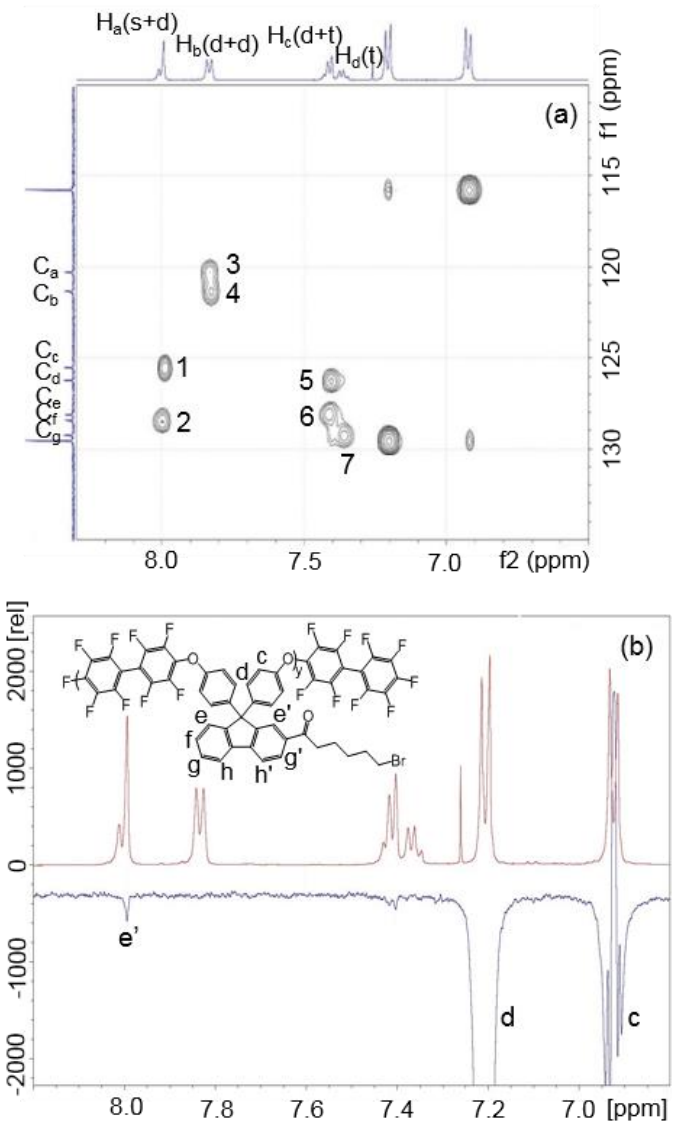

Figure 3.4 (a) Two-dimensional HSQC, and (b) one-dimensional NOE NMR spectra.

Thus, the tethers could only be attached at sites e, f, g or h on the backbone, shown in Figure 3.3(a). Two-dimensional HSQC and one-dimensional NOE NMR spectra, as shown in Figure 3.4(a) and 3.4(b), respectively, were used to identify the location of the tether attachment. In order to simplify the experiment, the hydrophilic oligomer with one tether after Friedel-Crafts reaction was used as the sample.

In the HSQC spectrum, the cross peaks show the coupling of carbon and proton bonded nuclei. Cross peaks 1 and 2 show that the corresponding protons H_a were linked to two different carbons C_c and C_f. Thus, the peaks for these protons in the ^1H NMR spectrum are an overlapping peak composed of a singlet and a doublet peak. Similarly, cross peaks 3 and 4 show that the peaks of the corresponding protons H_b in the ^1H NMR spectrum are composed of two overlapping doublet peaks. The protons H_c for cross peaks 5 and 6 were linked to carbon C_d and C_e, and show a doublet and triplet overlapped peak. The proton corresponding to cross peak 7 is a singlet peak and only linked to carbon C_g. There are two possible locations for the tether attachment which could show this set of peaks in the ^1H NMR spectrum: f or g site.

In order to further identify the tether attachment location, f or g, the one-dimensional NOE spectrum, which identifies spatially close atom pairs, was obtained. In Figure 3.4(b), the upper trace is the ^1H NMR spectrum of the aromatic protons of one-tether hydrophilic oligomer, and the lower trace is the corresponding NOE difference spectrum obtained from irradiation of proton d at 7.23 ppm. It shows that NOE can be seen between the proton of a singlet peak at 7.98 ppm and proton d, which means that these protons have spatial proximity. This proves that the Friedel-Crafts reaction occurred at the f site instead of the g site. The resulting singlet peak is attributed to aryl proton e' formed at the expense of the proton at f due to the attachment of tethers. The attachment at g site cannot result in the observed singlet peak.

The number of tethers attached to each monomer was calculated from the ratio of the integrated peaks i and the sum of the aromatic protons, shown in Figure 3.3(b). It was found that only one tether was attached per hydrophilic repeat unit, even though there

was excess 6-bromohexanoyl chloride reactant during the Friedel-Crafts reaction. This is due to the strong electron-withdrawing effect of the ketone group within the tether, which reduced the reactivity of aromatic rings.

As suggested by Hibbs[41], protons in the α-position of ketones are known to be acidic due to the formation of enolate ions, so the α-protons on the side chains might lead to degradation reactions under alkaline conditions. It was also shown that the corresponding reduction product was more stable in the alkaline stability test. The ketone groups of sidechains in BrKC6-mPEs were reduced by triethylsilane to methylene groups for better alkaline stability. The appearance of peak p (2.60 ppm), assigned to the methylene group adjacent to aromatic ring, and the shift of peak i, assigned to the α-protons, from 2.95 ppm to 1.60 ppm, in Figure 3.3(c) were clear evidence for the reduction of the ketone on the tether.

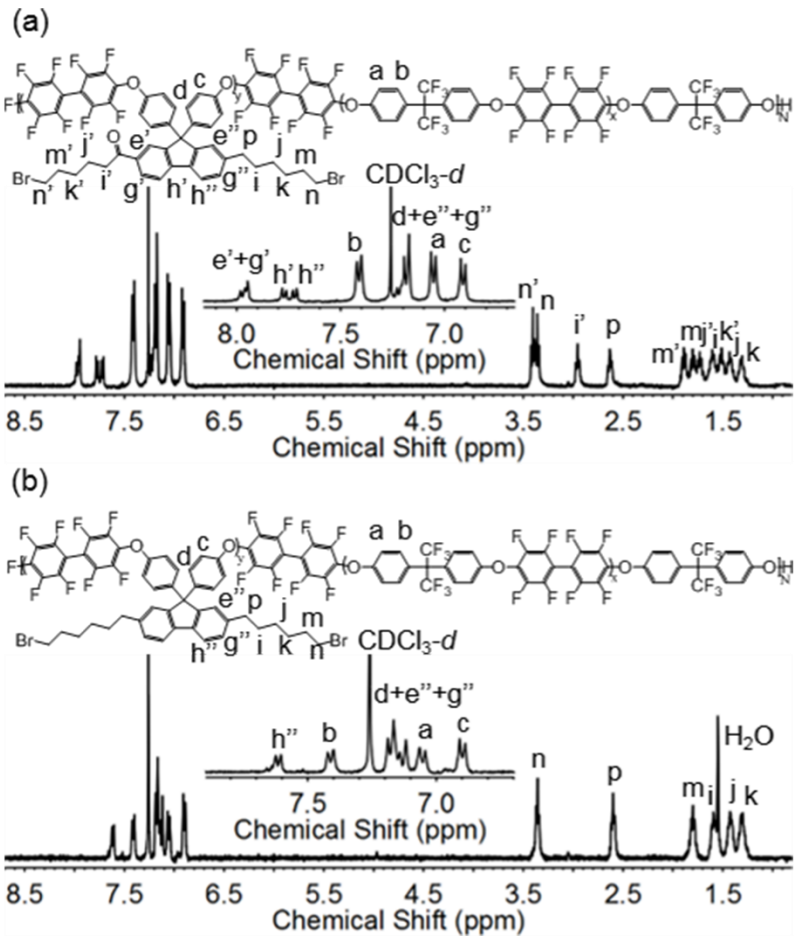

Figure 3.5 ^{1}H NMR spectra of (a) BrKC6-BrC6-mPEs, and (b) 2BrC6-mPEs.

After the ketone groups were reduced to methylene groups, the electron-withdrawing effect of the tether was eliminated and the aromatic rings were again susceptible to the Friedel-Crafts acylation reaction. Figure 3.5(a) and 3.5(b) show the ^{1}H NMR spectra of the Friedel-Crafts reaction product with new tethers, BrKC6-BrC6-mPEs, and the corresponding reduction product 2BrC6-mPEs, respectively. In Figure 3.5(a), the 1:1 ratio of the integration of peak areas of peak i', assigned to the new methylene group adjacent to benzyl ketone group, and peak p shows that a second tether was attached to the hydrophilic oligomer repeat unit on the remaining f site.

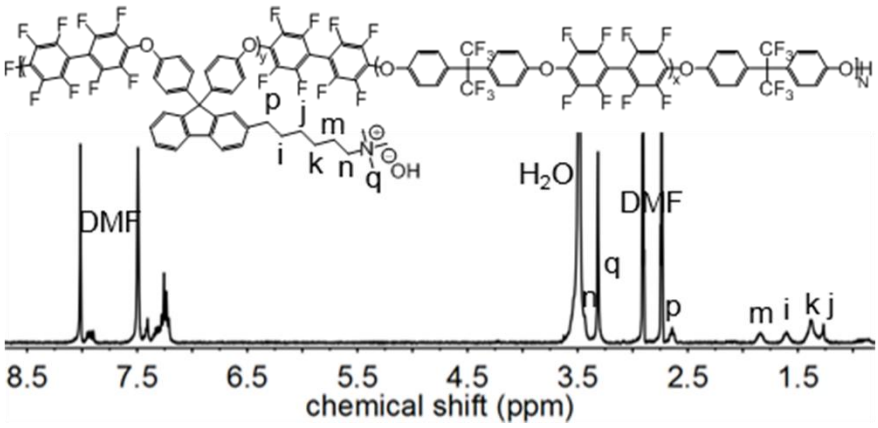

Figure 3.6 ^{1}H NMR spectrum of Q-mPEs.

The one-tether BrC6-mPEs and two-tether 2BrC6-mPEs were quaternized by reaction with trimethylamine (TMA). Figure 3.6 shows the ^{1}H NMR spectra of the quaternized multiblock copolymer Q-mPEs with one tether. The appearance of peak q, assigned to methyl groups of trimethyl quaternary ammonium ions, confirms the successful quaternization reaction. In addition, the 9:2 ratio of peak q to peak p (protons of methylene groups on the tether) shows that the methylene bromide was fully quaternized.

3.2.3 Morphology

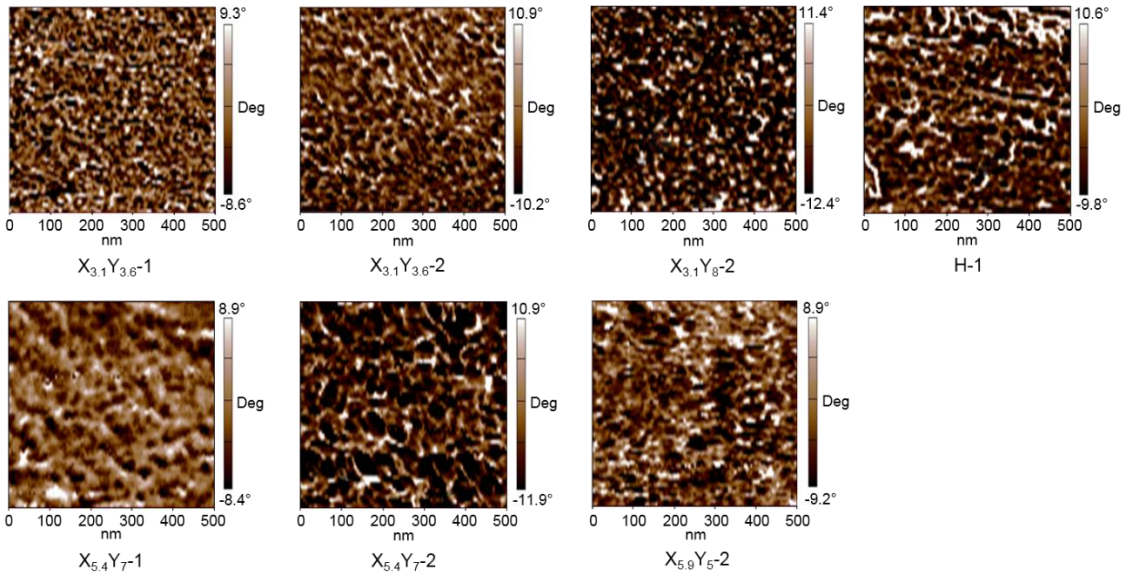

Figure 3.7 AFM phase images of mPEs membranes.

AFM phase images of the membranes (500 × 500 nm) were obtained for morphology analysis. Hydrophilic-hydrophobic phase separation was found for all multiblock copolymer membranes. Each had a different domain size and size distribution, as shown in Figure 3.7 The dark regions correspond to the hydrophilic domains and the bright regions correspond to the hydrophobic domains.[43, 52] The hydrophilic domains formed contiguous ion conductive nano-channels for ion transport. The resulting properties of the membranes, such as ionic conductivity and water uptake, were the result of the ion-channel size, density, and mobility of anions within the channels. The properties are summarized in Table 3.2. The sizes of the ionic channels were measured to be in the range of 7.8 to 22.5 nm. This channel size was determined by the length of the hydrophobic and hydrophilic blocks, tether size and number, and microstructure of the membrane. For example, mPE-$X_{3.1}Y_{3.6}$-1 and mPE-$X_{3.1}Y_{3.6}$-2 had the same backbone

structure with one and two tethers per monomer unit, respectively. The more tethers in mPE-$X_{3.1}Y_{3.6}$-2 resulted in a larger channel size. The channel size of mPE-$X_{3.1}Y_{8}$-2 was even larger, because it had a longer hydrophilic block. In addition, the pure hydrophilic oligomer based membrane, H-1, also showed a certain degree of phase segregation. However, the multiblock copolymer membranes consistently had a more uniform distribution of channel sizes.

3.2.4 Properties

3.2.4.1 Ion exchange capacity (IEC) and ionic conductivity

Table 3.2 Channel size, IEC, ionic conductivity, water uptake, hydration number, N_{free} and N_{bound} of mPEs membranes.

[a]Membrane	[b]Channel Size (nm)	[c]Overall IEC (meq/g)	[d]Local IEC (meq/g)	[e]Ionic conductivity (mS/cm)		[f]Water uptake (%)	Hydration number, λ	N_{free}	N_{bound}
				R. T.	80 °C				
H-1	16.5 ± 3.9	1.25	1.25	13.1	36.1	35.9	16.9	5.1	11.7
$X_{3.1}Y_{3.6}$-1	7.8 ± 1.2	0.66	1.25	16.4	51.5	5.6	4.7	0.2	4.5
$X_{5.4}Y_{7}$-1	9.7 ± 1.6	0.73	1.25	14.1	34.7	8.0	6.1	0.5	5.6
$X_{5.4}Y_{7}$-2	22.5 ± 2.9	1.30	2.08	38.2	119.7	50.8	21.7	11.9	9.8
$X_{3.1}Y_{8}$-2	15.3 ± 1.3	1.56	2.08	23.1	94.0	26.7	9.5	0.6	8.9
$X_{3.1}Y_{3.6}$-2	12.2 ± 1.4	1.19	2.08	25.8	85.0	25.0	11.7	1.8	9.9
$X_{5.9}Y_{5}$-2	11.3 ± 1.9	1.10	2.08	22.1	66.7	19.6	9.9	0.5	9.4

[a]1, 2: the number of tethers on each hydrophilic repeat unit; [b]Channel size: calculated by the average size measured on AFM phase image; [c]Overall IEC: with respect to the multiblock copolymer; [d]Local IEC: with respect to the hydrophilic block; [e]Ionic conductivity: tested in hydroxide ion form; [f]Water uptake: measured at room temperature in hydroxide ion form.

The overall IEC was calculated based on the multiblock copolymer, while the local IEC was calculated corresponding to hydrophilic blocks. As shown in Table 3.2, the

local IEC in the hydrophilic block was the same for each of the one-tether or two-tether mPEs copolymers. The introduction of hydrophobic blocks results in the overall IEC lower than the local IEC. The IEC was higher for two-tether block copolymer than one-tether ones with the same backbone structure. For example, the IEC of mPE-$X_{5.4}Y_7$-2 was higher than mPE-$X_{5.4}Y_7$-1, because each tether had an ionic head-group.

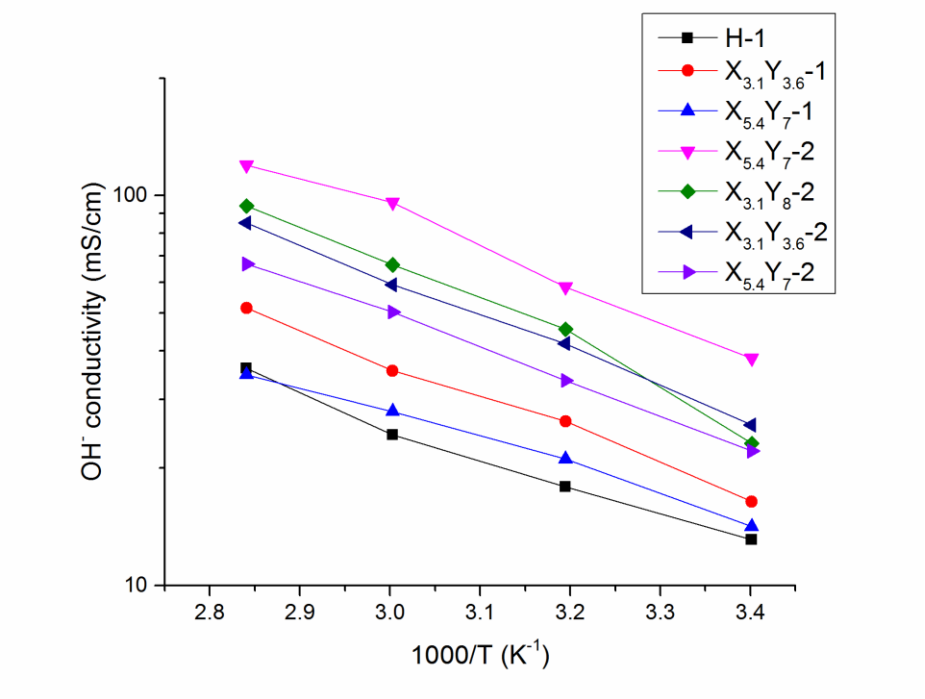

Figure 3.8 Arrhenius plot of ionic conductivity vs. inverse temperature.

Figure 3.8 shows the hydroxide conductivity of the membranes from 20 to 80 ℃. Generally, the ionic conductivity increases with temperature and follows an Arrhenius relationship. The slope of the Arrhenius plot corresponds to the activation energy for ionic conductivity. The mPE membranes shows a similar activation value, about 16 to 17 kJ/mol. Typically, the ionic conductivity increased with IEC.[9] With the same backbone

structure, mPE-$X_{5.4}Y_7$-2 showed higher ionic conductivity than mPE-$X_{5.4}Y_7$-1, because mPE-$X_{5.4}Y_7$-2 had a higher IEC. In addition, it is noted that the ionic conductivity of mPE-$X_{5.4}Y_7$-2 was more than twice of that of mPE-$X_{5.4}Y_7$-1, even though the number of head-groups of mPE-$X_{5.4}Y_7$-2 only doubled. This demonstrates a non-linear relationship between the number of head groups and ionic conductivity. With more head groups on the same backbone, the multiblock copolymer formed larger nano-channels for ion transport, resulting in higher ionic conductivity. However, even with the same number of head-groups per hydrophilic repeat unit, the mPEs multiblock copolymers had different ionic conductivities. This is because the mPEs multiblock copolymers formed different size nano-channels for ion transport due to the different size of the phases caused by the different ratio of hydrophobic to hydrophilic block lengths. For example, the multiblock copolymer membrane mPE-$X_{3.1}Y_{3.6}$-1 had a lower IEC than that of pure hydrophilic polymer based H-1, but higher ionic conductivity, which shows the efficiency of conductive nano-channels for ion transport. For all tested mPEs membranes, the larger the ion transport channel size in the multiblock copolymer, the higher the resulting ion conductivity. The mPE-$X_{5.4}Y_7$-2 had the highest ionic conductivity, up to 119 mS/cm at 80 ℃, however, not the highest IEC. This did not follow the typical relationship between IEC and ionic conductivity for random copolymers. In multiblock copolymers, the ion mobility within the channels also greatly affects the ionic conductivity. In other words, the optimum polymer structure will optimize the size of ion channels and mobility of hydroxide within the channel.

3.2.4.2 Water uptake (WU), hydration number (λ), number of freezable water molecules (N_{free}) and bound water molecules (N_{bound})

Water uptake is an important property for AEMs. AEMs need to maintain a certain amount of water for ion hydration and transport. However, excess, unbound water is not productive and swells the membrane, leading to poor performance of the membrane electrode assembly (MEA) and flooding of the ion conductive channels. In order to reduce the WU of AEMs, a fluorinated backbone was used in the mPEs multiblock copolymer to introduce greater hydrophobicity. The water uptake of the multiblock copolymer membranes, shown in Table 3.2, was less than the corresponding pure hydrophilic polymer. For example, H-1 had 35.9% WU and mPE-$X_{3.1}Y_{3.6}$-1 had much lower value of 5.6%. Similar to ionic conductivity, water uptake of mPEs membranes was affected by both the IEC and nano-channel size: higher IEC led to higher WU, and excessively large channels led to excessive WU. The proper channel size was important to acquire optimized WU. The two-tether mPEs membranes had higher WU than the one-tether membranes. The mPEs membranes with the same number of tethers showed different WU due to different ion conductive channel sizes.

The hydration number is the number of water molecules per ionic head-group (cation/anion pair). As shown in Table 3.2, multiblock copolymers had lower hydration numbers than the hydrophilic polymer H-1, except mPE-$X_{5.4}Y_{7}$-2, which shows that the efficiency of water utilization in the multiblock copolymer membrane for ion transport was higher. In other words, the multiblock copolymer membranes could efficiently utilize water in ion transport due to the well-developed nanophase separation. The reason for the

high hydration number of mPE-$X_{5.4}Y_7$-2 was that the ion conductive channel size was too large, which resulted in higher WU and more free water.

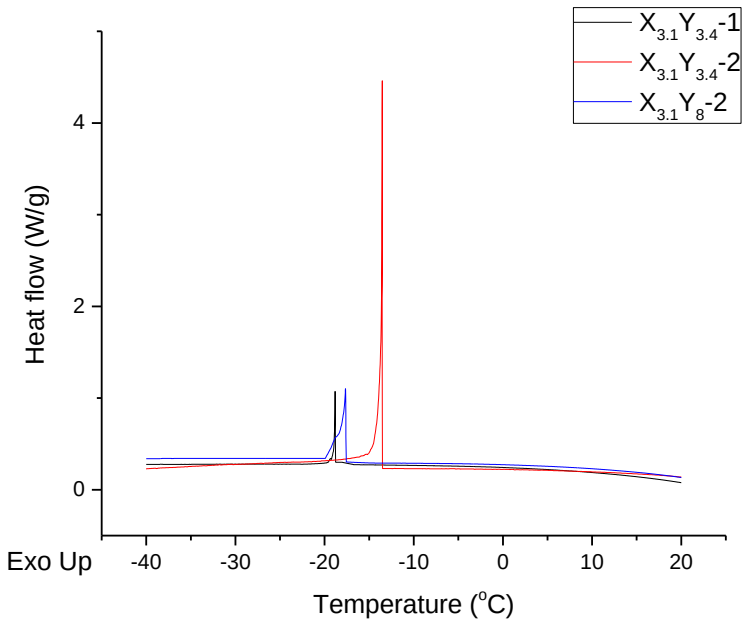

Figure 3.9 DSC thermograms of selected mPEs membranes.

To gain a deeper insight into water mobility and its effect on ion transport in AEMs, the state of water in the membranes, freezable and bound water (or non-freezable water), was investigated by DSC. Non-freezable water is bound to an ion or polar polymer segment and shows no characteristic thermal transition in DSC. Freezable water is associated with ion exchanges and frozen at subzero temperatures. Figure 3.9 shows the DSC thermograms of selected mPEs membranes. The integral of the freezing peak increased as water uptake increased, which suggests that the amount of freezable water increases. It was also observed that the higher water uptake lead to the lower freezing temperature depression, which implies that the excess freezable water molecules reduce the association of water to ionic exchange groups.

The sum of the numbers of freezable water and non-freezable water is the hydration number. The number of freezable water molecules (N_{free}) and non-freezable water molecules (N_{bound}) per head-group (or cation-hydroxide ion pear) are summarized in Table 3.2. It shows that all the two-tether multiblock copolymer mPEs had a similar amount of bound water, 9 to 10, per ionic pair, or 4.5 to 5 bound water per cation or anion, regardless of overall WU. The difference in hydration number was due to the presence of free, unbound water, in addition to the bound water of ion hydration. The number of bound water molecules per head-group for the one-tether mPEs membrane was lower because the ion conductive nano-channel size was small, which limited the water absorption and mobility in the membrane. Excess, unbound water could lead to flooding of the ion conductive channels, which reduces the efficiency of ion transport. As shown, the membranes could still maintain high ionic conductivity even with little freezable, unbound water, such as with mPE-$X_{3.1}Y_{8}$-2 and mPE-$X_{3.1}Y_{3.6}$-2. This implies that the dominant ion transport occurs close to the ion exchange groups through the assistance of non-freezable, bound water on the ions.

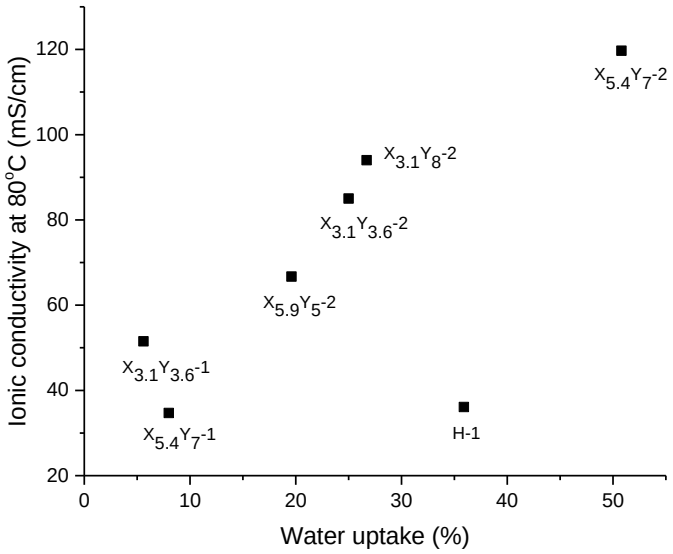

Figure 3.10 Relationship of ionic conductivity at 80 ℃ and water uptake of mPEs membranes.

Figure 3.10 shows the relationship between ionic conductivity and WU for mPEs membranes. It is desirable to have sufficient bound water for ion hydration and transport without excess, unbound water, the upper left region of Figure 3.10. Among all mPEs membranes, mPE-$X_{5.4}Y_7$-2 had the highest ionic conductivity, 119.7 mS/cm at 80 ℃, but relatively high water uptake, 50.8%. Although this value of WU is not excessive, it shows there were 11.9 unbound water molecules per head-group. There were only 9.8 water molecules per head-group needed for hydration. The reason for the excess free water was the large size of the nano-channels. Membrane mPE-$X_{3.1}Y_8$-2 had lower water uptake, 26.7%, and high ionic conductivity up to 94.0 mS/cm at 80 ℃. There were 8.9 bound water molecules per head-group, about the same as that for mPE-$X_{5.4}Y_7$-2, however, it had virtually no free water, only 0.6 water molecules per anion/cation pair. This is due to the optimized size of the nano-channels. In comparison, the pure hydrophilic polymer, H-

1 membrane, showed low ionic conductivity and high water uptake, which is in the lower right region in Figure 3.10. This is due to the lack of ion-channel formation and inefficient use of the ionic head-groups. Thus, phase segregation within the multiblock copolymer was beneficial to the improvement in ion conductivity and reduced WU.

3.2.4.3 Chemical, thermal and mechanical stability

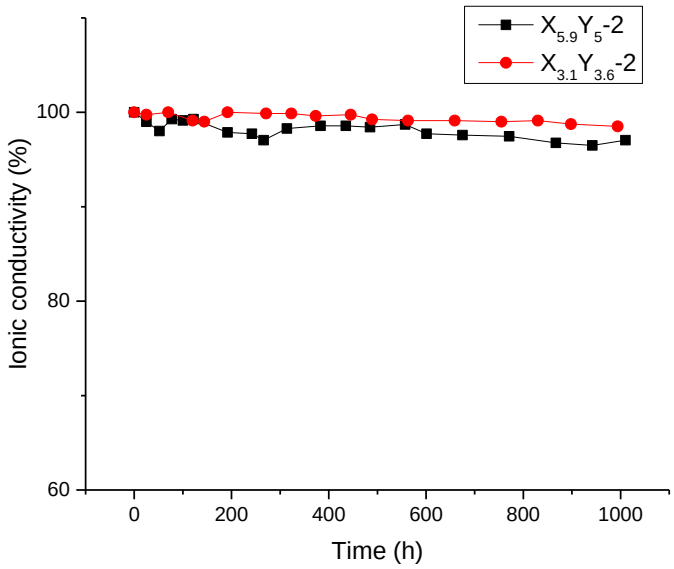

Figure 3.11 Alkaline stability of the mPEs membranes in 1 M NaOH solution at 60 ℃.

Long-term alkaline stability of AEMs is of great importance for fuel cell applications. The mPEs membranes with long tethers showed outstanding alkaline stability in strong alkaline solutions. The alkaline stability of mPE-$X_{3.1}Y_{3.4}$-2 and mPE-$X_{5.9}Y_5$-2 membranes were evaluated by the ionic conductivity loss in 1M NaOH solution at 60 ℃. As shown in Figure 3.11, nearly no change in ionic conductivity was observed after 1000 hours. The ionic conductivity loss of mPE-$X_{3.1}Y_{3.4}$-2 and mPE-$X_{5.9}Y_5$-2 were

1.2% and 3.0%, respectively. This result confirmed that long alkyl tether for quaternary ammonium ionic exchange groups greatly improved the alkaline stability.[27, 29]

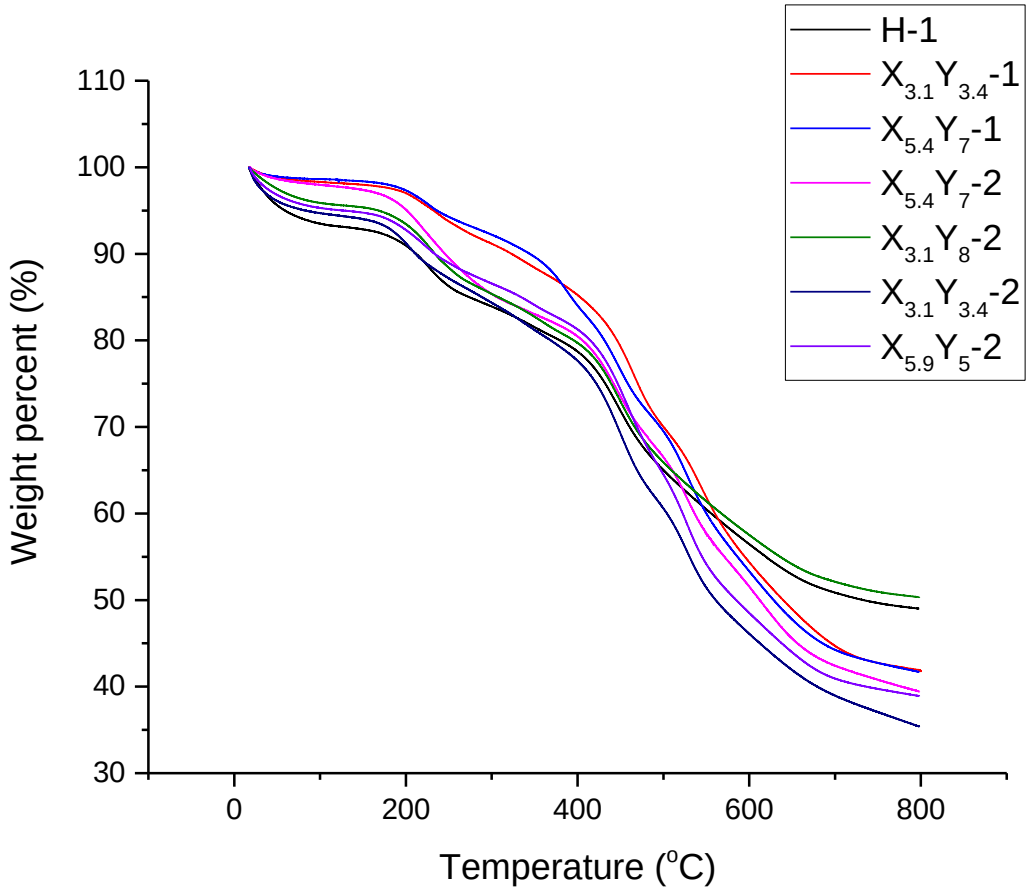

Figure 3.12 TGA curves of mPEs membranes under nitrogen atmosphere.

Figure 3.12 showed the thermal degradation behavior of mPEs membranes in their hydroxide form via TGA. All of the membranes had similar tendency. The initial weight loss below 100 ℃ corresponds to evaporation of bound water in the membranes. The mPEs membranes showed a three-stage weight loss. The first stage from 180 ℃ to 220 ℃ was assigned to the degradation of the quaternary ammonium groups. The second

stage from 220 ℃ to 400 ℃ was due to the degradation of the long alkyl side chains. All the membranes underwent polymer backbone degradation above 400 ℃. This trend of degradation was consistent with reported multi-block copolymer membranes with long alkyl side chains.[36, 51]

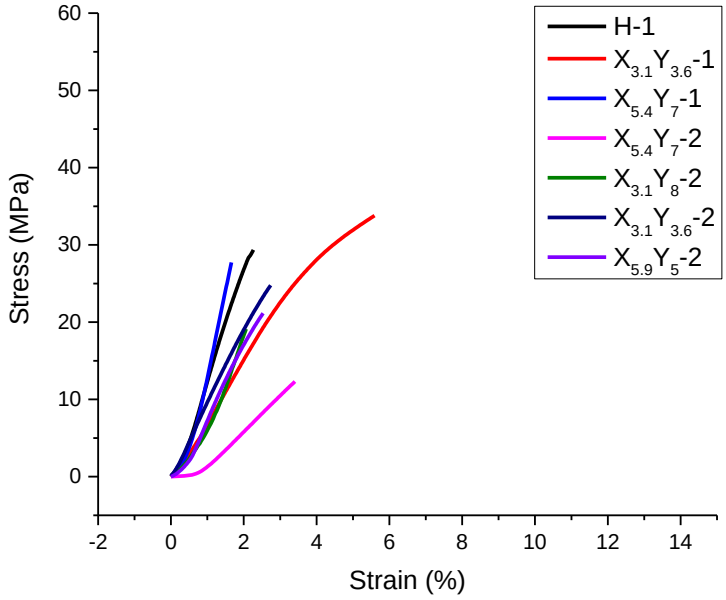

Figure 3.13 Stress-strain curve of mPEs membranes.

Table 3.3 Mechanical properties of mPEs membranes.

Membrane	Tensile strength (Mpa)	Young's modulus (Gpa)	Elongation at break (%)
H-1	29.4	1.6	2.3
$X_{3.1}Y_{3.6}$-1	33.4	0.8	5.5
$X_{5.4}Y_{7}$-1	27.7	2.3	1.7
$X_{5.4}Y_{7}$-2	12.3	0.5	3.4
$X_{3.1}Y_{8}$-2	19.1	1.3	2.1
$X_{3.1}Y_{4}$-2	24.8	0.9	2.7
$X_{5.9}Y_{5}$-2	21.2	1	2.5

Good mechanical stability is essential for the fabrication of electrode membrane assembly (EMA) and withstanding the pressure difference between two sides of the membrane during fuel cell operation. The mechanical properties, as summarized in Table 3.3, were obtained from stress-strain curves of mPEs membranes in Figure 3.13 measured by dynamic mechanical analysis (DMA). The tensile strength of all the membranes was in the range of 12.3 to 33.4 MPa, and the Young's modulus was in the range of 0.5 to 2.3 GPa, indicating that the membranes had proper mechanical properties to be used as polymer electrolyte. The tensile strength decreased as the increase of the tether amount and hydrophilic content. This was likely due to the increase of water content, which might act as a plasticizer[52] in the membranes and disintegrate the originally tightly arranged polymer chains.

3.2.4.4 Oxygen diffusivity and permeability

Table 3.4 Oxygen transport properties of Nafion®, Tokuyama A201, and mPEs block copolymers.

Sample	S (mass %)	D (cm^2/s)	P (mol/(bar*cm*s))
H-1	1.11	3.0E-11	1.1E-12
$X_{3.1}Y_{3.6}$-1	0.90	1.3E-08	4.0E-10
$X_{5.4}Y_{7}$-1	0.92	8.5E-09	2.7E-10
$X_{5.4}Y_{7}$-2	0.81	9.0E-10	2.5E-11
$X_{3.1}Y_{8}$-2	0.64	5.9E-09	1.3E-10
$X_{3.1}Y_{3.6}$-2	0.71	5.2E-09	1.3E-10
$X_{5.9}Y_{5}$-2	1.14	1.0E-08	3.9E-10
Nafion®	0.27	1.3E-07	1.2E-09
Tokuyama A201	0.38	2.0E-9	2.6E-11

The density of Nafion®, Tokuyama A201, and mPEs membranes used 1.1 g/cm^3 for calculation.

The oxygen solubility, diffusivity and permeability of all the membrane samples, Nafion®, and Tokuyama A201 are summarized in Table 3.4. Low oxygen diffusivity and permeability are desired for AEMs in order to get minimized oxygen crossover during fuel cell operation. The oxygen solubility of multiblock copolymer membrane was higher than that of Nafion®. However, the oxygen diffusivity and permeability was less than that of Nafion®. Compared with the commercial AEM copolymer material Tokuyama A201, the oxygen solubility of the multiblock copolymer membranes was higher. The oxygen diffusivity and permeability were on the same order of magnitude, 10^{-9} cm^2/s and 10^{-10} to 10^{-11} mol/(bar*cm*s), respectively. It is noted that the oxygen transport properties of mPE-$X_{5.4}Y_7$-2 were better than A201 membranes. By comparing mPE-$X_{3.1}Y_{3.6}$-1 and mPE-$X_{3.1}Y_{3.6}$-2 or mPE-$X_{5.4}Y_7$-1 and mPE-$X_{5.4}Y_7$-2, it can be concluded that the two tether mPEs membrane had lower oxygen diffusivity and permeability than the one tether membrane.

3.3 Conclusions

A systematic study of the effect of the hydrophilic and hydrophobic block lengths and ion exchange capacity of partially fluorinated multiblock copolymer mPEs with long head-group tethers was undertaken to explore the relationship of the chemical structure, morphology and properties of the mPEs AEMs. The chemical structure was studied via one-dimensional ^1H NMR, ^{19}F NMR, NOE, and two-dimensional HSQC NMR spectra. Only one tether could be attached per hydrophilic repeat unit at each time. The formation of ion conductive nano-channels for hydroxide ion transport due to nanophase separation of the multiblock copolymers greatly improved the ionic conductivity and reduced the water uptake. Multiblock copolymer mPE-$X_{5.4}Y_7$-2 showed the highest ionic conductivity,

119 mS/cm at 80 ℃, but not the highest IEC, because it formed efficient channels. The ratio of ionic conductivity to water uptake of the multiblock copolymers was high. For example, mPE-$X_{3.1}Y_8$-2 had very high ionic conductivity up to 94.0 mS/cm at 80 ℃, but only 26.7% water uptake. From DSC measurements of the number of freezable water and bound water molecules, the number of bound water molecules per ion of two-tether polymers was 4.5 to 5. In addition, the bound water played the dominant role in the hydroxide ion transport within the channels. The multiblock copolymer AEM showed good thermal, mechanical stability and excellent alkaline stability. The ionic conductivity was hardly changed after soaking the membrane in 1 M NaOH solution at 60 ℃ for 1000 h. Oxygen transport properties were also investigated. The mPEs AEM with higher ionic conductivity showed lower oxygen diffusivity and permeability, which means that the oxygen crossover problem was less severe.

CHAPTER 4. MULTIBLOCK COPOLYMER WITH MULTIPLE LONG HEAD-GROUP TETHERS FOR ANION EXCHANGE MEMBRANES

4.1 Introduction and objective

High ionic conductivity is needed for the successful use of anion exchange membranes. The goal is to achieve ionic conductivity greater than 100 mS/cm at 80 ℃ for acceptable fuel cell operation. Ionic conductivity is a function of two factors: ion exchange capacity (IEC) and ion mobility in the membranes. As discussed in Chapter 3, ion mobility can be improved by constructing efficient ion conductive channels in the membranes. One of the most effective methods to construct the ionic channels is through phase segregation of block copolymers and graft polymers in which the ionic groups are locally concentrated in the hydrophilic domains.

Another way to improve ionic conductivity is increasing the ion exchange capacity by increasing the number of fixed cation head-groups. However, water uptake also increases with higher IEC. High water uptake will cause membrane swelling, decrease in mechanical toughness, and water flooding of the ionic channels. There is a trade-off between ionic conductivity and water uptake. Therefore, in order to achieve the highest performance, the IEC has to balance high ionic conductivity and acceptable water uptake.

In this work, multiblock copoly(arylene ether)s (mPEs) were synthesized with different IECs by attaching a different number of cationic head-groups via long alkyl

chain tethers. The goal is to explore the relationship between the morphology and properties of the AEMs with different IECs. The number of the tethers and ionic groups attached to the polymer backbone can be precisely controlled by use of the unique characteristics of the Friedel-Crafts reaction and reduction reaction. Each tether was attached one at a time and repeated to form the hydrophilic block. Specifically, 1, 2, 3, and 4 ionic groups were attached on each repeat unit in the hydrophilic block of the block copolymer. It is noted that the 4-tether mPE membrane had an exceptionally high IEC value in hydrophilic blocks, 3.13 meq/g, as compared to previously reported AEMs. The size of the ion conductive channels, ionic conductivity, water uptake, number of freezable and bound water molecules in the membranes were also evaluated.

4.2 Results and discussion

4.2.1 Synthesis and structural analysis of 1, 2, 3 or 4-tether multiblock copoly(arylene ether)s

The structures of the 1, 2, 3 and 4-tether multiblock copoly(arylene ether)s (mPEs) are shown in Figure 4.1. All the samples had the same multiblock backbone structure (X_3Y_5), synthesized via polymer condensation reaction of hydrophobic oligomers (x = 3 repeat units) and hydrophilic oligomers (y = 5 repeat units), as previously described[65]. The molecular weight of the polymer backbone mPE-X_3Y_5 measured by GPC was 67.2 kDa. The ionic head groups with long tethers were attached to the multiblock copolymer mPEs backbone via a Friedel-Crafts reaction with 6-bromohexanoyl chloride and $AlCl_3$, followed by a reduction reaction to reduce the tether's ketone group. The reactivity of the fluorene aromatic rings is low due to the electron-withdrawing nature of the ketone group

on the tether. Thus, only one head-group tether can be attached on each hydrophilic repeat unit with each Friedel-Crafts reaction, even though 6-bromohexanoyl chloride was used in excess and multiple sites are available for tether attachment. However, after the reduction of the ketone group to an alkyl, the aromatic group ring regains its reactivity, and an additional tether can be attached. This one-at-a-time characteristic of the tether attachment reaction has been used to precisely control the number of the ionic head-groups attached to each hydrophilic repeat unit of the polymer backbone. Multi-tether, multiblock copolymers were synthesized via repeated Friedel-Crafts followed by reduction reactions. From our previous structural analysis of ^{1}H NMR spectra[65], the first two tethers were attached at f position, as shown in Figure 4.2.

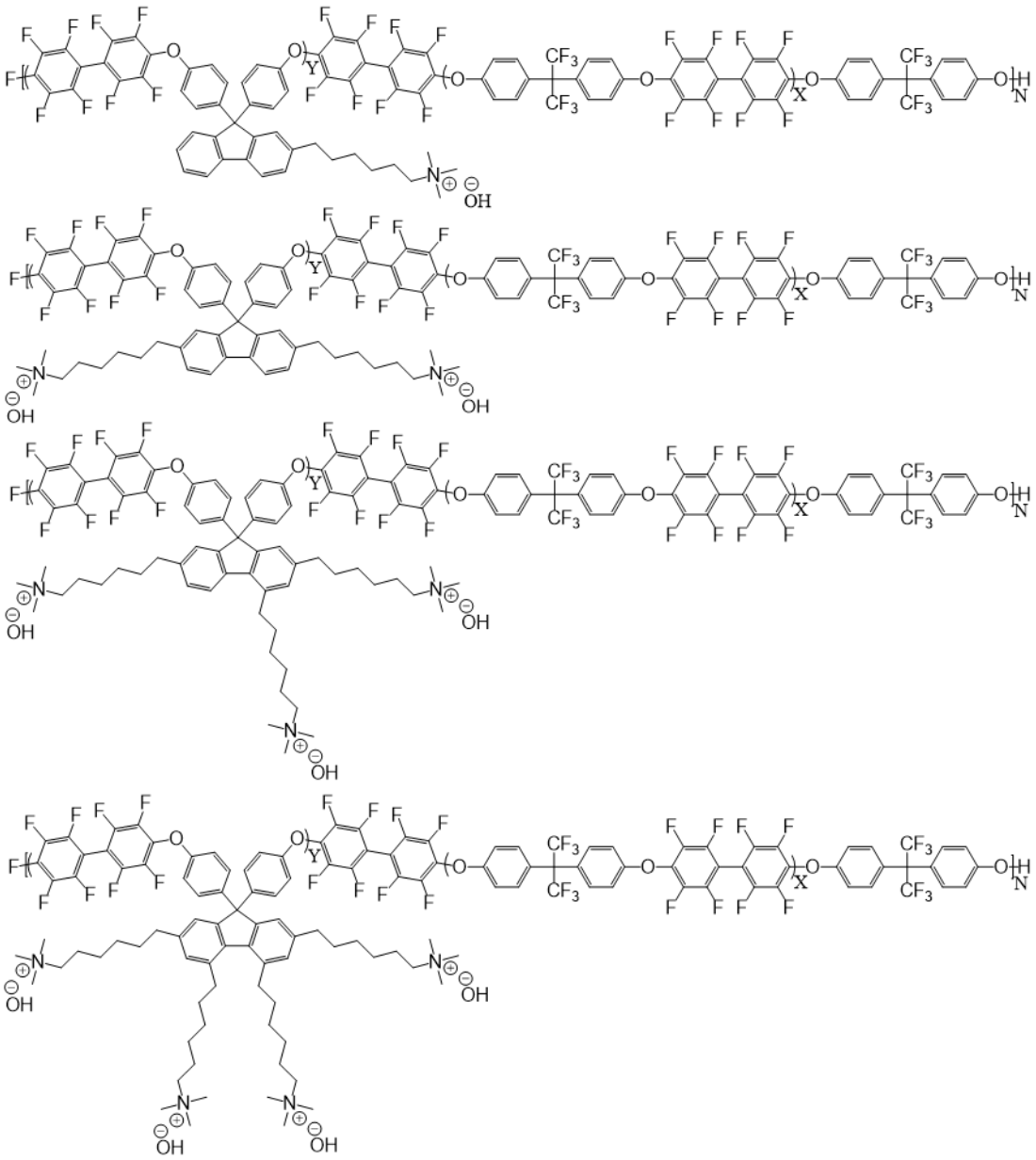

Figure 4.1 Structure of multiblock copoly(arylene ether)s with 1, 2, 3, and 4 long alkyl tethers.

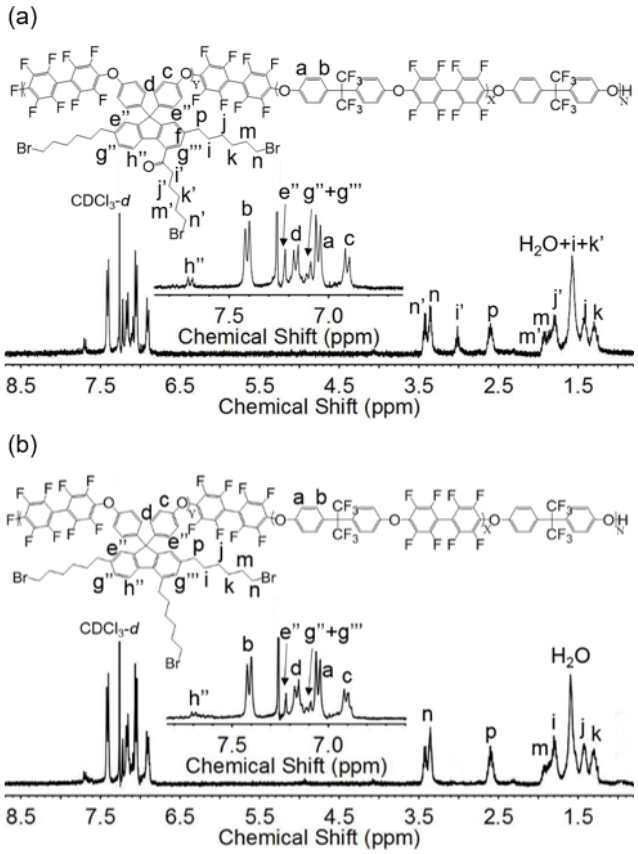

Figure 4.2 ^{1}H NMR spectra of (a) 3-tether BrKC6-2BrC6-mPEs, and (b) 3-tether 3BrC6-mPEs.

The third and fourth tether were attached at position h'' on the fluorene aromatic ring. This was shown by integration area of the proton peak h'' at 7.70 ppm. The h'' peak was reduced to half of its amount after the third tether was attached, as shown in Figure 4.2(a). The singlet peak at 7.22 ppm corresponds to the aromatic protons at position e''. The overlapping singlet and doublet peak at 7.10 ppm was attributed to the g'' and g''' protons. The integration areas of these two peaks were twice that of peak h'', which is another piece of evidence showing attachment of the third tether at position h''. The 1:2 ratio of the peak areas for the protons at positions i' and p confirm the successful attachment of the third tether. The 1:6 ratio of the peak area for the proton at h'' on the

fluorene aromatic ring and the overlapping peaks n and n', attributed to the methylene protons adjacent to the bromide groups, is another piece of evidence for the third tether attachment. After the ketone group of the third tether was reduced, the i' peak disappeared and the peak ratio for the protons at n and p became 1:1, as shown in Figure 4.2(b). The attachment of the fourth tether was shown by the disappearance of the h'' peak and 1:3 peak ratio of protons i' and p, shown in Figure 4.3(a). After reduction of the ketone group, the i' peak disappeared and the peak ratio of protons at n and p changed back to 1:1, as in Figure 4.3(b).

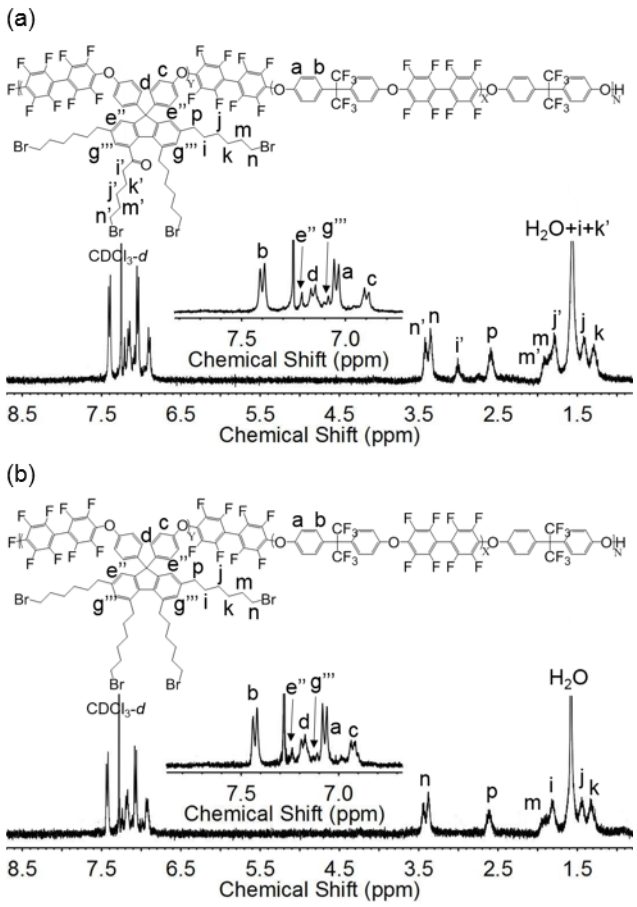

Figure 4.3 ^{1}H NMR spectra of (a) 4-tether BrKC6-3BrC6-mPEs, and (b) 4-tether 4BrC6-mPEs.

4.2.2 Morphology

Small angle X-ray scattering (SAXS) measurements were performed to investigate the microstructure of the membranes with a different number of alkyl chains terminated with quaternary ammonium head-groups. The polymers were tested dry with an iodide counter ion. The average separation length between inhomogeneities in the membrane, or interdomain spacing, d, was calculated from the position of the scattering maximum (q_{max}) via Braggs law. The multiblock AEM copolymers with 1, 2, 3, and 4 ionic head-groups on each hydrophilic repeat unit showed scattering peaks with q_{max} values, 0.140, 0.112, 0.107 and 0.105 nm^{-1}, respectively, as shown in Figure 4.4. This corresponds to interdomain spacing, d, of 44.8, 56.1, 58.7, and 59.8 nm, respectively, as summarized in Table 4.1. This magnitude of the separation d suggests that the scattering was due to phase segregation of the multiblock copolymer structure, rather than simply the formation of ion clusters in a random polymer which would have only showed a small value for d.[29] The size of ion conductive channels was influenced by the length of the hydrophobic and hydrophilic blocks, the length of head-group tethers, and the ionic group density. These results show that an increase in the number of the alkyl chain tethered quaternary ammonium groups results in an increase in the size of the ion conductive channels. The large difference in the d values for the 1 and 2-tether polymers indicates that the density of tethered ionic groups had a significant influence on the channel size. However, this influence became less dramatic with additional tethers.

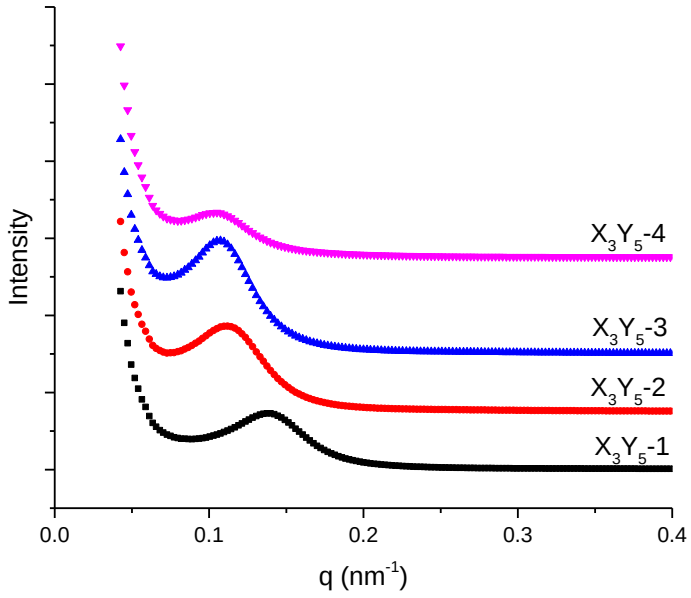

Figure 4.4 SAXS data of mPE membranes with 1, 2, 3, and 4 long alkyl side chains tethered trimethyl quaternary ammoniums in iodide form. The data have been shifted vertically for clarity and the arrowheads indicate q_{max}.

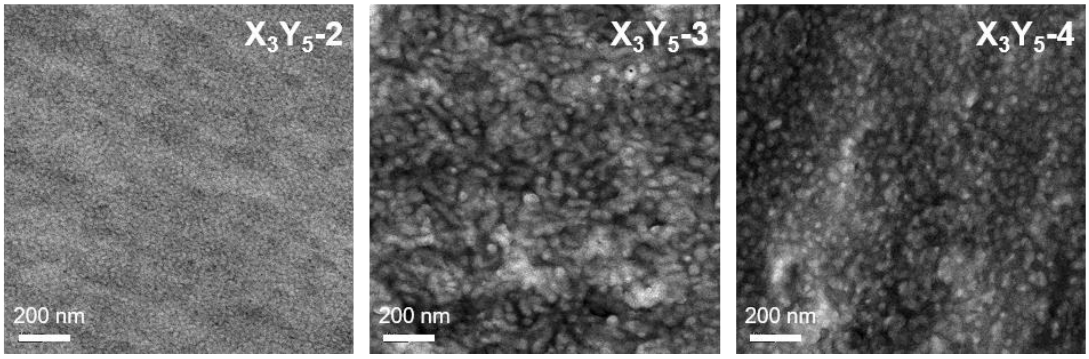

Figure 4.5 TEM images of mPEs membranes in bromide form.

TEM images were obtained to examine the morphology of the membranes, as shown in Figure 4.5. Phase separation is observed in the images of 2, 3, and 4-tether membranes in bromide form. The dark regions correspond to hydrophilic domains and the bright regions correspond to hydrophobic domains.[48] The hydrophilic domains appear

to form contiguous ion conductive channels. The average size of the ion conductive channels of 2, 3, 4-tether samples were about 18, 28, and 38 nm, respectively. This also confirmed that with the increase of the number of ionic groups, or ion concentration in hydrophilic blocks, the size of the channels increased.

4.2.3 Ion exchange capacity (IEC) and ionic conductivity

As shown in Table 4.1, the overall IEC was calculated for the multiblock copolymer. The local IEC was calculated corresponding to the density of ionic groups within only the hydrophilic blocks. It can be seen that both the overall IEC and local IEC increased with the number of tethers attached to the hydrophilic repeat units. The local IEC of 4-tether mPE membrane reached 3.13 meq/g, which is large compared with other AEM membranes reported in the literature.

Table 4.1 Properties of the AEMs with 1, 2, 3, and 4 tethered ionic groups.

[a]Membrane	[b]Interdomain spacing, d (nm)	[c]Overall IEC (meq/g)	[d]Local IEC (meq/g)	[e]Ionic conductivity (mS/cm)		[f]σ/IEC	[g]Water uptake (%)	Hydration number, λ	N_{free}	N_{bound}
				25 °C	80 °C					
X_3Y_5-1	44.8	0.76	1.25	10.6	42.2	55.5	11.5	8.4	0.7	7.7
X_3Y_5-2	56.1	1.35	2.08	26.8	86.1	63.8	24.8	10.2	1.5	8.7
X_3Y_5-3	58.7	1.83	2.68	41.9	130.6	71.4	58.3	17.7	6.9	10.8
X_3Y_5-4	59.8	2.23	3.13	48.3	141.0	63.2	82.5	20.5	9.6	10.9

[a]1, 2, 3, 4: the number of head-group tethers on each hydrophilic repeat unit; X: hydrophobic block (3 repeat units); Y: hydrophilic block (5 repeat units); [b]Channel size: average separation length between inhomogeneities (d) measured from SAXS; [c]Overall IEC: corresponding to the multiblock copolymer; [d]Local IEC: corresponding to the hydrophilic block; [e]Ionic conductivity: tested in hydroxide ion form; [f]σ/IEC: ratio of ionic conductivity at 80 °C to IEC; [g]Water uptake: measured at room temperature in hydroxide ion form.

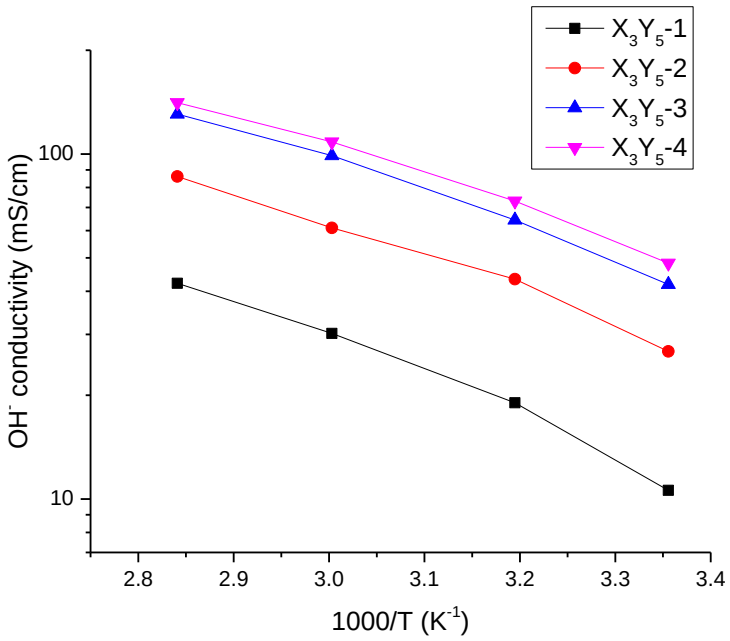

Figure 4.6 Arrhenius plot of ionic conductivity vs. inverse temperature.

Figure 4.6 shows the hydroxide conductivity of the membranes at 20, 40, 60 and 80 °C. The ionic conductivity increases with temperature and follows an Arrhenius relationship. The slope of the Arrhenius plot corresponds to the activation energy for the ionic conductivity, which was in the range of 17 to 22 kJ/mol. The ionic conductivity increased with the increasing of IEC, resulting from the increase of the number of ionic groups. This observation was also demonstrated in other studies.[43] Membranes with a greater number of ionic groups form larger ion conductive channels, which facilitates ion transport in the membrane, resulting in higher ionic conductivity. The ratio of the ionic conductivity to IEC was calculated to evaluate the effectiveness of the ionic groups, as shown in Table 4.1. The ionic conductivity/IEC value increased with the ionic group concentration, however, it reached a maximum with the 3-tether membrane, suggesting that this structure demonstrates the highest ionic group efficiency. The efficiency

decreased as the fourth tether was attached, even though the 4-tether membrane showed the highest absolute ionic conductivity.

4.2.4 Water uptake (WU), hydration number (λ), number of freezable water molecules (N_{free}) and bound, non-freezable water molecules (N_{bound})

A critical amount of water is necessary for ion hydration and conduction in the membranes. However, excess water, especially in the form of free-water, in the membranes results in membrane swelling, lower mechanical toughness, and flooding of the ion conductive channels. The phase segregation of block copolymers and the partial fluorination of the backbone structure, which introduces great hydrophobicity, can effectively control the water uptake at a relatively low level. The water uptake of the membranes with 1, 2, 3 and 4 long alkyl side chain tethered ionic groups in hydroxide ion form at room temperature is shown in Table 4.1. With the increase of the number of ionic groups (or IEC), the water uptake increased. The 2-tether membrane had an ionic conductivity of 86.1 mS/cm with only 26% water uptake. The 3-tether membrane showed 130.6 mS/cm ionic conductivity with 50% water uptake which is relative low in membranes compared to membranes with very high ionic conductivity. Though the 4-tether membrane also showed a very high ionic conductivity, the water uptake was also very high, which leads to excess swelling. This is due to the relatively large ion conductive channel and high density of head groups.

The hydration number (λ) is the number of water molecules per ionic head-group (cation/anion pair). Excess water in the form of free (unbound) water is not desirable or productive for ion conduction. The hydration number also increased somewhat as the

number of ionic groups in hydrophilic blocks, as shown in Table 4.1. The water molecules in the membrane can be divided into two states: freezable water molecules slightly associated with ion exchange groups, and non-freezable (bound) water molecules bound to an ion or polymer matrix. The number of freezable (N_{free}) and non-freezable (N_{bound}) water molecules was investigated by DSC and summarized in Table 4.1. The freezable water will show a characteristic freezing peak at temperatures below 0 ℃, while non-freezable water will show no peaks in DSC thermogram. Our previous work showed that the two-tether multiblock copolymer mPEs membranes had a similar amount of bound water molecules: 9 to 10, per ionic pair, or 4.5 to 5, per cation or anion.[65] In this work, the 2-tether sample showed a similar result. In addition, the number of bound water molecules for the 3 and 4-tether membranes was also in this range. Therefore, the increase of the number of head-groups (> 2 tethers) had little effect on the increase of the number of bound water molecules per head group. In contrast, the increase in density of head groups greatly affected the freezable water content in the membranes. 1 and 2-tether membrane showed very little freezable water, while 3 and 4-tether polymers had a large amount of freezable water. This explained the high water uptake of 3 and 4-tether sample. It also suggests that the ion conductive channels must be large enough for the bound water and have enough room for the freezable water. The 4-tether sample had a large amount of freezable water, resulting in 82.5% water uptake and lower ionic conductivity/IEC.

4.2.5 Alkaline stability

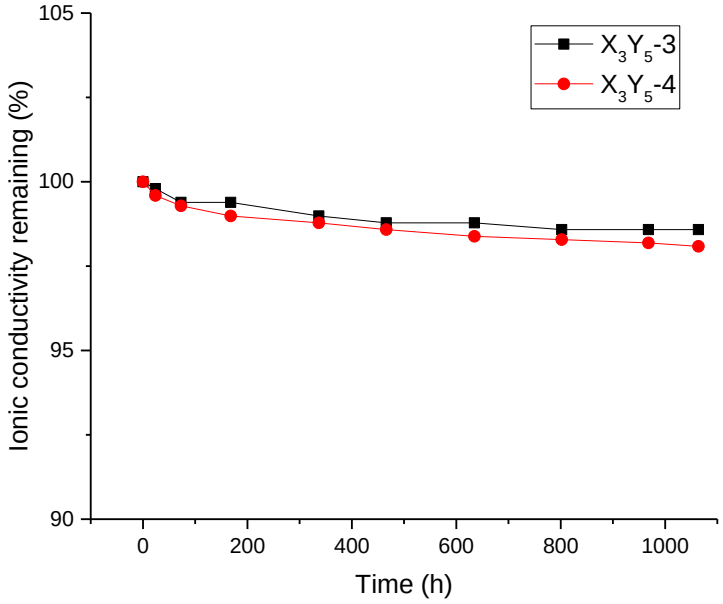

Figure 4.7 Alkaline stability of the mPEs membranes with 1, 2, 3, and 4 long alkyl side chain tethered ionic groups in 1 M NaOH solution at 60 ℃.

It was reported previously[65] that the 1 or 2-tether mPEs membranes with long tether attached quaternary trimethyl ammonium showed outstanding alkaline stability in strong base solutions. After soaking in 1M NaOH solution at 60˚C for 1000 h, there was only 1-3% drop in ionic conductivity. The 3-tether and 4-tether mPEs membranes were tested at the same condition, and it also showed that the ionic conductivity of the X_3Y_5-3 and X_3Y_5-4 membrane reduced only 1.4 and 1.9%, respectively. Therefore, it can be concluded that the long alkyl tether for quaternary trimethylammonium ionic exchange groups have greatly improved the alkaline stability compared to many other AEM materials with benzyl trimethylammonium groups.

4.2.6 Thermal stability

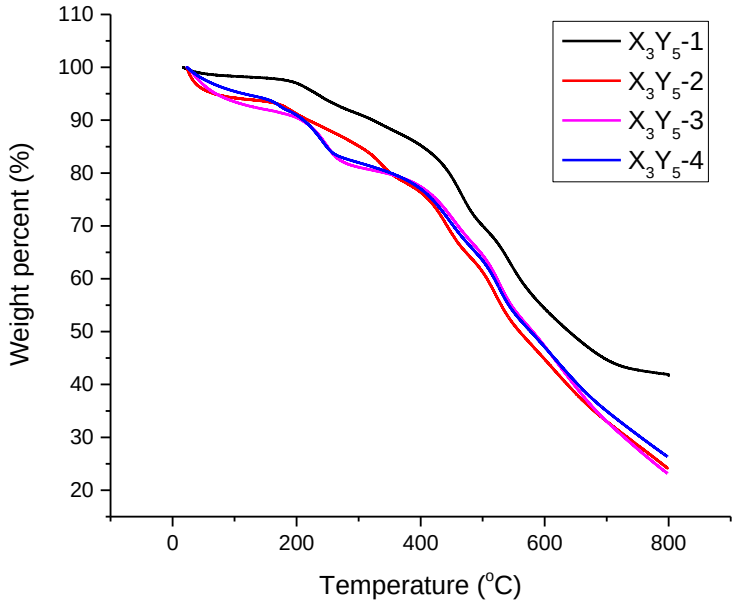

Figure 4.8 TGA curve of mPEs membranes with 1, 2, 3, and 4 long alkyl side chain tethered ionic groups under nitrogen atmosphere.

Figure 4.8 shows the thermal degradation behavior of mPEs membranes with a different number of tethers in the hydroxide form via TGA. Regardless of the number of the tethers, these membranes showed similar thermal degradation pattern. The initial weight loss below 100˚C was due to the evaporation of bound and unbound water in the membrane. The mPEs membranes followed a three-stage weight loss. From 180˚C to 220˚C, the weight loss was due to the degradation of the quaternary ammonium groups. From 220˚C to 400˚C, it was the degradation of the long alkyl side chains. Above 400˚C, polymer backbone started to degrade. Therefore, the membranes are thermally stable

enough under the common operation temperature of fuel cells or electrolyzers (i.e. below 100 ℃).

4.2.7 Mechanical properties

Good mechanical stability of the membrane is indispensable for the fabrication of the membrane electrode assembly and the operation of electrochemical devices. Devices often have a pressure difference between the two sides of the membrane. The mechanical properties were obtained from stress-strain curve of mPEs membranes tested from DMA, as summarized in Table 4.2.

Table 4.2 Mechanical properties of mPEs membranes with 1, 2, 3, and 4 ionic groups.

Membrane	Tensile strength (Mpa)	Young's modulus (Gpa)	Elongation at break (%)
X_3Y_5-1	30.4	0.8	5.0
X_3Y_5-2	22.3	1.1	3.1
X_3Y_5-3	19.3	0.9	2.8
X_3Y_5-4	18.7	1.2	2.1

The values of tensile strength, Young’s modulus, and elongation at break show that the membranes had adequate mechanical strength for many applications. It was observed that the tensile strength and the elongation at break decreased with the increase in the number of ionic groups. This was likely due to the increase of water content, which might act as a plasticizer in the membranes and disintegrate tightly arranged polymer chains. In addition, with the increase of the tether structure, the arrangement of polymer chains was further disrupted.

4.3 Conclusions

The effect of ionic concentration in hydrophilic block of multiblock copolymers on the morphology and properties of anion exchange membranes were investigated in this work. The multiblock copolymer mPEs with 1, 2, 3 and 4 long alkyl chain tethered ionic groups on each repeat unit in hydrophilic block, resulting in different ion exchange capacity (IEC), were synthesized and compared. Only one head-group tether can be attached on each hydrophilic repeat unit at a time. Thus, the tether amount can be precisely controlled. As the ionic concentration increased, the ionic conductivity and water uptake of the membranes increased. This was due to the increase of the size of ion conductive channels. 3-tether membrane showed the highest ionic conductivity/IEC, which means that its ionic groups were most efficient for contributing to the ionic conductivity. In addition, the number of freezable and non-freezable water molecules were investigated. 2, 3, 4-tether membrane showed similar number of bound water, while the number of freezable water increased with the number of ionic groups. The excess freezable water led to high water uptake and low ionic conductivity/IEC ratio (i.e. X_3Y_5-4). Therefore, X_3Y_5-3 showed the best properties, 130.6 mS/cm ionic conductivity and 58.3% water uptake, with an IEC of 1.83 meq/g. All of the membranes showed the same thermal and alkaline stability. As the number of ion groups increased, the mechanical strength of the membranes declined.

CHAPTER 5. MULTIBLOCK COPOLYMER WITH LONG ALKYL CHAIN TETHERED CATIONS AS ANION EXCHANGE MEMBRANES

5.1 Introduction and objectives

Benzyl trimethyl quaternary ammonium (BTMA) is a common cation group in anion exchange membranes due to its convenient synthesis and lack of beta-hydrogens (i.e. hydrogens on the beta carbon). Beta-hydrogens are known to undergo Hoffman degradation.[66] However, it has been reported that it is susceptible to other degradation processes under alkaline including direct nucleophilic substitution of hydroxide ions, [21-22] and elimination via yield formation.[21, 23] In Chapter 3, it was shown that long alkyl chain tethered trimethyl ammonium had excellent alkaline stability with only 1-3% loss of ionic conductivity after soaking in 1 M NaOH at 60 ℃ for 1000 h. Several other studies confirmed stability of the alkyl, quaternary ammonium head group.[27, 66] The long alkyl chain reduces the electron-withdrawing inductive effect and the resonance effect of the benzene ring when a benzyl attachment is used.[66] It was hypothesized that the high electron density around the beta-hydrogens and the steric shielding in the β-positions can prevent Hofmann elimination.[30-31] Apart from trimethyl quaternary ammonium cations, other cation groups, such as quinuclidium,[19] phosphonium,[33, 64] imidazolium, [32] and guanidinium[34] have also been studied as alternative to BTMA.

Quinuclidium, or 1-azaoniumbicyclo[2,2,2]octane, a quaternary ammonium cation formed by quaternization of a polycyclic amine 1-azabicyclo[2,2,2]octane

(ABCO), was first reported by Zhou et al.[19] used in the ionomer for alkaline electrode in fuel cells. Quinuclidium has a larger van der Waals volume than the trimethyl ammonium head group, which may facilitate the formation of larger ion conductive channels to enhance ion mobility in the membrane. Arges et al.[67] studied the alkaline stability of quinuclidium with poly(2,6-dimethyl 1,4-phenylene)oxide (PPO) backbone. Although no degradation of quinuclidium was found by 1D or 2D NMR, the decrease in IEC after exposure to alkaline solutions and the decline in the fuel cell performance after 12 h indicated cation degradation. They postulated that quinuclidium degraded through direct nucleophilic substitution (S_N1) of OH^- ions (debenzylation – cleavage of the cation site to benzyl alcohol).

Phosphonium cation has a central atom of phosphorus instead of nitrogen. Yan et al.[33, 64] developed a stabilized quaternary phosphonium cation, benzyl tri(2,4,6-trimethoxyphenyl)phosphonium, designed with nine methoxy groups to provide strong electron donation and steric hindrance. A high ionic conductivity up to 45 mS/cm at 20 ℃ was observed in polysulfone AEM with an IEC of 1.17 meq/g. They also reported that the membrane retained its flexibility and ionic conductivity for 30 days after exposure to 1 M KOH at 60 ℃. However, Arges et al.[67] reported that polysulfone AEM with benzyl tri(2,4,6-trimethoxyphenyl)phosphonium showed cation degradation via NMR analysis. The degradation pathway was thought to be direct nucleophilic substitution (S_N2) of OH^- ion (removal of a methoxy substituent from the cation site) to a tertiary phosphine and subsequent oxidation to phosphorus oxide.

In this chapter, multiblock copoly(arylene ether)s (mPEs) with partial fluorination and two long alkyl head-group tethers on each hydrophilic repeat unit with quaternary

trimethyl ammonium (TMHA), quinuclidium (ABCO), and tris(2,4,6-trimethoxyphenyl)phosphonium (TTMPP) were synthesized. Their morphology and properties (*i.e.* ionic conductivity, water uptake, alkaline stability, mechanical and thermal properties) were compared in order to understand the effects of the size and type of cations on the morphology and physical properties. The cation with the best properties were identified. To our knowledge, this work was the first to combine quinuclidium and phosphonium cations with long alkyl tethers in anion exchange membranes. The alkaline stability of this alkyl tethered quinuclidium and phosphonium cations was also compared with benzyl linkages.

5.2 Results and discussion

5.2.1 Synthesis of anion conductive multiblock copolymer with long alkyl tethered trimethylammonium (TMHA), quinuclidium (ABCO), and tris(2,4,6-trimethoxyphenyl)phosphonium (TTMPP)

The multiblock copolymer with long alkyl side chain terminated with a cation head-group was synthesized via polycondesation reaction and Friedel-Crafts acylation followed by reduction of the ketone, as described in Chapter 2. In this chapter, the multiblock copolymer used is X_3Y_7-2, which has a hydrophobic block (X) with 3 repeat units in each block, a hydrophilic block (Y) with 7 repeat units in each block, and 2 alkyl head-group tethers on each of the hydrophilic repeat unit. The block copolymer was quaternized with trimethylamine (TMA), quinuclidine, and tris(2,4,6-trimethoxyphenyl)phosphine to form three types of head groups. The resulting cations were: alkyl tethered trimethylammonium (TMHA), quinuclidium (ABCO), and tris(2,4,6-

trimethoxyphenyl)phosphonium (TTMPP), respectively, with bromide ion as the counter ion. The detailed procedure was described in Section 2.2. The membranes were solvent cast after quaternization reactions. Another membrane with alkyl trimethylammonium (TMHA) was quaternized after the membrane was cast. This was used as a comparison with the membranes quaternized before casting. The membranes were converted to the hydroxide ion form by soaking them in NaOH solution. The structure of the multiblock copolymer with these three cations are shown in Figure 5.1.

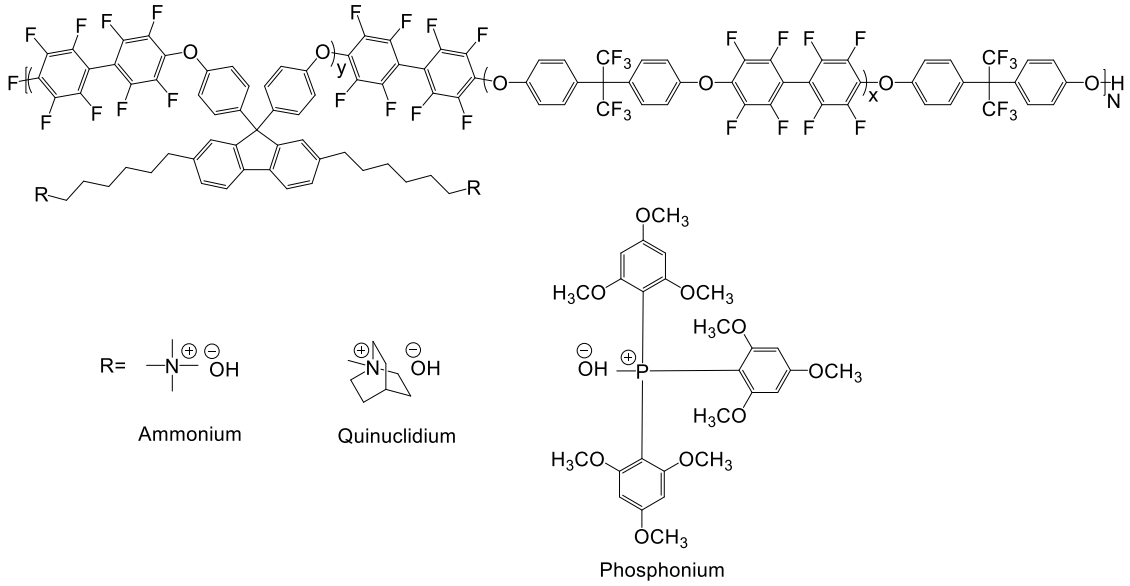

Figure 5.1 Structure of the multiblock copolymer with alkyl tethered trimethylammonium (TMHA), quinuclidium (ABCO), and tris(2,4,6-trimethoxyphenyl)phosphonium (TTMPP) cation groups.

5.2.2 Morphology

The morphology of the dry membranes with the three cations in bromide form were characterized via small angle X-ray scattering (SAXS), as shown in Figure 5.2. The size of the ion conductive channels was evaluated by calculating the average separation length, or interdomain spacing, d, between inhomogeneities in a membrane. This was

calculated from the position of the scattering maximum (q_{max}) via Braggs law. The multiblock copolymer AEMs with alkyl trimethylammonium X_3Y_7-A1, X_3Y_7-A2, quinuclidium X_3Y_7-Q, and phosphonium X_3Y_7-P showed scattering peaks with q_{max} values of 0.124, 0.167, 0.153 and 0.132 nm^{-1}, respectively, which corresponds to interdomain spacing d of 50.6, 37.6, 41.0 and 47.6 nm, respectively, Table 5.1. The d values obtained from the SAXS data confirmed phase segregation from the multiblock copolymers, rather than just small ion clusters in the membranes which would show a small value of d.

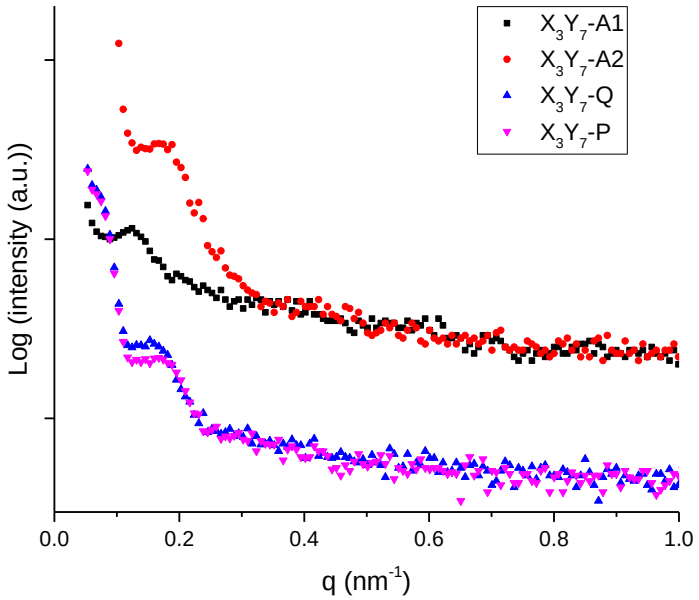

Figure 5.2 SAXS data of the membranes with alkyl trimethylammonium (TMHA), quinuclidium (ABCO), and tris(2,4,6-trimethoxyphenyl)phosphonium (TTMPP) cations.

Since the membranes had the same backbone structure (i.e. same length of hydrophobic and hydrophilic blocks) and the same number of head-group tethers on each repeat unit in the hydrophilic block, the difference in the interdomain spacing d was

primarily due to the different cation effects. By comparing X_3Y_7-A2, X_3Y_7-Q, and X_3Y_7-P, it was found that the size of the ion conductive channels increased with the size of the cation head group. In addition, the preparation method of the membrane also affected the phase segregation and the size of the ion conductive domains. The membrane quaternized after casting, X_3Y_7-A1, showed much larger interdomain spacing d than that of the membrane quaternized before casting, X_3Y_7-A2. Quaternization before casting allowed better phase segregation of the block copolymers because the block copolymer with the ionic groups attached has higher χ, the Flory Huggins interaction parameter characterizing the effective interaction of monomers in the hydrophilic and hydrophobic blocks. In addition, casting the membrane before quaternization may not provide the needed volume expansion formation of the cation head group.

5.2.3 Properties

5.2.3.1 Ion exchange capacity (IEC) and ionic conductivity

The ion exchange capacity (IEC) of the membranes with different cations are summarized in Table 5.1. Since all the membranes had the same structure other than the cation head group, the difference in the IEC values are a result of the molecular weight differences for the cation head groups. As the size of cation group increase, the IEC declined. For example, the membrane with alkyl trimethylammonium, X_3Y_7-A1 and X_3Y_7-A2 had an IEC of 1.49 meq/g, while the membrane with alkyl tris(2,4,6-trimethoxyphenyl)phosphonium, X_3Y_7-P, only had an IEC of 0.87 meq/g.

Table 5.1 Properties of the AEMs with alkyl trimethylammonium (TMAH), quinuclidium (ABCO), and tris(2,4,6-trimethoxyphenyl)phosphonium (TTMPP) cations.

[a]Membrane	[b]Interdomain spacing d (nm)	[c]Theoretical IEC (meq/g)	[d]Ionic conductivity (mS/cm)		[e]σ/IEC	[f]Water uptake (%)	Hydration number, λ	N_{free}	N_{bound}
			25 °C	80 °C					
X_3Y_7-A1	40	1.49	26.7	92.2	61.8	26.0	9.7	0.6	9.1
X_3Y_7-A2	36	1.49	27.8	101.2	67.9	24.4	9.1	0.4	8.7
X_3Y_7-Q	35	1.38	21.1	68.2	49.4	11.1	4.5	0.2	4.3
X_3Y_7-P	45	0.87	14.2	46.1	52.9	22.4	14.3	1.7	12.6

[a]X: hydrophobic block (3 repeat units); Y: hydrophilic block (5 repeat units); [b]Interdomain spacing: average separation length between inhomogeneities (d) measured from SAXS; [c]Theoretical IEC: calculated assuming 100% quaternization; [d]Ionic conductivity: tested in hydroxide ion form; [e]σ/IEC: ratio of ionic conductivity at 80 °C to IEC; [f]Water uptake: measured at room temperature in hydroxide ion form.

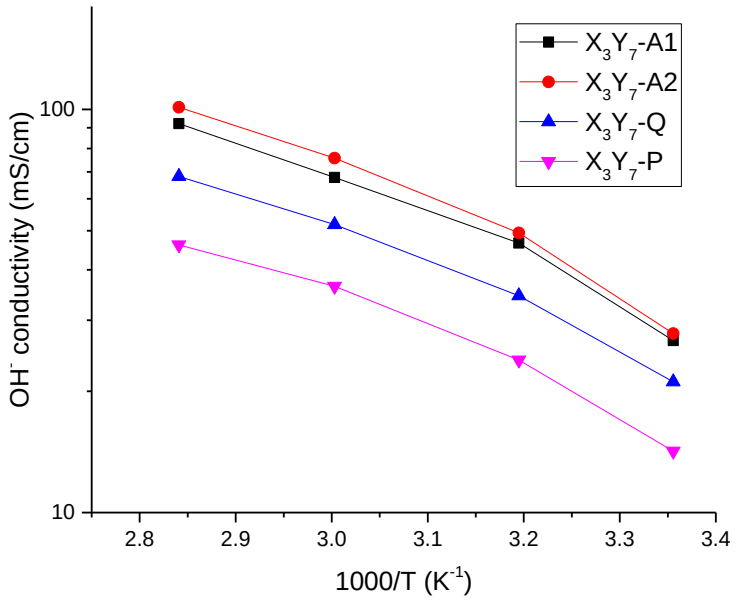

Figure 5.3 Arrhenius plot of ionic conductivity vs. inverse temperature.

The hydroxide conductivity of the membranes at 20, 40, 60 and 80 °C was shown in Figure 5.3. The ionic conductivity increased with temperature and follows an

Arrhenius relationship. The slope of the Arrhenius plot corresponds to the activation energy for ionic conductivity. The energy of activation is 19.6, 20.6, 18.8, and 18.9 kJ/mol for X_3Y_7-A1, X_3Y_7-A2, X_3Y_7-Q, and X_3Y_7-P, respectively.

By comparing the ionic conductivity of the membranes with different cations, it can be seen that the ionic conductivity increased with IEC even though the materials had the same backbone, tether, and the same number of ionic head groups attached to each repeat unit in the hydrophilic segment. The difference in membrane conductivity is due to their different IECs. The quaternary trimethylammonium is a more efficient and compact head group, which has a smaller van der Waals volume. Thus, though alkyl trimethylammonium formed the smallest channels, it showed the highest ionic conductivity.

In addition, the preparation method of the membranes also affects the ionic conductivity. The membrane quaternized after casting, X_3Y_7-A1, exhibited lower ionic conductivity than the membrane quaternized before casting, X_3Y_7-A2, although the membranes were otherwise the same. As a result, X_3Y_7-A1 had larger ion conductive channels. However, this did not result in higher conductivity. X_3Y_7-A2 had the higher conductivity which may be due to a more optimum and efficient channel size due to a more continuous and less tortuous ion pathway.

The ratio of the ionic conductivity to IEC was calculated to evaluate the efficiency of the ionic groups to the ionic conductivity, as shown in Table 5.1. The result shows that X_3Y_7-A1 and X_3Y_7-A2 had higher ionic conductivity/IEC ratio than X_3Y_7-Q and X_3Y_7-P, which reflects the higher efficiency of the channels in the alkyl trimethylammonium (TMHA) head groups. In addition, X_3Y_7-A2 showed a slightly

higher ratio than X_3Y_7-A1, which confirms that quaternization before casting leads to better ion transport in the membrane, in this case.

5.2.3.2 Water uptake (WU), hydration number (λ), number of freezable water molecules (N_{free}) and bound water molecules (N_{bound})

An optimum amount of water uptake is essential for ion hydration and conduction in the membranes. However, excess free water can result in swelling, reducing the mechanical toughness, and water flooding in the ion conductive channels. The water uptake of the membranes in hydroxide ion form at room temperature is shown in Table 5.1. X_3Y_7-Q membrane with quinuclidium (ABCO) had the lowest water uptake, and the X_3Y_7-A1 membrane with alkyl trimethylammonium (TMHA) had the highest. This is another indication that quaternization before membrane casting can result in preferred phase segregation for more efficient ion conductive channels.

Hydration number (λ) is the number of water molecules per cation/anion pair, which characterizes the efficiency of utilization of water in the membranes. Hydration number includes all the water molecules in the membrane: freezable water molecules which is only slightly associated with the ion exchange groups, and non-freezable water molecules which are bound to an ion or polymer matrix. The number of freezable (N_{free}) and non-freezable (N_{bound}) water molecules was investigated by DSC and summarized in Table 5.1. In the DSC thermogram, the freezable water showed a characteristic freezing peak at subzero temperature while non-freezable water did not.

The membrane with alkyl trimethylammonium, X_3Y_7-A1and X_3Y_7-A2, had a hydration number in the range as discussed in Chapter 3, about 9 bound water molecules

per ionic pair and very little free-water. This is consistent with the previous results where two-tether multiblock copolymer membranes with alkyl tethered quaternary ammonium groups. However, in the case of alkyl quinuclidium, X_3Y_7-Q, it had a low hydration number of only 4.5 with very little freezable water. The membrane with alkyl phosphonium, X_3Y_7-P, had a very high hydration number, up to 14.3 with a bound water value of 12.6, which is much higher than that of alkyl trimethylammonium groups.

5.2.3.3 Relationship of morphology, IEC, ionic conductivity, and water uptake

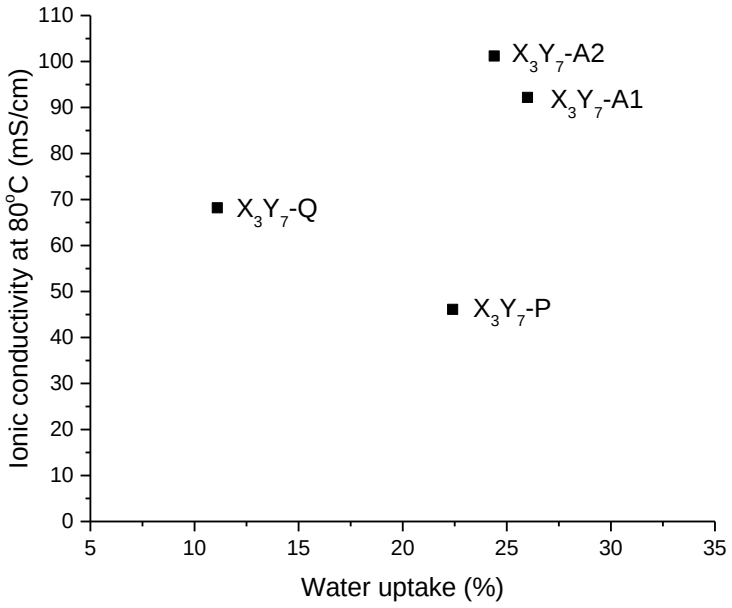

Figure 5.4 Relationship of ionic conductivity at 80 ℃ and water uptake of membranes with different cations.

The size of cation groups affects the morphology and properties of AEMs with a common backbone. Alkyl trimethylammonium (THMA) has the smallest size and forms the smallest ion conductive channels, as determined by SAXS measurements. It has the

highest ionic conductivity, up to 101.2 mS/cm at 80 ℃ and highest water uptake, 24.4% due to its high IEC (1.49). Alkyl quinuclidium (ABCO) also has a very low water uptake, only 11.1%. This corresponds to four bound waters per cation/anion pair. Alkyl tris(2,4,6-trimethoxyphenyl)phosphonium (TTMPP) has the largest size and forms the largest ion conductive channels. It has relatively low ionic conductivity, and higher water uptake than quinuclidium (ABCO). Thus, alkyl trimethylammonium is the preferred head group for this backbone in terms of IEC, ionic conductivity and water uptake.

5.2.3.3 Chemical stability

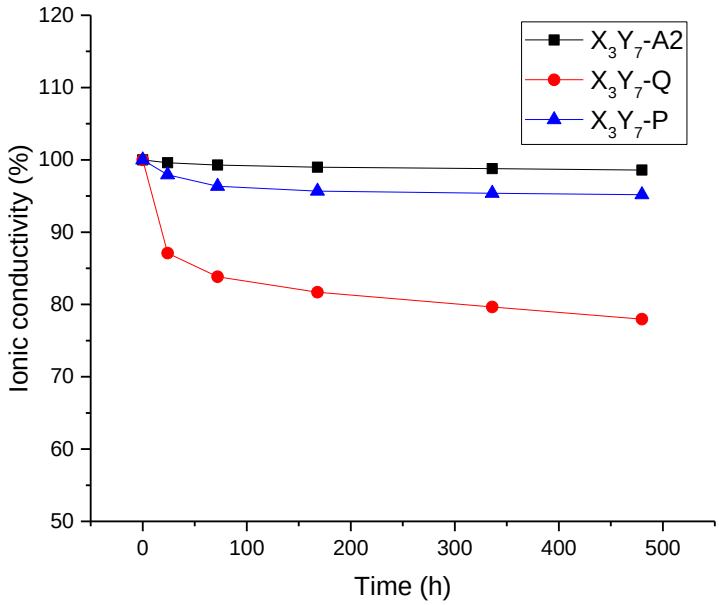

Figure 5.5 Alkaline stability of the membranes with alkyl trimethylammonium (TMHA), quinuclidium, and tris(2,4,6-trimethoxyphenyl)phosphonium (TTMPP) cations in 1 M NaOH solution at 60 ℃.

The alkaline stability of the membranes with the three cations were evaluated by tracking the change of ionic conductivity with exposure time in 1 M NaOH at 60 ℃. As

shown in Figure 5.5, the X_3Y_7-A2 membrane with alkyl trimethylammonium showed the best alkaline stability, with only 1% ionic loss over 480 h. This was consistent with the result of alkyl trimethylammonium group stability reported in Chapters 3 and 4. Several other studies also confirmed that alkyl trimethylammonium has no degradation at 60 °C for 30 days.[27, 66]

X_3Y_7-P with alkyl tris(2,4,6-trimethoxyphenyl)phosphonium (TTMPP) showed 4.8% ionic conductivity loss in 480 h. Yan et al.[64] reported no ionic conductivity loss for benzyl TTMPP after exposure to 1 M KOH at 60 °C for 30 days. However, Arges et al.[68] reported about 90% of the cations remained after the same exposure. In addition, they proposed the degradation pathway to be direct nucleophilic S_N2 substitution of the OH^- ion (*i.e.* removal of a methoxy substituent from the cation site), creating a tertiary phosphine followed by oxidation to phosphorus oxide. It is believed that the same degradation mechanism also happened in this case, but the long alkyl side chain mitigates the degradation. Yan et al.[69] suggested alternate structure of alkyl tris(2,4,6-trimethylphenyl)phosphonium without the methoxy groups for better alkaline stability.

X_3Y_7-Q with alkyl quinuclidium showed 22% ionic conductivity loss after 480 h at 60 °C. Degradation was also observed in other studies by Agres et al.[67] on benzyl quinuclidium where the IEC dropped from 1.8 to 0.5 meq/g in 1 M NaOH at 60 °C after 30 days. This was due to direct nucleophilic S_N1 substitution at the benzylic methyl (debenzylation). Mohanty et al.[66] reported no degradation of a series small molecules based long alkyl tether quaternary ammonium groups in 1 M NaOH at 60 °C. The ionic conductivity loss of alkyl quinuclidium in this study may have been caused by the low

number of bound water molecules (N_{bound}) (i.e. 4) around the cation/anion groups resulting in a higher local OH^- concentration accelerating the degradation.

5.2.3.4 Thermal stability

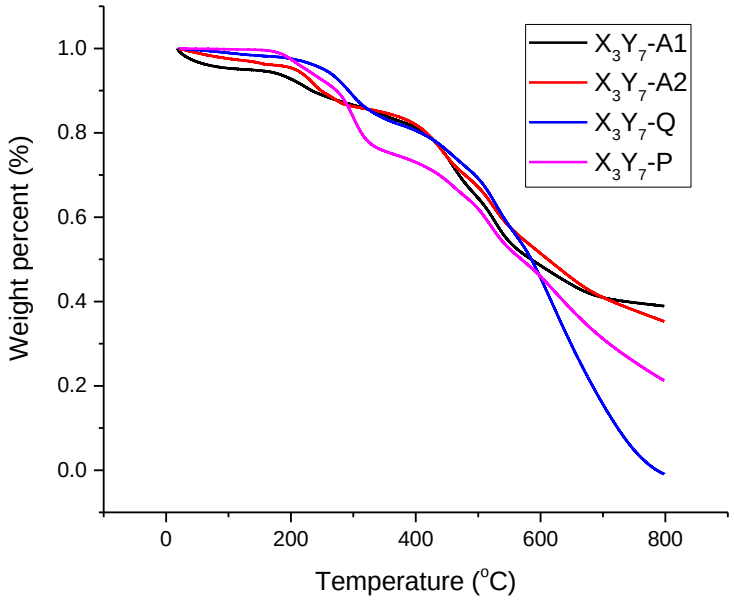

Figure 5.6 TGA curves of the membranes with alkyl trimethylammonium, quinuclidium, phosphonium cations under nitrogen.

Figure 5.6 showed the thermal degradation behavior of the membranes with the three cations in the hydroxide ion form via TGA. All the four samples showed a three-stage degradation upon heating under nitrogen. The initial weight loss below 100 ℃ was attributed to the evaporation of bound water in the membrane, which is not membrane degradation. The first degradation stage was the thermal degradation of ionic exchange groups which occurred at slightly different temperatures for the three cations. The starting temperatures for degradation were 180, 200, and 190 ℃ for trimethylammonium, quinuclidium, and tris(2,4,6-trimethoxyphenyl)phosphonium cations, respectively. The

second stage was the thermal degradation of long alkyl side chains in the temperature range of 250 to 400 ℃. Above 400 ℃, the degradation of polymer backbone occurred. The thermal degradation was not affected by the film casting method, as the chemical structure of the X_3Y_7-A1 and X_3Y_7-A2 were the same. All of the membranes are thermally stable at the common operation temperature, below 100 ℃, which is of interest for fuel cells and electrolyzers.

5.2.3.5 Mechanical properties

Table 5.2 Mechanical properties of the membranes with alkyl trimethylammonium, quinuclidium, and tris(2,4,6-trimethoxyphenyl)phosphonium cations.

Membrane	Tensile strength (Mpa)	Young's modulus (Gpa)	Elongation at break (%)
X_3Y_7-A1	21.4	1.3	2.7
X_3Y_7-A2	23.2	1.2	5.3
X_3Y_7-Q	27.5	0.9	6.6
X_3Y_7-P	17.1	1.9	2.5

The mechanical properties of the membranes with the three cations in hydroxide ion form were obtained from the stress-strain curve, as summarized in Table 5.2. The membranes were soaked in deionized water. Excess water was wiped off the surface before the test. The values of the tensile strength, Young's modulus, and elongation at break show that these membranes had adequate mechanical strength and flexibility to be considered for polymer electrolytes. The membrane with the quinuclidium cation showed the highest mechanical strength, while the membrane with tris(2,4,6-trimethoxyphenyl)phosphonium showed the lowest. This can be explained by the water content (i.e. hydration number) in the membranes, as water might act as a plasticizer to degrade the quality of the film. In addition, the bulky structure of the phosphonium cation

also reduced the flexibility of the polymer chains, which results in lower elongation at break and more brittle membranes. It was also observed that the solvent casting method affected the mechanical properties of the membrane. X_3Y_7-A2, quaternized before solvent casting, showed better mechanical properties than X_3Y_7-A1, quaternized after membrane casting. This is due to tighter entanglement and better rearrangement of polymer chains in the membrane if cast after quaternization.

5.3 Conclusions

Multiblock copoly(arylene ether)s based anion exchange membranes with alkyl tethered trimethylammonium (TMHA), quinuclidium (ABCO), and tris(2,4,6-trimethoxyphenyl)phosphonium (TTMPP) cations were synthesized and characterized. The relationship of the size and structure of the cations with the morphology and properties of AEMs was investigated. A larger cation led to larger ion channels. However, larger cation also caused lower IEC and consequently lower ionic conductivity despite the channel size of the cation. Quinuclidium showed low water uptake with a lower number of bound water for each ion pair. Tris(2,4,6-trimethoxyphenyl)phosphonium showed high water uptake due to a large number of bound water. TMHA is the most stable cation after exposure to 1 M NaOH solution at 60 ℃ after 20 days, while quinuclidium showed a 22% ionic conductivity loss due to high hydroxide ion concentration in the local area of ionic groups caused by low bound water content. TMHA also had the best mechanical properties, while phosphonium was the poorest. Therefore, alkyl trimethylammonium appears to be the best cation head group among the three cations studied for this backbone. Finally, the membrane preparation method impacts the morphology and properties of the AEMs. Quaternization before membrane

casting resulted in better properties than quaternization after membrane casting due to greater phase segregation.

CHAPTER 6. ANION CONDUCTING IONOMERS FOR FUEL CELLS AND ELECTROLYZERS

The work in this chapter was also contributed by John Ahlfield and Garrett Huang for fuel cell and electrolyzer fabrication and testing.

6.1 Introduction and objectives

The design of new anion exchange ionomers for use in electrochemical devices is a critical step in improvement of anionic fuel cells and electrolyzers. Although these materials share some targeted goals with anion exchange membranes (AEMs), there are several different property requirements. Since ionomers are used within electrode layers, they do not serve as a primary separator for fuel and air. Rather, they act as a transport facilitator in the electrode where a high degree of mass transport is required.

Fuel cells and electrolyzers electrodes can be fabricated by spraying a slurry of catalyst and ion conducting polymer (i.e. ionomer) onto a gas diffusion layer. The electrode is then bonded to the ion conducting membrane to form a membrane electrode assembly. Because ionomers and membranes serve different functions in the cell, the materials used for these functions should be different and optimized for each purpose. For example, the membrane should have low oxygen permeability and high mechanical strength while the ionomer for the air-cathode should have high oxygen permeability. Free-standing mechanical strength is not an issue for the ionomer. Some properties, such as ion conductivity and chemical stability, are common to both.

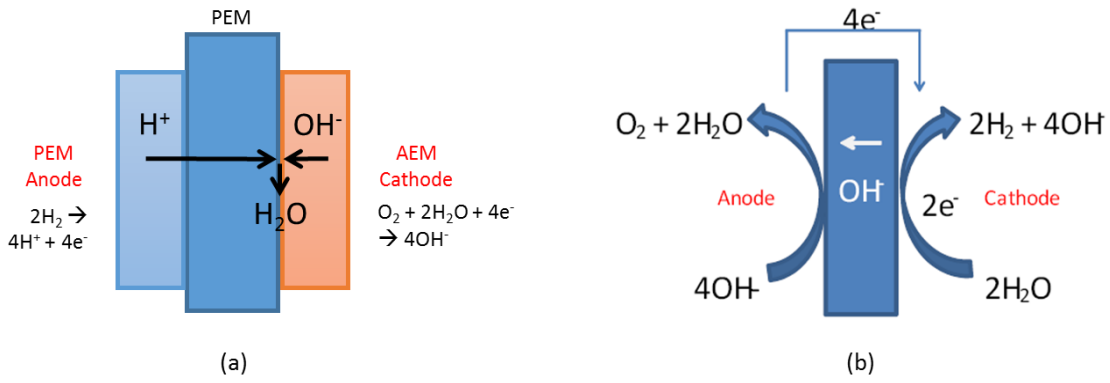

Figure 6.1 (a) Cathode hybrid fuel cell configuration and (b) alkaline electrolyzer configuration.[70]

In previous AEM ionomers studies, the anion conducting ionomer was used in conjunction with an anion exchange membrane, which made deconvolution of ionomer from membrane performance difficult. For this study, a bipolar (or hybrid) cell configuration is used, Figure 6.1(a), in an attempt to combine the established PEM architecture with the advantages potentially offered by AEMs. In a bipolar configuration, the fuel cell (or electrolyzer) has one electrode operated at low pH while the other operates at high pH. The bipolar device offers advantages compared to fully acidic or alkaline fuel cells.[71] It allows for the study and evaluation of AEM ionomers separately from anion exchange membranes, which has resulted in a few materials being developed explicitly as ionomers rather than membranes.

In this study, a series of anionic ionomers was synthesized and tested in fuel cells and electrolyzers. These ionomers are based on a series of materials which include block copolymer AEMs with alkyl tethers that have been modified to be used as anion conductors. The newly synthesized ionomers tested for their viability as anion conductors in the cathodic electrode for the cathode hybrid fuel cell depicted in Figure 6.1(a) and as

the anodic electrode of an alkaline electrolyzer in Figure 6.1(b). In this case, the selected materials will be evaluated in both oxygen-consuming (i.e. oxygen reduction reaction (ORR)) and oxygen-producing electrodes (i.e. oxygen evolution reaction (OER)).

6.2 Devices fabrication

6.2.1 Fuel cell fabrication

The membranes used in this study were Nafion 117, which was pre-treated by sequential boiling steps in 3% H_2O_2, H_2O, 1 M H_2SO_4, and again in H_2O. Each boil lasted approximately 1 hour. All membranes were stored in distilled water until MEA fabrication. A 5% Nafion dispersion in alcohol was used as the anodic PEM ionomer, while the cathodic AEM ionomer was varied among the choices in Table 6.1 and Tokuyama AS-4. All other chemicals were used as received.

The PEM anode and AEM cathode were both fabricated via slurry method. The PEM anode slurry consisted of Pt/Ru alloy catalyst (75% metal weight), Nafion dispersion (15% by weight with respect to the catalyst), and a mixture of water/isopropanol. The slurry was sprayed onto hydrophilic Toray 2050 L carbon paper and dried at room temperature. The target metal loading was 4 mg/cm^2 for this low pH electrode. The AEM cathode slurry contained a Pt/C catalyst (40% metal weight), anion exchange ionomer (10% weight with respect to catalyst), and dimethylformamide (DMF). The slurry was sprayed onto hydrophobic Toray TGPH-090 carbon paper and dried at room temperature. The target metal loading for the high pH electrodes was 2 mg/cm^2. After drying, the electrodes were soaked in 0.1 M NaOH overnight to exchange

completely to OH^- form. Finally, the electrodes were rinsed in distilled water to remove any excess OH^- ions from the surface.

The membrane electrode assembly (MEA) was prepared by spraying 50 μL of a 1:2 Nafion:IPA solution onto each electrode surface prior to assembly. Each electrode was then placed directly onto the prepared Nafion 117 film. The entire MEA was hot-pressed for 10 min at 2 MPa and 60 °C. The MEA was placed into a BioLogic Fuel Cell Test Station FCT 150S. Humidified oxygen and hydrogen were fed at 55 °C to the cathode and anode at 25 and 10 sccm respectively. Electrochemical measurements were obtained using a Princeton PAR 2273 potentiostat/galvanostat. The device testing protocol consisted of 5 h chronoamperometry at 250 mV, followed by forward and reverse linear sweep voltammetry and electrochemical impedance spectroscopy taken at 300 and 600 mV. This cycle was repeated 4 times for 20 h total run time.

6.2.2 Electrolyzer fabrication

The membrane used in this study was Tokuyama A201 for all devices. A commercially available AEM ionomer, Tokuyama AS-4, was used as a reference for comparison to the various synthesized anode ionomers. Prefabricated cathode HER electrodes with a proprietary design were provided by Proton OnSite and were used as received.

The AEM electrolyzer anode was fabricated via a slurry method. The anode slurry consisted of an iridium oxide catalyst, ionomer, and dimethylformamide. The slurry was sprayed onto a platinized titanium gas diffusion layer (GDL) and dried at room

temperature. The target metal loading was 4 mg/cm^2. An additional layer of ionomer (20% mass of slurry) was sprayed on top of the catalyst layer of the anode.

The MEA was prepared by soaking electrodes and membrane in 0.5 M NaOH for approximately 2 h prior to testing to exchange the materials completely to OH^- form. Each electrode was stacked vertically in a heated cell block with cathode on bottom, followed by membrane, and finally anode. Deionized water was fed to the anode side of the cell to reduce water content in the product hydrogen. Electrochemical measurements were obtained using a Princeton PAR 2273 potentiostat/galvanostat. The device testing protocol consisted of a 24 h chronopotentionmetry at 200 mA/cm^2, followed by a forward linear sweep voltammetry and electrochemical impedance spectroscopy taken at 1.8 V. This cycle was repeated until either the cell voltage reached a 3 V cutoff threshold or some other technical failure which shortened the duration of the experiment. Typical runtime for each cell was approximately 100 h.

6.3 Results and Discussion

6.3.1 Synthesis of anion exchange ionomers

The low molecular weight anion conducting ionomers were synthesized as described in Chapter 2. The ionomers include hydrophilic oligomer based homopolymers and multiblock copolymers with one or two long alkyl chain tethered quaternary ammonium groups, as shown in Figure 6.2.

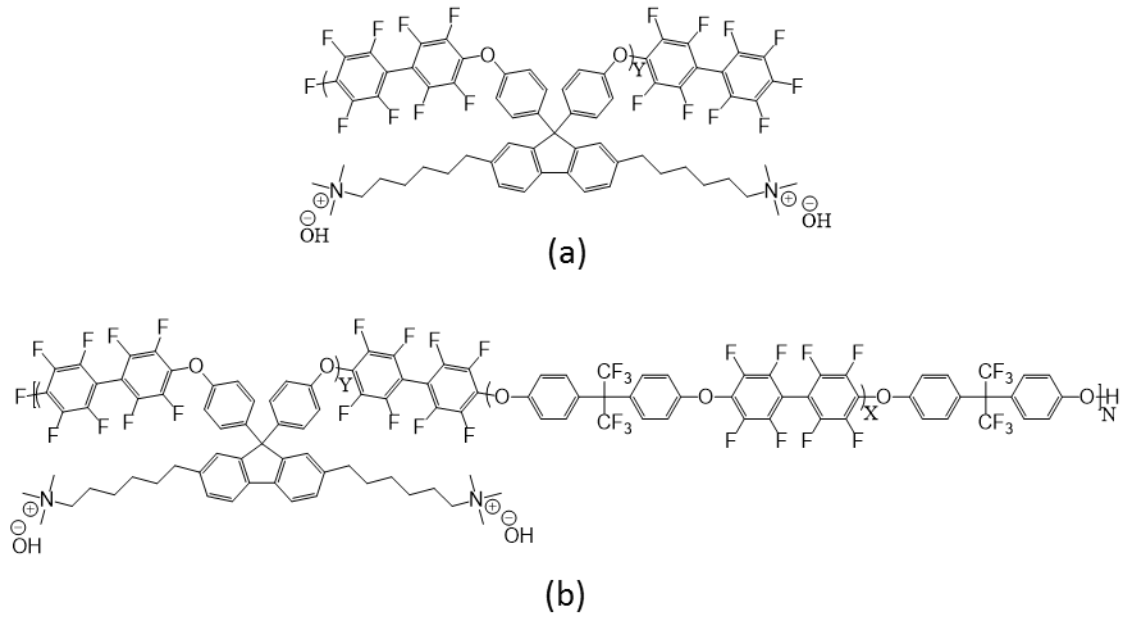

Figure 6.2 Structure of poly(aryl ether) homo- (a) and block- (b) copolymers used in this study.

Table 6.1 Description of ionomer samples.

Sample Name	Description
3k1T	3k MW hydrophilic oligomer, 1 tether
3k2T	3k MW hydrophilic oligomer, 2 tether
4k2T	4k MW hydrophilic oligomer, 2 tether
19k2T	19k MW hydrophilic oligomer, 2 tether
33k2T	33k MW hydrophilic oligomer, 2 tether
B20k1T	20k MW block copolymer, 1 tether
B20k2T	20k MW block copolymer, 2 tether

The AEM ionomers are summarized in Table 6.1. Variations of each of class of materials will be tested in-situ in both fuel cell and electrolysis devices. The homopolymers vary in molecular weight from 3 kDa – 33 kDa, and select samples also contain either 1 or 2 ionic groups per monomer in order to vary the IEC for similar samples. The sample names denote the molecular weight of each sample (i.e. 3k), the

number of tethers per monomer unit (1T or 2T), and whether it is a copolymer (indicated by B).

6.3.2 Fuel Cell Testing

The polarization curves after 20 h operation are shown in Figure 6.3 for the samples achieving the highest overall power densities, 3k1T and 4k2T. These results support the hypothesis that lower molecular weight ionomers exhibit superior performance to higher molecular weight samples, as shown in an earlier study.[72]

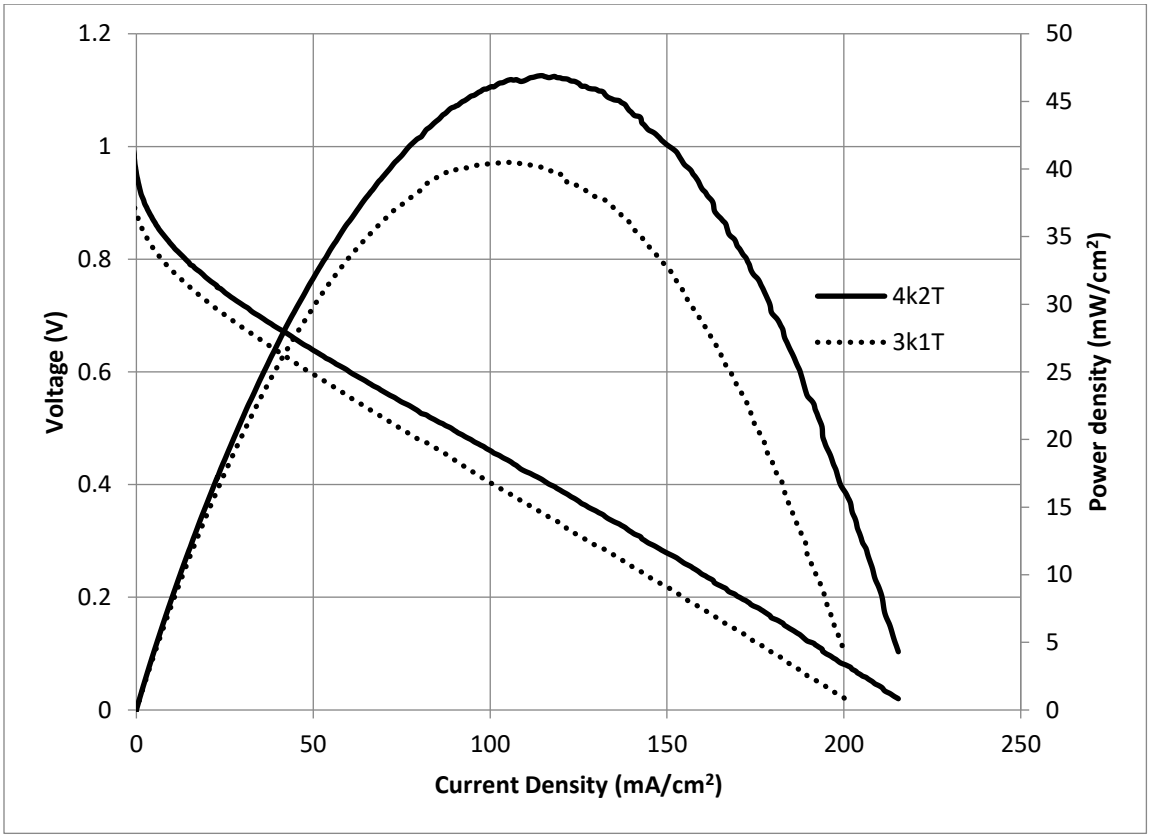

Figure 6.3 Polarization curves for the highest performing ionomers.

However, the performance does not solely correlate with ionomer molecular weight. Table 6.2 shows the peak power density (PPD) obtained from voltammetry for

each ionomer sample tested. For the oligomeric samples consisting of only the hydrophilic material, it is clear that increasing molecular weight results in decreased power output. The block copolymer sample breaks that trend, far outperforming the oligomer sample of similar molecular weight (19k2T), and in fact exhibiting power output much closer to the lower molecular weight ionomers tested.

Table 6.2 Peak power density for every ionomer sample.

Sample	Peak Power Density (mW/cm^2)
4k2T	46.9
3k1T	40.5
3k2T	38.1
B20k1T	35.9
B20k2T	33.9
19k2T	19.4
33k2T	14.7

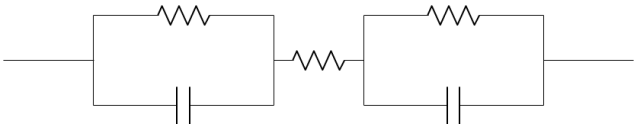

Figure 6.4 Equivalent circuit for CPE model.

To probe this result further, electrochemical impedance spectroscopy (EIS) data was collected for each device at 300 mV. The data was analyzed using a model consisting of two parallel resistance-capacitance circuit elements, one representing the anode and one representing the cathode, and a series resistance representing all other ohmic losses (Figure 6.4). The low- and high-frequency loops are attributed to the cathode and anode respectively.[73] The high-frequency intercept is the smallest total resistance collected and is taken to be the sum of the membrane ionic resistance, contact resistance with any

electrical hardware, and interfacial resistance between the electrodes and the membrane (i.e. resistive part of the two parallel RC elements). Because the same membrane and hardware was used for all devices, any detectable differences in the high-frequency intercept can be attributed to the varying interfacial quality between the electrodes and the membrane. Table 6.3 shows the high-frequency resistance at each testing interval for the samples. For the samples which have identical molecular weights but varying number of ionic head groups, the 1 tether samples showed significantly lower interfacial resistance, approximately 0.4 Ω less than their 2 tether counterparts. This may be due to the critical role the ionic density plays in the interfacing of membranes and electrodes.

Table 6.3 High-frequency intercept values (in Ω) at every testing interval.

Ionomer	PPD (mW/cm^2)	0 h	5 h	10 h	15 h	20 h
4k2T	46.9	1.37	0.83	1.01	1.01	1.03
3k1T	40.5	1.11	0.27	1.01	1.00	0.99
3k2T	38.1	3.61	1.84	1.56	1.46	1.37
B20k1T	35.9	0.87	0.86	0.83	0.83	0.84
B20k2T	33.9	1.89	1.51	0.26	0.26	1.23
19k2T	19.4	1.38	1.27	1.20	1.18	1.14
33k2T	14.7	1.97	1.82	1.84	1.88	1.89

In addition to measuring the interfacial resistance, EIS can also be used to determine the resistance within the electrode layers (i.e. ohmic resistance in each of the two RC parallel networks), typically denoted as charge transfer resistance. These data are tabulated in Table 6.4. After 20 h, the samples with smallest charge transfer resistance are those which had the highest power output. However, the block copolymer sample with 2 tethers showed consistently lower charge transfer resistance than its 1 tether counterpart, while the 3k oligomer samples showed very similar values to each other.

Table 6.4 Charge transfer resistance values (in Ω) at every testing interval.

Ionomer	PPD (mW/cm2)	0 h	5 h	10 h	15 h	20 h
4k2T	46.9	9.50	2.25	0.55	0.55	0.56
3k1T	40.5	0.73	1.09	0.68	0.63	0.66
3k2T	38.1	1.22	0.39	0.65	0.63	0.61
B20k1T	35.9	1.03	1.15	1.16	1.18	1.23
B20k2T	33.9	4.00	0.92	0.99	0.99	0.85
19k2T	19.4	2.68	3.82	3.54	3.04	2.93
33k2T	14.7	3.16	3.14	3.52	3.92	4.00

The summation of the resistances in Tables 6.3 and 6.4 provides a clear trend – the power output of each device increased as the *total* resistance decreased. The composition of the resistances may provide a blueprint to further anion conducting ionomer materials. The block copolymer sample with a single head group tether provided the lowest interfacial resistance, while lower molecular weight samples exhibited lower charge transfer resistance. For future optimization of these materials, controlled morphologies of low molecular weight polymers should provide an improvement in overall device performance.

6.3.3 Electrolyzer Testing

Results of an initial 12 h aging survey of all ionomers are shown in Figure 6.5. Long-term chronopotentiometry data is provided in Figure 6.6 for the three best performing ionomers, 3k2T, 4k2T and B20k2T. Tokuyama AS-4 data is also provided as a reference. Lower cell potential during chronopotentionmetry is indicative of a more efficient water electrolysis process (smaller overpotentials) and therefore a better performing ionomer. Among the hydrophilic oligomeric materials, lower molecular

weight materials were found to have superior performance than higher molecular weight samples. Table 6.5 shows cell potentials of all ionomer samples at 200 mA/cm2 after 12 h of constant current aging. It was found that the 2-tether versions (i.e. 2T) of these ionomers were also better performing than their 1-tether counterparts. Both of these results are consistent with what was found in fuel cell configuration.

Table 6.5 Cell potential (in V) for every ionomer sample after 12 h at 200 mA/cm^2. Samples with * did not complete the full 12 h experiment and cell potential is based on measurement just before cell failure.

Sample	Cell Potential
B20k2T	2.293
4k2T	2.443
3k2T	2.470
AS-4	2.523
3k1T	2.715
33k2T	3.304*
19k2T	4.252*

Several factors influenced which ionomer samples were down selected for extended aging. The 1-tether samples were immediately omitted from extended testing due to their inferior performance compared to the 2-tether versions during the initial performance evaluation as shown in Figure 6.5. The high molecular weight ionomer samples were also found to be unsuitable for long term testing largely due to mechanical issues with adhering the iridium oxide catalyst and the titanium GDL.

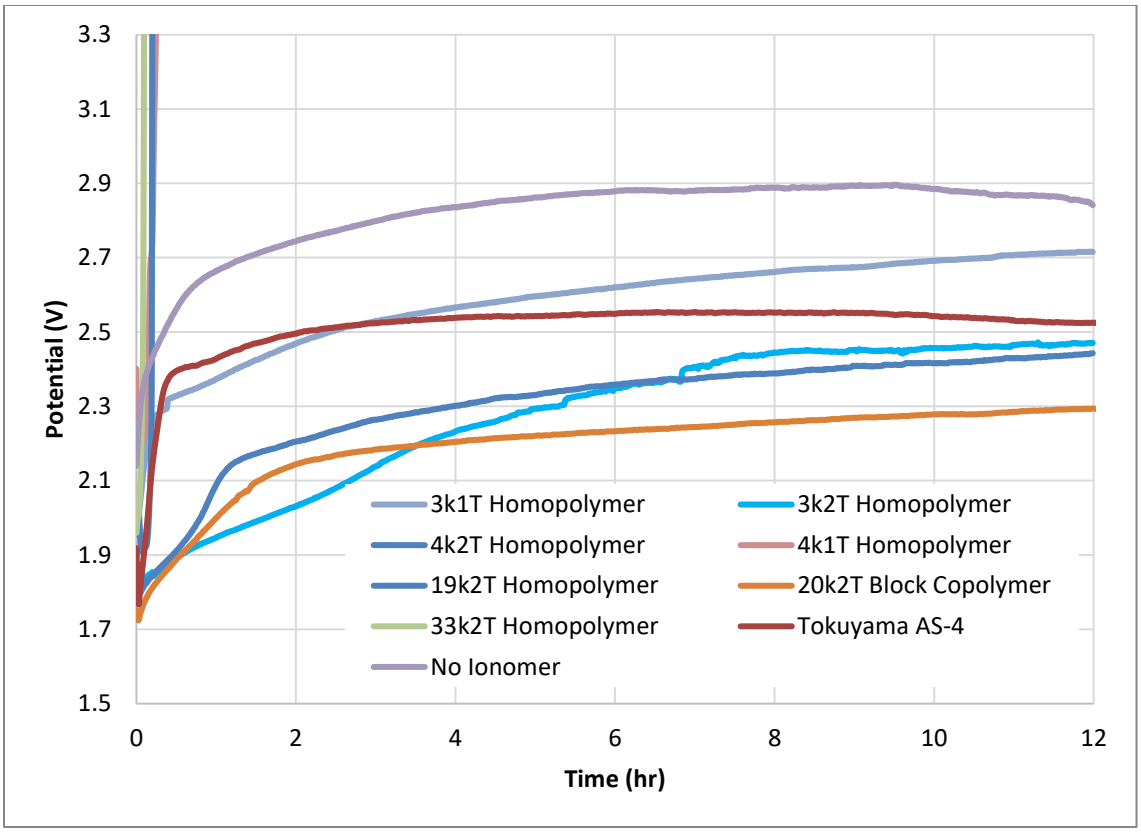

Figure 6.5 Initial 12 h survey of all ionomers.

When performing the extended aging experiments, it was found that many of the tests needed to be terminated prematurely due to the mechanical durability of the Tokuyama A201 membrane. This membrane typically formed small pin holes across the entire active area within 40-100 hours of aging which would cause short circuiting in the MEA. Therefore, the observed performance degradation of the ionomer cannot easily be deconvoluted from the effects of the short circuiting. This is most relevant to the block copolymer sample which was not aged to the same extent as the other ionomer samples for this reason. Nevertheless, this material outperformed all of the other ionomers, including the commercial ionomer AS-4. It should be noted that it is unlikely that degradation of the ionomer is the cause of these abbreviated experiments. These materials

have all been demonstrated to be stable at this time scale in alkaline conditions in a previous study.[65]

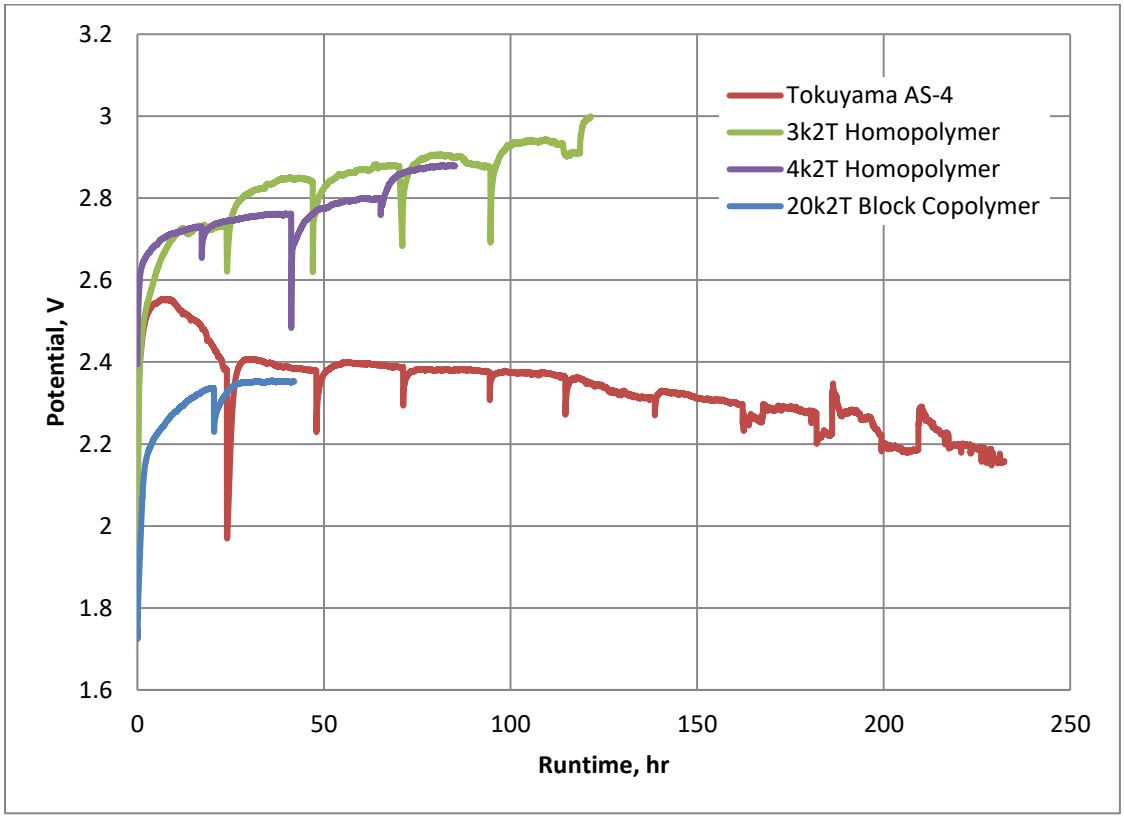

Figure 6.6 Extended aging data for the highest performing ionomers. Discontinuities in potential indicate when chronopotentiometry experiment was interrupted to perform EIS and voltammetry measurements.

Electrochemical impedance spectroscopy (EIS) data was collected for the top performing cells approximately every 24 h throughout the duration of each experiment. As in the fuel cell experiments above, the same membrane and hardware was used for all devices, therefore any detectable differences in the high-frequency intercept can be attributed to the varying interfacial quality between the electrodes and the membrane.

Table 6.6 shows the high-frequency resistance for the first 48 h of testing for the high performing samples.

Table 6.6 High-frequency intercept values (in Ω-cm^2) through the first 48 h of testing.

Ionomer	0 h	24 h	48 h	Cell Potential (V @ 200 mA/cm^2 after 48 h)
B20k2T	0.445	2.290	3.193	2.352
AS-4	0.422	0.930	2.022	2.383
4k2T	0.611	2.214	2.120	2.689
3k2T	0.448	2.259	2.557	2.845

There was little discernable difference among interfacial resistances of the best performing cells through the first 48 h of experimentation, prompting us to investigate the resistance within the electrode layers. This is typically referred to as the charge transfer resistance and can be extracted from the EIS data using an appropriate model. For a system with two different time constants, a first approximation can attribute each to an electrode process: the hydrogen evolution reaction (HER) at the cathode and the oxygen evolution reaction (OER) at the anode.[74] The experimental impedance measured in this study have been modeled using a resistor and two constant phase elements (CPE) connected in series to approximate the interfacial resistances and each electrode charge transfer resistance, respectively (Figure 6.4). The difficulty with this approach is that for a non-ideally polarized electrode with irreversible uniform charge transfer, the CPE is coupled not only to the solution resistance but also the charge-transfer resistance (or more generally to the faradaic impedance), if it is caused by heterogeneity of the electrode surface.[75] For these reasons, our model was not able to definitively assign resistance contributions to each electrode process. Still, the low-frequency intercept of the EIS data,

should provide some insight as it is determined by the collective contributions of the charge transfer resistances as well as the interfacial resistances. To our knowledge, this level of EIS analysis has not been widely reported on AEM electrolysis cells. However, our results in Table 6.7 clearly show that the cells with the lowest charge transfer resistance are unsurprisingly also the cells that performed the best through 48 h of testing. Table 6.8 shows the difference of the low-frequency and high-frequency value, which would normally be a measure of the charge transfer resistance assuming ideal behavior.

Table 6.7 Low-frequency intercept values (in Ω-cm^2) through the first 48 hours of testing.

Ionomer	0 h	24 h	48 h	Cell Potential (V @ 200 mA/cm^2 after 48 h)
B20k2T	1.090	8.711	11.080	2.352
AS-4	1.504	2.619	9.305	2.383
4k2T	2.316	25.715	25.183	2.689
3k2T	1.618	23.988	27.192	2.845

Table 6.8 Charge transfer resistance values (in Ω-cm^2) through the first 48 hours of testing.

Ionomer	0 h	24 h	48 h	Cell Potential (V @ 200 mA/cm^2 after 48 h)
B20k2T	0.645	6.421	7.887	2.352
AS-4	1.082	1.689	7.283	2.383
4k2T	1.705	23.501	23.063	2.689
3k2T	1.170	21.729	24.635	2.845

Comparing the low-frequency resistances of the two best performing materials, the commercial ionomer Tokuyama AS-4 had the lowest measured charge transfer

resistance yet it still did not perform as well as the block copolymer ionomer. We believe that the introduction of a hydrophobic block promotes systematic phase segregation, which allows the hydrophilic block to create more efficient ion conduction and gas diffusion channels. From this it can be inferred that the electrolyte wetting of the 3-dimensional interfacial area in the gas diffusion electrode is increased, thereby reducing mass transfer resistances and improving the overall cell performance. For future optimization of these materials, an investigation of the specific morphologies of block copolymers should drive improvement in device performance.

6.4 Conclusions

In this work, a new set of anionic conductive ionomers was tested for its viability in both oxygen consuming (fuel cell) and oxygen producing (electrolysis) electrodes. The two sets of results show similar trends – for a homopolymer, lower molecular weight materials provide superior performance compared to their higher molecular weight counterparts. Additionally, the introduction of phase segregation via block copolymer further increased performance in both types of devices. Future work on optimizing anionic ionomer materials in oxygen-based electrodes should be focused on reducing the molecular weight of phase segregated materials in order to optimize ionomeric performance.

CHAPTER 7. CONCLUSIONS AND FUTURE WORK

7.1 General conclusions

Multiblock copolymers with partial fluorination and long head-group tethers was designed to improve the ionic conductivity, the alkaline stability, and lower water uptake of AEMs. A systematic study of the effect of the hydrophilic and hydrophobic block lengths and ion exchange capacity of partially fluorinated multiblock copolymer mPEs with long head-group tethers was undertaken to explore the relationship of the chemical structure, morphology and properties of the AEMs. The formation of ion conductive nano-channels for hydroxide ion transport due to nanophase separation of the multiblock copolymers greatly improved the ionic conductivity and reduced the water uptake. Multiblock copolymer mPE-$X_{5.4}Y_7$-2 showed the highest ionic conductivity, 119 mS/cm at 80 ℃, but not the highest IEC, because it formed efficient channels. Partial fluorination of the polymer backbone was used to lower water uptake of the membrane by increasing the hydrophobicity. From DSC measurements of the number of freezable water and bound water molecules, the number of bound water molecules per ion of two-tether polymers was 4.5 to 5. In addition, the bound water played the dominant role in the hydroxide ion transport within the channels. The multiblock copolymer AEM showed good thermal, mechanical stability and excellent alkaline stability. Long head-group tether was used to improve the chemical stability of the membrane at high pH, as this structure prevents several possible degradation mechanisms of the commonly used benzylic structure. The ionic conductivity was hardly changed after soaking the membrane in 1 M NaOH solution at 60 ℃ for 1000 h. The mPEs AEM with higher ionic

conductivity showed lower oxygen diffusivity and permeability, which means that the oxygen crossover problem was less severe.

Second, the effect of the number of ionic groups in the hydrophilic segment on the morphology and properties of AEMs was studied. Multiblock copoly(arylene ether)s (mPEs) were synthesized with different ion exchange capacity (IEC) by attaching a different number of cationic head-groups via long alkyl chain tethers. The multiblock copolymer mPEs with 1, 2, 3 and 4 long alkyl chain tethered ionic groups on each repeat unit in hydrophilic block, resulting in different IECs, were compared. Only one head-group tether can be attached on each hydrophilic repeat unit at a time. Thus, the tether amount can be precisely controlled. As the ionic concentration increased, the ionic conductivity and water uptake of the membranes increased. This was due to the increase of the size of ion conductive channels. 3-tether membrane showed the highest ionic conductivity/IEC, which means that its ionic groups were most efficient for contributing to the ionic conductivity. In addition, the number of freezable and non-freezable water molecules were investigated. 2, 3, 4-tether membrane showed similar number of bound water, while the number of freezable water increased with the number of ionic groups. The excess freezable water led to high water uptake and low ionic conductivity/IEC ratio. Therefore, 3-tether membrane showed the best properties, 130.6 mS/cm ionic conductivity and 58.3% water uptake, with an IEC of 1.83 meq/g. As the number of ion groups increased, the mechanical strength of the membranes declined.

Third, the effect of the cationic groups (*i.e.* size, central atom, *etc.*) was investigated. Multiblock copoly(arylene ether)s (mPEs) with partial fluorination and two long alkyl head-group tethers on each hydrophilic repeat unit with quaternary trimethyl

mmonium (TMHA), quinuclidium (ABCO), and tris(2,4,6-trimethoxyphenyl)phosphonium (TTMPP) were synthesized. Their morphology and properties (*i.e.* ionic conductivity, water uptake, alkaline stability, mechanical and thermal properties) were compared in order to understand the effects of the size and type of cations on the morphology and physical properties. A larger cation led to larger ion channels. However, larger cation also caused lower IEC and consequently lower ionic conductivity despite the channel size of the cation. Quinuclidium showed low water uptake with a lower number of bound water for each ion pair. Tris(2,4,6-trimethoxyphenyl)phosphonium showed high water uptake due to a large number of bound water. TMHA is the most stable cation after exposure to 1 M NaOH solution at 60 ℃ after 30 days, while quinuclidium showed a 22% ionic conductivity loss due to high hydroxide ion concentration in the local area of ionic groups caused by low bound water content. TMHA also had the best mechanical properties, while phosphonium was the poorest. Therefore, alkyl trimethylammonium appears to be the best cation head group among the three cations studied for this backbone. In addition, the membrane preparation method impacts the morphology and properties of the AEMs. Quaternization before membrane casting resulted in better properties than quaternization after membrane casting due to greater phase segregation.

Lastly, a series of anionic ionomers was synthesized and tested in fuel cells and electrolyzers. These ionomers are based on a series of materials which include block copolymer AEMs with alkyl tethers that have been modified to be used as anion conductors. The ionomers were tested for their viability as anion conductors in the cathodic electrode for the cathode hybrid fuel cell and as the anodic electrode of an

alkaline electrolyzer. In this case, the selected materials will be evaluated in both oxygen-consuming (*i.e.* oxygen reduction reaction (ORR)) and oxygen-producing electrodes (*i.e.* oxygen evolution reaction (OER)). The two sets of results show similar trends: for a homopolymer, lower molecular weight materials provide superior performance compared to their higher molecular weight counterparts. Additionally, the introduction of phase segregation via block copolymer further increased performance in both types of devices.

7.2 Suggested future works

7.2.1 Hydro-carbon backbone structure

As discussed in Chapter 1.2, chemical stability of anion exchange membranes at high pH is one of the most crucial obstacles to its wide application in electrochemical devices. Polymer backbone stability is of vital importance of AEM alkaline stability. Various polymer backbone structures including polyphenylenes,[41] poly(phenylene oxide)s,[28, 42] poly(arylene ether sulfone)s,[40] and poly(arylene ether)s[44] have been used, and their alkaline stability and degradation mechanism have also been investigated.

Recent study indicates that polymer backbones with only hydrocarbon structure, which gets rid of any aryl ether, sulfone, or ketone groups, show excellent alkaline stability at 80 °C without any reported IEC or ionic conductivity loss and any degradation from NMR analysis. Lee et al.[26] synthesized fluorene-based AEMs with only hydrocarbon structures in polymer backbone, which showed excellent alkaline stability and no structural change from NMR analysis after soaking in 1 M NaOH solution at 80 °C for 30 days. Mohanty et al.[76] prepared polystyrene-*b*-poly(ethylene-*co*-butylene)-*b*-polystyrene (SEBS) triblock copolymer based elastomeric AEMs with benzyl- and alkyl-

substituted quaternary ammonium groups for fuel cell applications. Their results showed that after 4 weeks in 1 M NaOH at 80 ℃, the membranes remained chemically stable. In addition to good chemical stability in alkaline media owing to its absence of aryl ether bonds, SEBS also provide good mechanical properties with its rubbery ethylene-butylene block and enhanced ion conductivity via nano-phase segregation of its block copolymer structure. A perfluorinated anion exchange membrane[77], which has similar backbone structure as Nafion, was also reported with excellent chemical stability. Other hydro-carbon backbone structures, such as polypropylene[53] and polyethylene[73], were also reported to exhibit excellent alkaline stability.

Therefore, hydro-carbon backbone structure is highly recommended. Some possible candidates can be considered in the future, including poly(norbornene), poly(styrene-ethylene-butylene-styrene) (SEBS), etc.

7.2.2 Long alkyl side chain tethered quaternary trimethylammonium or aliphatic-heterocyclic quaternary ammonium cations

Apart from polymer backbone stability, cationic group stability is another important issue of AEM materials. Quaternary ammoniums are still the most commonly employed cationic groups. The quaternary benzyl trimethyl ammonium (BTMA) is widely acknowledged as the benchmark, but it has been reported to be unstable under alkaline condition at high pH.

However, long alkyl side chain tethered trimethylammonium groups have demonstrated superior alkaline stability. This has been demonstrated in Chapter 3 in this work. In addition, Bae and co-workers[27] analyzed the byproducts after degradation of a

variety of cationic groups attached on small molecule benzene via NMR. They reported that TMHA (hexyl chain tethered trimethyl ammonium) showed the greatest stability after alkaline degradation under 60 ℃ and 120 ℃, which was much better than the well-known BTMA. This long alkyl side chain structure also facilitates the phase segregation of the polymers, which improves the formation of the ion-conducting channels within the membrane. Dang and co-workers[28] showed that a five-carbon tether performed the best by comparing different cationic alkyl side chain designs. Therefore, such long alkyl tethered quaternary trimethyl ammonium structure is highly recommended in future structure design.

Aliphatic-heterocyclic quaternary ammonium cationic groups have also attracted a lot of interests recently, as these structures contain β-H with the C-C bond rotationally restricted by the ring geometry which may provide good alkaline stability. Varcoe and co-workers[78] compared the stability of AEMs with various cycloaliphatic benzyl quaternary ammonium groups, and it turned out that the N-methylpiperidinium and N-methylpyrrolidium showed better alkaline stability than BTMA. Especially, N-methylpyrrolidium AEM exhibited the highest relative chemical stability, conductivity, and *in situ* fuel cell performance. However, this work used the benzylic linkage between the polymer backbone and the head groups, which may be attacked by hydroxide ions. Therefore, long alkyl chain tethered N-methylpyrrolidium head-group structure is recommended for future work. Dang et al.[79] reported that poly(phenylene oxide)s carrying quaternary piperidinium cations via a hexyl-tether exhibited very high ionic conductivity (up to 69 and 186 mS/cm at 20 and 80 ℃) and no degradation from NMR analysis after storage in 1 M NaOH at 90 ℃ during 8 days. Lin et al.[80] also reported a

triblock copolymer with the long alkyl chain tethered quaternary N-methylpiperidinium groups showed ionic conductivity up to 105 mS/cm at 80 ℃ and high retention of hydroxide conductivity (88.9%) and IEC (91.2%) after storage in 1 M KOH solution at 80 ℃ for 480 h.

In summary, it is recommended that long alkyl chain tethered quaternary ammonium groups, either trimethylammonium or cycloaliphatic quaternary ammonium (N-methylpiperidinium and N-methylpyrrolidium), are used for excellent ionic conductivity and alkali stability in future work. Combining the hydro-carbon backbone and these cation groups will provide AEM materials with superior alkaline stability while retaining high ionic conductivity, which will promote the wide commercialization of AEM materials.

7.2.3 Strong mechanical strengths and dimensional stability of AEMs from cross-linking and interpenetrating network

Strong mechanical properties and dimensional stability are highly desired for anion exchange membranes. Mechanical stability of AEMs is essential during the membrane fabrication process and device operation since a pressure difference usually exists between the two electrodes. Traditionally, the preparation of AEMs is usually based on post-modification of pristine polymers, followed by quaternization via immersing the membranes into a trimethylamine aqueous solution. Membranes made this way usually do not exhibit enough mechanical strengths.

Cross-linking has been widely used for preparing AEMs with improved dimensional stability. The most common cross-linking strategy is connecting polymer

matrix using cross-linkers such as diols, dihalides, diamine and hydrazoate.[81-82] Lin et al.[83] presented a strategy for preparing crosslinked AEMs without using catalyst and the crosslinked moiety is away from the ionic domain in order not to affect the ionic conductivity. The crosslinking was carried out by converting the trifluorovinyl groups into perfluorocyclobutane groups via thermal treatment. Lai et al.[84] enhanced dimensional stability of AEMs via cross-linking of ion cluster regions. Click reaction was also reported to be used for end-group cross-linking for anion exchange membranes. It has been shown that cross-linking is effective in enhancing the mechanical strengths of AEMs, the ionic conductivity of these membranes, however, may be confined due to the tortuous ionic channels.

Interpenetrating polymer networks (IPNs) or semi interpenetrating polymer networks (sIPNs), as shown in Figure 7.1, are used to improve the mechanical strengths and dimensional stability of AEMs. IPNs are unique class of polymer alloys, consisting of two or more cross-linked polymers with no covalent bonds or grafts between them. sIPNs are polymeric composites obtained by interpenetrating of a linear or branched polymer within a network of another covalent cross-linked polymer.[11] IPNs and sIPNs possess excellent electrochemical and mechanical properties since the aggregation of hydrophilic and hydrophobic polymer segments may induce dual-phase continuity structure. Meanwhile, the unique dynamically forced compatibility feature of IPNs could decrease macro-phase segregation between different polymer components in the membranes to provide dimensional stability.[85] However, the ionic conductivity of the membranes may be limited due to the tight interlock of polymer chains feature restricting the flexibility of polymer chains and ion clusters aggregation.

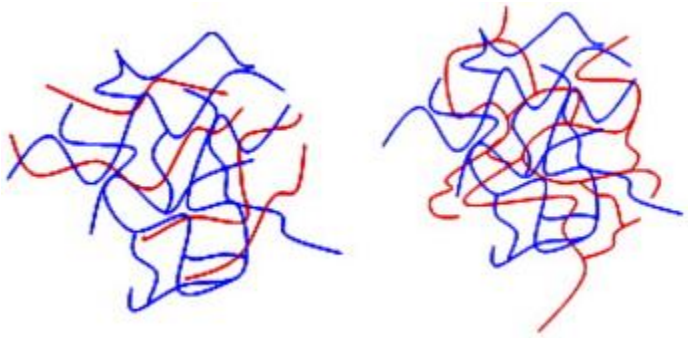

Figure 7.1 Sketch of a semi-interpenetrated polymer network (left) and an interpenetrated polymer network (right).[11]

Lin et al.[85] prepared the thermoplastic interpenetrating polymer network (TIPN) anion exchange membranes (AEMs) based on poly [2,2'-(p-oxydiphenylene)-5,5'-bibenzimidazole] (OPBI) and poly(1,2-dimethy-3-allylimidazolium) (PDAIm) (PBI/DAIm TIPN) with DAIm polymerization in presence of OPBI polymer chains. Two kinds of uncrosslinked polymer chains (i.e. PDAIm and OPBI) interpenetrate with each other to form a physically crosslinking network, which provided the AEM with low swelling ratio (4.4%) and high tensile strength (48.2 MPa).

In summary, cross-linking and interpenetrating polymer network are two effective methods to improve the mechanical strength and dimensional stability of anion exchange membranes with certain degree of sacrifice of ionic conductivity. High IEC polymeric AEMs are strongly recommended to incorporate these methods to achieve an excellent combination of electrochemical and mechanical properties.

REFERENCES

1. Steele, B. C. H.; Heinzel, A., Materials for fuel-cell technologies. *Nature* **2001,** *414* (6861), 345-352.

2. Varcoe, J. R.; Atanassov, P.; Dekel, D. R.; Herring, A. M.; Hickner, M. A.; Kohl, P. A.; Kucernak, A. R.; Mustain, W. E.; Nijmeijer, K.; Scott, K.; Xu, T.; Zhuang, L., Anion-exchange membranes in electrochemical energy systems. *Energy & Environmental Science* **2014,** *7* (10), 3135-3191.

3. Li, N.; Guiver, M. D., Ion Transport by Nanochannels in Ion-Containing Aromatic Copolymers. *Macromolecules* **2014,** *47* (7), 2175-2198.

4. Leng, Y.; Chen, G.; Mendoza, A. J.; Tighe, T. B.; Hickner, M. A.; Wang, C.-Y., Solid-State Water Electrolysis with an Alkaline Membrane. *Journal of the American Chemical Society* **2012,** *134* (22), 9054-9057.

5. Zeng, K.; Zhang, D., Recent progress in alkaline water electrolysis for hydrogen production and applications. *Progress in Energy and Combustion Science* **2010,** *36* (3), 307-326.

6. Alotto, P.; Guarnieri, M.; Moro, F., Redox flow batteries for the storage of renewable energy: A review. *Renewable and Sustainable Energy Reviews* **2014,** *29*, 325-335.

7. Vermaas, D. A.; Veerman, J.; Yip, N. Y.; Elimelech, M.; Saakes, M.; Nijmeijer, K., High Efficiency in Energy Generation from Salinity Gradients with Reverse Electrodialysis. *ACS Sustainable Chemistry & Engineering* **2013,** *1* (10), 1295-1302.

8. Peighambardoust, S. J.; Rowshanzamir, S.; Amjadi, M., Review of the proton exchange membranes for fuel cell applications. *International Journal of Hydrogen Energy* **2010,** *35* (17), 9349-9384.

9. Hickner, M. A.; Herring, A. M.; Coughlin, E. B., Anion exchange membranes: Current status and moving forward. *Journal of Polymer Science Part B: Polymer Physics* **2013,** *51* (24), 1727-1735.

10. Merle, G.; Wessling, M.; Nijmeijer, K., Anion exchange membranes for alkaline fuel cells: A review. *Journal of Membrane Science* **2011,** *377* (1–2), 1-35.

11. Couture, G.; Alaaeddine, A.; Boschet, F.; Ameduri, B., Polymeric materials as anion-exchange membranes for alkaline fuel cells. *Progress in Polymer Science* **2011,** *36* (11), 1521-1557.

12. Varcoe, J. R.; Slade, R. C. T., Prospects for Alkaline Anion-Exchange Membranes in Low Temperature Fuel Cells. *Fuel Cells* **2005,** *5* (2), 187-200.

13. Schiller, G.; Henne, R.; Mohr, P.; Peinecke, V., High performance electrodes for an advanced intermittently operated 10-kW alkaline water electrolyzer. *International Journal of Hydrogen Energy* **1998,** *23* (9), 761-765.

14. Rasten, E.; Hagen, G.; Tunold, R., Electrocatalysis in water electrolysis with solid polymer electrolyte. *Electrochimica Acta* **2003,** *48* (25–26), 3945-3952.

15. Wei, G.; Wang, Y.; Huang, C.; Gao, Q.; Wang, Z.; Xu, L., The stability of MEA in SPE water electrolysis for hydrogen production. *International Journal of Hydrogen Energy* **2010,** *35* (9), 3951-3957.

16. Manolova, M.; Schoeberl, C.; Freudenberger, R.; Ellwein, C.; Kerres, J.; Stypka, S.; Oberschachtsiek, B., Development and testing of an anion exchange membrane electrolyser. *International Journal of Hydrogen Energy* **2015,** *40* (35), 11362-11369.

17. Parrondo, J.; Arges, C. G.; Niedzwiecki, M.; Anderson, E. B.; Ayers, K. E.; Ramani, V., Degradation of anion exchange membranes used for hydrogen production by ultrapure water electrolysis. *RSC Advances* **2014,** *4* (19), 9875-9879.

18. Energy, U. S. D. o. *Integration and Optimization of Novel Ion Conducting Solids (Ionics)*; 2016.

19. Zhou, J.; Joseph, K.; Ahlfield, J. M.; Park, D.-Y.; Kohl, P. A., Poly(arylene ether) Ionomers with Pendant Quinuclidium Groups and Varying Molecular Weight for Alkaline Electrodes. *Journal of The Electrochemical Society* **2013,** *160* (6), F573-F578.

20. Zhang, Z.; Chalkova, E.; Fedkin, M.; Wang, C.; Lvov, S. N.; Komarneni, S.; Chung, T. C. M., Synthesis and Characterization of Poly(vinylidene fluoride)-g-sulfonated Polystyrene Graft Copolymers for Proton Exchange Membrane. *Macromolecules* **2008,** *41* (23), 9130-9139.

21. Chempath, S.; Einsla, B. R.; Pratt, L. R.; Macomber, C. S.; Boncella, J. M.; Rau, J. A.; Pivovar, B. S., Mechanism of Tetraalkylammonium Headgroup Degradation in Alkaline Fuel Cell Membranes. *The Journal of Physical Chemistry C* **2008,** *112* (9), 3179-3182.

22. Chempath, S.; Boncella, J. M.; Pratt, L. R.; Henson, N.; Pivovar, B. S., Density Functional Theory Study of Degradation of Tetraalkylammonium Hydroxides. *The Journal of Physical Chemistry C* **2010,** *114* (27), 11977-11983.

23. Long, H.; Kim, K.; Pivovar, B. S., Hydroxide Degradation Pathways for Substituted Trimethylammonium Cations: A DFT Study. *The Journal of Physical Chemistry C* **2012,** *116* (17), 9419-9426.

24. Edson, J. B.; Macomber, C. S.; Pivovar, B. S.; Boncella, J. M., Hydroxide based decomposition pathways of alkyltrimethylammonium cations. *Journal of Membrane Science* **2012,** *399-400* (Supplement C), 49-59.

25. Sata, T.; Tsujimoto, M.; Yamaguchi, T.; Matsusaki, K., Change of anion exchange membranes in an aqueous sodium hydroxide solution at high temperature. *Journal of Membrane Science* **1996,** *112* (2), 161-170.

26. Lee, W.-H.; Mohanty, A. D.; Bae, C., Fluorene-Based Hydroxide Ion Conducting Polymers for Chemically Stable Anion Exchange Membrane Fuel Cells. *ACS Macro Letters* **2015,** *4* (4), 453-457.

27. Mohanty, A. D.; Bae, C., Mechanistic analysis of ammonium cation stability for alkaline exchange membrane fuel cells. *Journal of Materials Chemistry A* **2014,** *2* (41), 17314-17320.

28. Dang, H.-S.; Jannasch, P., Exploring Different Cationic Alkyl Side Chain Designs for Enhanced Alkaline Stability and Hydroxide Ion Conductivity of Anion-Exchange Membranes. *Macromolecules* **2015,** *48* (16), 5742-5751.

29. Jannasch, P.; Weiber, E. A., Configuring Anion-Exchange Membranes for High Conductivity and Alkaline Stability by Using Cationic Polymers with Tailored Side Chains. *Macromolecular Chemistry and Physics* **2016,** *217* (10), 1108-1118.

30. Komkova, E. N.; Stamatialis, D. F.; Strathmann, H.; Wessling, M., Anion-exchange membranes containing diamines: preparation and stability in alkaline solution. *Journal of Membrane Science* **2004,** *244* (1), 25-34.

31. Tomoi, M.; Yamaguchi, K.; Ando, R.; Kantake, Y.; Aosaki, Y.; Kubota, H., Synthesis and thermal stability of novel anion exchange resins with spacer chains. *Journal of Applied Polymer Science* **1997,** *64* (6), 1161-1167.

32. Gu, F.; Dong, H.; Li, Y.; Si, Z.; Yan, F., Highly Stable N3-Substituted Imidazolium-Based Alkaline Anion Exchange Membranes: Experimental Studies and Theoretical Calculations. *Macromolecules* **2013,** *47* (1), 208-216.

33. Gu, S.; Cai, R.; Luo, T.; Jensen, K.; Contreras, C.; Yan, Y., Quaternary Phosphonium-Based Polymers as Hydroxide Exchange Membranes. *ChemSusChem* **2010,** *3* (5), 555-558.

34. Sajjad, S. D.; Hong, Y.; Liu, F., Synthesis of guanidinium-based anion exchange membranes and their stability assessment. *Polymers for Advanced Technologies* **2014,** *25* (1), 108-116.

35. Rao, A. H. N.; Thankamony, R. L.; Kim, H.-J.; Nam, S.; Kim, T.-H., Imidazolium-functionalized poly(arylene ether sulfone) block copolymer as an anion exchange membrane for alkaline fuel cell. *Polymer* **2013,** *54* (1), 111-119.

36. Rao, A. H. N.; Nam, S.; Kim, T.-H., Comb-shaped alkyl imidazolium-functionalized poly(arylene ether sulfone)s as high performance anion-exchange membranes. *Journal of Materials Chemistry A* **2015,** *3* (16), 8571-8580.

37. Kim, D. S.; Fujimoto, C. H.; Hibbs, M. R.; Labouriau, A.; Choe, Y.-K.; Kim, Y. S., Resonance Stabilized Perfluorinated Ionomers for Alkaline Membrane Fuel Cells. *Macromolecules* **2013,** *46* (19), 7826-7833.

38. Ran, J.; Wu, L.; Varcoe, J. R.; Ong, A. L.; Poynton, S. D.; Xu, T., Development of imidazolium-type alkaline anion exchange membranes for fuel cell application. *Journal of Membrane Science* **2012,** *415–416*, 242-249.

39. Zhang, Q.; Li, S.; Zhang, S., A novel guanidinium grafted poly(aryl ether sulfone) for high-performance hydroxide exchange membranes. *Chemical Communications* **2010,** *46* (40), 7495-7497.

40. Park, D.-Y.; Kohl, P. A.; Beckham, H. W., Anion-Conductive Multiblock Aromatic Copolymer Membranes: Structure–Property Relationships. *The Journal of Physical Chemistry C* **2013,** *117* (30), 15468-15477.

41. Hibbs, M. R., Alkaline stability of poly(phenylene)-based anion exchange membranes with various cations. *Journal of Polymer Science Part B: Polymer Physics* **2013,** *51* (24), 1736-1742.

42. Yang, Z.; Zhou, J.; Wang, S.; Hou, J.; Wu, L.; Xu, T., A strategy to construct alkali-stable anion exchange membranes bearing ammonium groups via flexible spacers. *Journal of Materials Chemistry A* **2015,** *3* (29), 15015-15019.

43. Weiber, E. A.; Meis, D.; Jannasch, P., Anion conducting multiblock poly(arylene ether sulfone)s containing hydrophilic segments densely functionalized with quaternary ammonium groups. *Polymer Chemistry* **2015,** *6* (11), 1986-1996.

44. Shimada, M.; Shimada, S.; Miyake, J.; Uchida, M.; Miyatake, K., Anion conductive aromatic polymers containing fluorenyl groups: Effect of the position and number of ammonium groups. *Journal of Polymer Science Part A: Polymer Chemistry* **2016,** *54* (7), 935-944.

45. Fujimoto, C.; Kim, D.-S.; Hibbs, M.; Wrobleski, D.; Kim, Y. S., Backbone stability of quaternized polyaromatics for alkaline membrane fuel cells. *Journal of Membrane Science* **2012,** *423–424*, 438-449.

46. Nuñez, S. A.; Hickner, M. A., Quantitative 1H NMR Analysis of Chemical Stabilities in Anion-Exchange Membranes. *ACS Macro Letters* **2013,** *2* (1), 49-52.

47. Sturgeon, M. R.; Macomber, C. S.; Engtrakul, C.; Long, H.; Pivovar, B. S., Hydroxide based Benzyltrimethylammonium Degradation: Quantification of Rates and Degradation Technique Development. *Journal of The Electrochemical Society* **2015,** *162* (4), F366-F372.

48. Pan, J.; Chen, C.; Li, Y.; Wang, L.; Tan, L.; Li, G.; Tang, X.; Xiao, L.; Lu, J.; Zhuang, L., Constructing ionic highway in alkaline polymer electrolytes. *Energy & Environmental Science* **2014,** *7* (1), 354-360.

49. Dorenbos, G.; Morohoshi, K., Chain architecture dependence of pore morphologies and water diffusion in grafted and block polymer electrolyte fuel cell membranes. *Energy & Environmental Science* **2010,** *3* (9), 1326-1338.

50. Tanaka, M.; Fukasawa, K.; Nishino, E.; Yamaguchi, S.; Yamada, K.; Tanaka, H.; Bae, B.; Miyatake, K.; Watanabe, M., Anion Conductive Block Poly(arylene ether)s: Synthesis, Properties, and Application in Alkaline Fuel Cells. *Journal of the American Chemical Society* **2011,** *133* (27), 10646-10654.

51. Li, L.; Yue, X.; Wu, W.; Yan, W.; Zeng, M.; Zhou, Y.; Liao, S.; Li, X., Multi-block copolymers with fluorene-containing hydrophilic segments densely functionalized by side-chain quaternary ammonium groups as anion exchange membranes. *RSC Advances* **2016,** *6* (47), 41453-41464.

52. Lai, A. N.; Wang, L. S.; Lin, C. X.; Zhuo, Y. Z.; Zhang, Q. G.; Zhu, A. M.; Liu, Q. L., Phenolphthalein-based Poly(arylene ether sulfone nitrile)s Multiblock Copolymers As Anion Exchange Membranes for Alkaline Fuel Cells. *ACS Applied Materials & Interfaces* **2015,** *7* (15), 8284-8292.

53. Zhang, M.; Liu, J.; Wang, Y.; An, L.; Guiver, M. D.; Li, N., Highly stable anion exchange membranes based on quaternized polypropylene. *Journal of Materials Chemistry A* **2015,** *3* (23), 12284-12296.

54. Lee, W.-H.; Kim, Y. S.; Bae, C., Robust Hydroxide Ion Conducting Poly(biphenyl alkylene)s for Alkaline Fuel Cell Membranes. *ACS Macro Letters* **2015,** *4* (8), 814-818.

55. Karlsson, L. E.; Wesslén, B.; Jannasch, P., Water absorption and proton conductivity of sulfonated acrylamide copolymers. *Electrochimica Acta* **2002,** *47* (20), 3269-3275.

56. Wu, X.; He, G.; Gu, S.; Hu, Z.; Yan, X., The state of water in the series of sulfonated poly (phthalazinone ether sulfone ketone) (SPPESK) proton exchange membranes. *Chemical Engineering Journal* **2010,** *156* (3), 578-581.

57. Kim, D. S.; Park, H. B.; Jang, J. Y.; Lee, Y. M., Synthesis of sulfonated poly(imidoaryl ether sulfone) membranes for polymer electrolyte membrane fuel cells. *Journal of Polymer Science Part A: Polymer Chemistry* **2005,** *43* (22), 5620-5631.

58. Hwang, B.-J.; Joseph, J.; Zeng, Y.-Z.; Lin, C.-W.; Cheng, M.-Y., Analysis of states of water in poly (vinyl alcohol) based DMFC membranes using FTIR and DSC. *Journal of Membrane Science* **2011,** *369* (1), 88-95.

59. Lu, Z.; Polizos, G.; Macdonald, D. D.; Manias, E., State of Water in Perfluorosulfonic Ionomer (Nafion 117) Proton Exchange Membranes. *Journal of The Electrochemical Society* **2008,** *155* (2), B163-B171.

60. Lue, S. J.; Shieh, S.-J., Water States in Perfluorosulfonic Acid Membranes Using Differential Scanning Calorimetry. *Journal of Macromolecular Science, Part B* **2009,** *48* (1), 114-127.

61. Mecheri, B.; Felice, V.; Zhang, Z.; D'Epifanio, A.; Licoccia, S.; Tavares, A. C., DSC and DVS Investigation of Water Mobility in Nafion/Zeolite Composite Membranes for Fuel Cell Applications. *The Journal of Physical Chemistry C* **2012,** *116* (39), 20820-20829.

62. Moster, A. L.; Mitchell, B. S., Hydration and proton conduction in Nafion/ceramic nanocomposite membranes produced by solid-state processing of powders from mechanical attrition. *Journal of Applied Polymer Science* **2009,** *113* (1), 243-250.

63. Nicotera, I.; Coppola, L.; Rossi, C. O.; Youssry, M.; Ranieri, G. A., NMR Investigation of the Dynamics of Confined Water in Nafion-Based Electrolyte Membranes at Subfreezing Temperatures. *The Journal of Physical Chemistry B* **2009,** *113* (42), 13935-13941.

64. Gu, S.; Cai, R.; Luo, T.; Chen, Z.; Sun, M.; Liu, Y.; He, G.; Yan, Y., A Soluble and Highly Conductive Ionomer for High-Performance Hydroxide Exchange Membrane Fuel Cells. *Angewandte Chemie International Edition* **2009,** *48* (35), 6499-6502.

65. Liu, L.; Ahlfield, J.; Tricker, A.; Chu, D.; Kohl, P. A., Anion conducting multiblock copolymer membranes with partial fluorination and long head-group tethers. *Journal of Materials Chemistry A* **2016,** *4* (41), 16233-16244.

66. Mohanty, A. D.; Tignor, S. E.; Sturgeon, M. R.; Long, H.; Pivovar, B. S.; Bae, C., Thermochemical Stability Study of Alkyl-Tethered Quaternary Ammonium Cations for Anion Exchange Membrane Fuel Cells. *Journal of The Electrochemical Society* **2017,** *164* (13), F1279-F1285.

67. Arges, C. G.; Wang, L.; Parrondo, J.; Ramani, V., Best Practices for Investigating Anion Exchange Membrane Suitability for Alkaline Electrochemical Devices: Case Study Using Quaternary Ammonium Poly(2,6-dimethyl 1,4-phenylene)oxide Anion Exchange Membranes. *Journal of The Electrochemical Society* **2013,** *160* (11), F1258-F1274.

68. Arges, C. G.; Ramani, V., Investigation of Cation Degradation in Anion Exchange Membranes Using Multi-Dimensional NMR Spectroscopy. *Journal of The Electrochemical Society* **2013,** *160* (9), F1006-F1021.

69. Zhang, B.; Kaspar, R. B.; Gu, S.; Wang, J.; Zhuang, Z.; Yan, Y., A New Alkali-Stable Phosphonium Cation Based on Fundamental Understanding of Degradation Mechanisms. *ChemSusChem* **2016,** *9* (17), 2374-2379.

70. Ayers, K. E.; Anderson, E. B.; Capuano, C. B.; Niedzwiecki, M.; Hickner, M. A.; Wang, C.-Y.; Leng, Y.; Zhao, W., Characterization of Anion Exchange Membrane Technology for Low Cost Electrolysis. *ECS Transactions* **2013,** *45* (23), 121-130.

71. Ünlü, M.; Zhou, J.; Kohl, P. A., Hybrid Anion and Proton Exchange Membrane Fuel Cells. *The Journal of Physical Chemistry C* **2009,** *113* (26), 11416-11423.

72. Zhou, J. F.; Joseph, K.; Ahlfield, J. M.; Park, D. Y.; Kohl, P. A., Poly(arylene ether) Ionomers with Pendant Quinuclidium Groups and Varying Molecular Weight for Alkaline Electrodes. *J Electrochem Soc* **2013,** *160* (6), F573-F578.

73. Zhou, J.; Guo, J.; Chu, D.; Chen, R., Impacts of anion-exchange-membranes with various ionic exchange capacities on the performance of H2/O2 fuel cells. *Journal of Power Sources* **2012,** *219* (Supplement C), 272-279.

74. Millet, P.; Mbemba, N.; Grigoriev, S. A.; Fateev, V. N.; Aukauloo, A.; Etiévant, C., Electrochemical performances of PEM water electrolysis cells and perspectives. *International Journal of Hydrogen Energy* **2011,** *36* (6), 4134-4142.

75. Brug, G. J.; van den Eeden, A. L. G.; Sluyters-Rehbach, M.; Sluyters, J. H., The analysis of electrode impedances complicated by the presence of a constant phase element. *Journal of Electroanalytical Chemistry and Interfacial Electrochemistry* **1984,** *176* (1), 275-295.

76. Mohanty, A. D.; Ryu, C. Y.; Kim, Y. S.; Bae, C., Stable Elastomeric Anion Exchange Membranes Based on Quaternary Ammonium-Tethered Polystyrene-b-poly(ethylene-co-butylene)-b-polystyrene Triblock Copolymers. *Macromolecules* **2015,** *48* (19), 7085-7095.

77. Liu, X.; Gao, H.; Chen, X.; Hu, Y.; Pei, S.; Li, H.; Zhang, Y., Synthesis of perfluorinated ionomers and their anion exchange membranes. *Journal of Membrane Science* **2016,** *515* (Supplement C), 268-276.

78. Ponce-Gonzalez, J.; Whelligan, D. K.; Wang, L.; Bance-Soualhi, R.; Wang, Y.; Peng, Y.; Peng, H.; Apperley, D. C.; Sarode, H. N.; Pandey, T. P.; Divekar, A. G.; Seifert, S.; Herring, A. M.; Zhuang, L.; Varcoe, J. R., High performance aliphatic-heterocyclic benzyl-quaternary ammonium radiation-grafted anion-exchange membranes. *Energy & Environmental Science* **2016,** *9* (12), 3724-3735.

79. Dang, H.-S.; Jannasch, P., Alkali-stable and highly anion conducting poly(phenylene oxide)s carrying quaternary piperidinium cations. *Journal of Materials Chemistry A* **2016,** *4* (30), 11924-11938.

80. Lin, C. X.; Wang, X. Q.; Li, L.; Liu, F. H.; Zhang, Q. G.; Zhu, A. M.; Liu, Q. L., Triblock copolymer anion exchange membranes bearing alkyl-tethered cycloaliphatic quaternary ammonium-head-groups for fuel cells. *Journal of Power Sources* **2017,** *365* (Supplement C), 282-292.

81. Chen, X.; Jiang, Y.; Yang, S.; Pan, J.; Yan, R.; Bruggen, B. V. d.; Sotto, A.; Gao, C.; Shen, J., Internal cross-linked anion exchange membranes with improved dimensional stability for electrodialysis. *Journal of Membrane Science* **2017,** *542* (Supplement C), 280-288.

82. Zhou, J.; Ünlü, M.; Anestis-Richard, I.; Kohl, P. A., Crosslinked, epoxy-based anion conductive membranes for alkaline membrane fuel cells. *Journal of Membrane Science* **2010,** *350* (1), 286-292.

83. Lin, C. X.; Zhuo, Y. Z.; Hu, E. N.; Zhang, Q. G.; Zhu, A. M.; Liu, Q. L., Crosslinked side-chain-type anion exchange membranes with enhanced conductivity and dimensional stability. *Journal of Membrane Science* **2017,** *539* (Supplement C), 24-33.

84. Lai, A. N.; Guo, D.; Lin, C. X.; Zhang, Q. G.; Zhu, A. M.; Ye, M. L.; Liu, Q. L., Enhanced performance of anion exchange membranes via crosslinking of ion cluster regions for fuel cells. *Journal of Power Sources* **2016,** *327* (Supplement C), 56-66.

85. Lin, J.; Yan, X.; He, G.; Chen, W.; Zhen, D.; Li, T.; Ma, L.; Wu, X., Thermoplastic interpenetrating polymer networks based on polybenzimidazole and poly (1, 2-dimethy-3-allylimidazolium) for anion exchange membranes. *Electrochimica Acta* **2017,** *257* (Supplement C), 9-19.